

SPECTRAL VARIABILITY IN CELESTIAL X-RAY SOURCES

by

ROBERT HALL

Thesis submitted to the University of Leicester
for the degree of Doctor of Philosophy

December 1983

X-ray Astronomy Group
Department of Physics
University of Leicester

UMI Number: U346442

All rights reserved

INFORMATION TO ALL USERS

The quality of this reproduction is dependent upon the quality of the copy submitted.

In the unlikely event that the author did not send a complete manuscript and there are missing pages, these will be noted. Also, if material had to be removed, a note will indicate the deletion.



UMI U346442

Published by ProQuest LLC 2015. Copyright in the Dissertation held by the Author.
Microform Edition © ProQuest LLC.

All rights reserved. This work is protected against
unauthorized copying under Title 17, United States Code.



ProQuest LLC
789 East Eisenhower Parkway
P.O. Box 1346
Ann Arbor, MI 48106-1346



x75002-1615

DECLARATION

I hereby declare that no part of this thesis has been previously submitted to this or any other University as part of the requirement for a higher degree. The work described herein was conducted by the undersigned except for the contributions from colleagues and other workers which are acknowledged in the text, and in the following note on publications.

R. Hall

Robert Hall

December 1983

PUBLICATIONS

Some of the work reported here has been published elsewhere as follows:

Chapter 4

Ricketts, M.J., Hall, R., Page C.G. and Pounds, K.A. Proceedings of 25th ESLAB Symposium, Amsterdam, 1981. p.399. "Observation of an outburst from the X-ray pulsator 0115+63".

Hall, R., Ricketts, M.J. and Kloss, R. Workshop on "Accreting Neutron Stars", Garching, 1982. "Pulse phase spectroscopy of 0115+63 and an observation of 4U1223-62".

Ricketts, M.J., Hall, R., Page, C.G., Whitford, C.H. and Pounds, K.A. M.N.R.A.S. (1982). 201, 759. "GX 1+4: pulse period measurement and detection of phase-variable Iron line emission".

Chapter 5

Hall, R., Ricketts, M.J., Page, C.G. and Pounds, K.A. Proceedings of 25th ESLAB Symposium, Amsterdam, 1981. p.47. "Ariel-6 medium energy spectral observations of active galaxies".

This thesis is dedicated to

Mum, Dad

&

Angie

ACKNOWLEDGEMENTS

I would like to thank Dr Martin Ricketts for his help and guidance during the years of my research studentship, Dr Clive Page for his help, and also for reading the first draft of this thesis; Nigel Marshall for many comments and for the office decorations.

I would also like to thank Professor K A Pounds for his support and patience whilst this work was completed, and many other colleagues, too numerous to mention, who at some time or other have made constructive comments about this thesis.

I take this opportunity to thank the S.E.R.C. for providing me with a studentship whilst I conducted my research.

ABSTRACT

The Ariel-6 spacecraft was launched during 1979 and remained operational for ~ 3 years. The satellite payload is discussed, with an emphasis on the medium energy detectors, their calibration and performance. We present observations of spectral variability, in both galactic and extra-galactic sources, made with this instrument in the 1 - 50 keV energy range.

Three galactic sources were observed, these consisted of two X-ray pulsators, 4U0115+63 and GX 1+4; the former being fortuitously seen during outburst. Both sources were found to show a significant phase dependence in their X-ray spectra. In GX 1+4 an Iron emission feature was detected, the equivalent width of which was also phase dependent. Pulse timing was performed on the data from both sources and in the case of 4U0115+63 yields a revised set of orbital parameters. The third galactic source presented is 3A1822-371, we find that our data are not only consistent with the presence of an accretion disc corona in the system, but strongly suggests the presence of such a corona in many disc fed systems.

Three Seyfert galaxies, NGC 4151, MCG 8-11-11 and III Zw2 were observed, this being the first reported X-ray spectrum of III Zw2. NGC 4151 was found to have a spectrum consistent with that seen ~ 3 years earlier, whilst MCG 8-11-11 was softer than seen hitherto and now shows evidence for an Iron emission line. The BL Lac, Mkn 421 was found to have a two component spectrum; comparison with earlier reported spectra indicates that both components vary independently of each other and therefore arise in physically differing regions of the source.

Finally a forward-look is made which considers the improvements in medium energy spectroscopy that can be anticipated over the next decade or so.

CONTENTS

<u>1</u>	<u>Introduction</u>	1
<u>2</u>	<u>Instrumentation and Data Analysis</u>	5
2.1	Instrumentation	5
2.1.1	General Description of the Ariel-6 Satellite	5
2.1.2	Power Supply	8
2.1.3	Attitude Determination and Control	9
2.1.4	Onboard Data Storage and Telemetry	12
2.1.5	Timing	13
2.1.6	The Cosmic Ray Gas Scintillator	13
2.1.7	The Low Energy X-ray Instrument	14
2.1.8	The Medium Energy Instrument	15
	a) Description	15
	b) Data Storage and Modes of Operation	22
2.2	Data Handling and Analysis	27
2.2.1	Data Handling	27
2.2.2	Temporal Analysis	29
2.2.3	Spectral Analysis	30
<u>3</u>	<u>Inflight Performance and Calibration</u>	37
3.1	Inflight Performance	37
3.1.1	Spurious Command Reception	37
3.1.2	High Spacecraft Temperatures	39
3.1.3	Battery Failures	40
3.1.4	Tape Recorders	41
3.1.5	Coning Angle	41
3.1.6	Timing	43
3.1.7	Attitude	43

3.2	Calibration	45
3.2.1	By the Calibration Sources	45
3.2.2	Detector Background Spectrum	47
3.2.3	The Crab Nebula	55
<u>4</u>	<u>Ariel-6 Observations of Galactic Sources</u>	<u>58</u>
4.1	Introduction	58
4.2	4U0115+63	62
4.2.1	The Ariel-6 Observations	63
4.2.2	The Outburst	63
4.2.3	Pulse Timing Analysis	68
4.2.4	Pulse Profiles	71
4.2.5	Pulse Phase Spectroscopy	73
4.2.6	Discussion	75
4.3	GX 1+4	79
4.3.1	The Pulse Period and Profile	80
4.3.2	Spectra: The Continuum	85
4.3.3	Spectra: Iron Fluorescence	89
4.3.4	Discussion	90
4.4	3A1822-371	96
4.4.1	Ariel-6 Observations	99
4.4.2	Discussion	108
<u>5</u>	<u>Ariel-6 Observations of Active Galaxies</u>	<u>111</u>
5.1	Introduction	111
5.2	Energy Generation	114
5.3	Ariel-6 Observations	117
5.3.1	Seyferts	117
	NGC 4151	118
	MCG 8-11-11	126
	III Zw2	131

5.3.2 BL Lac Objects	135
Mkn 421	135
<u>6 Conclusions and Forward Look</u>	140
<u>References</u>	147

Chapter 1

Introduction

The potential for understanding the physical processes acting within an X-ray emitting region, using spectroscopic data, is obvious. Detection of features in an X-ray spectrum would make it possible to determine elemental abundancies, local ionization states and the temperature of the plasma in the line formation region. Similarly, the detection of absorption edges, such as those of Iron at energies >7.1 keV, enables an accurate measure of the column density of the material local to the source, since the value indicated by the decreased flux at low energies may be an underestimate due to the reduced opacity of the material along the line of sight at high temperatures, when its lighter constituents may be ionised.

The relative inefficiency of dispersive techniques, such as Bragg and Grating spectroscopy, compared to photometric methods has meant that in the 1 - 10 keV energy range observations of astrophysical plasmas have been mainly performed by instruments which typically have resolutions of $\sim 20\%$ at 6 keV. Astrophysical X-ray spectroscopy has therefore been little more than a determination of the different types of source continua and the detection of strong features against the surrounding continuum. Observations of this type, and their interpretation using simple models, do have the capability to constrain the possible X-ray emission mechanisms however, consider for example the detection of the thermal spectra, some containing Iron line features, from clusters of galaxies (Mushotzky et al. 1978a). Not only was the emission mechanism found directly in this case, but the presence of the lines revealed that the gas had originated in the constituent galaxies of the cluster.

In the case of compact X-ray sources the structure of the emitting region will determine the characteristics of the observed spectra. The presence of gas streams in a binary system, either connecting the companion to an accretion disc around the compact object or in a stellar wind from the mass donating star, may be detected by the attenuation of the X-ray spectrum at low energies. Similarly the presence of a disc may be inferred from periodic variability of the low energy X-ray spectrum. In the specific case of the active galaxies the signal to noise obtained with the current instrumentation is generally insufficient to enable a significant distinction to be made between power-law and thermal bremsstrahlung models. However, in the case of the Seyfert type 1 galaxies, the X-ray spectra appear to be approximately identical and favour a power-law interpretation (Mushotzky et al. 1980). Whether this power-law arises due to non-thermal processes, such as the inverse compton scattering of synchrotron photons, or by the comptonisation of an initially thermal spectrum can not generally be determined by the observations over a limited dynamic range that are currently performed. Distinction will be possible however, as it is expected that X-rays which had a thermal origin will also have a spectral break in the 100 keV - 10 MeV energy range, whilst no such break should exist if the emission was from a non-thermal process (Holt and McCray 1982).

The detection of spectral variability can be a far more powerful diagnostic tool in the determination of the X-ray emission and radiative transfer processes than crude spectroscopy alone. Consider for example, the interpretation of the black body spectra seen during X-ray bursts as the changing radius of a photosphere of material blown off a neutron star

during a thermonuclear flash (Lewin et al. 1983). Variability, therefore, implies that changes have occurred in the physical structure of the source, and it is expected that the characteristics of this variability will place restrictions on the range of X-ray emission models available.

It is the purpose of this work to show how observations of spectral variability made with the medium energy (1 - 50 keV) instrument on Ariel-6 have contributed to our understanding of the physical processes acting in both galactic and extragalactic X-ray sources. The importance of even low resolution observations of this type as a diagnostic tool is underlined.

The observations described in this work were made with the Ariel-6 satellite during the period 1979 - 81. In Chapter 2 therefore, the scientific payload and control of the spacecraft are reviewed, with a particular emphasis on the description of the medium energy instrument. Data preparation and spectral analysis techniques relevant to this work are also discussed.

Chapter 3 gives details of several faults that were evident in the spacecraft following launch, these severely restricted the data acquisition and therefore the methods which were used to avoid these problems are also given. Included in this chapter are the determination of the medium energy instrument's background spectrum and its inflight calibration, with both the onboard sources and by observations of the Crab nebula.

Chapter 4 presents data obtained on three galactic X-ray sources, two pulsators (4U0115+63 and GX 1+4) and a short period binary, 3A1822-371. The ~ 3.6 s transient pulsator 4U0115+63 was fortuitously observed in outburst during late 1980; we find its X-ray spectrum to be very hard and highly

phase dependent. Similarly the ~ 110 s pulsator GX 1+4 was found to exhibit a significant phase dependence in both its continuum and Iron line emission. 3A1822 - 371 is an ~ 5.6 hr binary and is the progenitor of what has become a class of X-ray sources, all of which are thought to contain a compact object residing in a shell or corona of hot, ionised material, our observations are consistent with the presence of such a corona.

Observations were made of four active galaxies and these are presented in Chapter 5. The sources were the Seyfert galaxies NGC 4151, MCG 8-11-11 and III Zw 2; also the BL Lac object Mkn 421. III Zw 2 is included as an example of the Ariel-6 medium energy instrument's sensitivity to weak sources, this being the first reported X-ray spectrum. NGC 4151 is perhaps the most studied of all the active galaxies and is included, slightly out of context in this work, as an example of spectral non-variability, the inferences that we may draw from this are discussed. Both MCG 8-11-11 and Mkn 421 show evidence of spectral variability on a timescale of years, upon comparison of our data with previously published results. MCG 8-11-11 was found to have an Iron emission feature, whilst Mkn 421 shows a distinct two component spectrum.

Chapter 6 presents the conclusions that were drawn from the Ariel-6 observations and provides a forward look, discussing the improvements in medium energy spectroscopy that are to be expected within the next few years.

Chapter 2

Instrumentation and

Data Analysis

2.1 Instrumentation

2.1.1 General Description of the Ariel-6 Satellite

The Ariel-6 satellite was placed in orbit on the 2nd June 1979 by a Scout rocket launched from the NASA Wallops Island range off the east coast of Virginia, USA.

In order to minimise the post launch costs of the mission the satellite was designed to use only one ground station, based in the United Kingdom at Winkfield, near Ascot. To achieve contact with this ground station Ariel-6 was placed in a highly inclined ($\sim 55^\circ$) orbit. Due to the inherent precession there were only five or six orbits per day which could be seen from Winkfield. During the short time that Ariel-6 was above the Winkfield horizon the onboard instruments were commanded, manouvres programmed and scientific and housekeeping data collected. The Ariel-6 orbital elements are given in Table 2.1 and the in-orbit satellite configuration is shown in Fig 2.1.

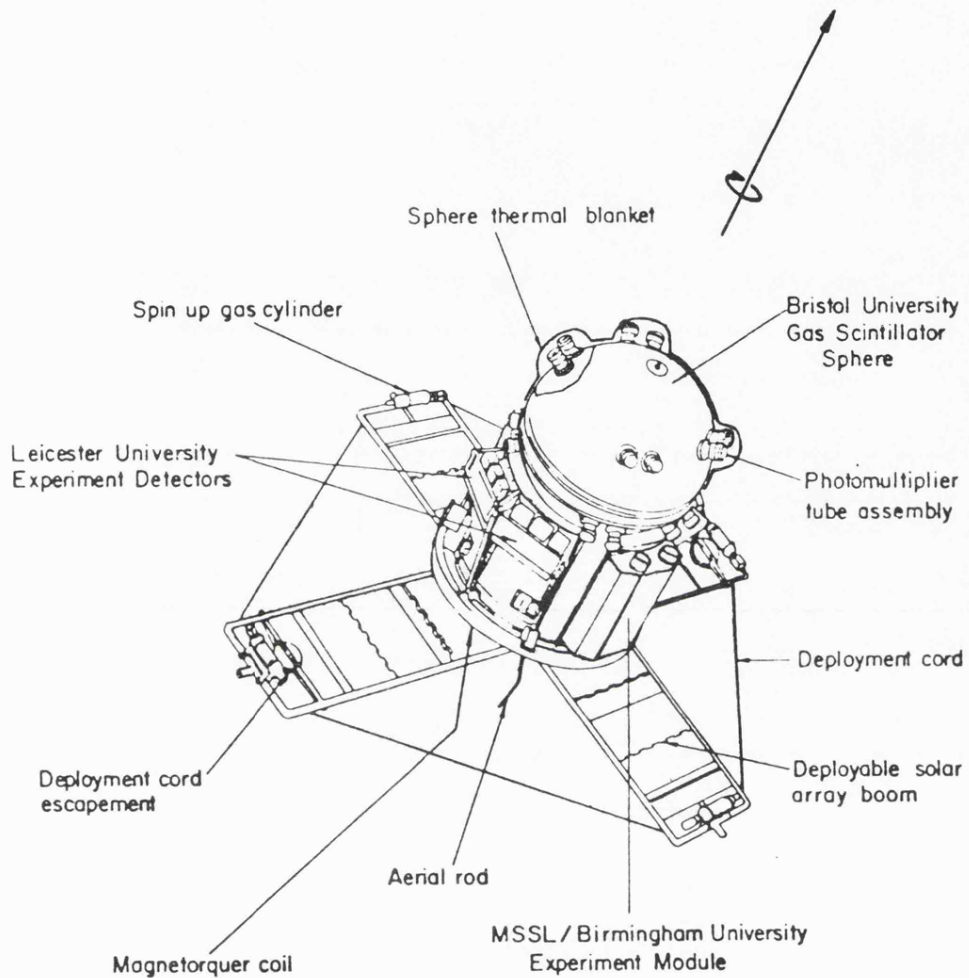
Attitude stability was obtained by spinning the satellite at ~ 60 rpm, this spin rate decreased to ~ 15 rpm after 100 days in orbit. It was possible to "spin-up" the satellite on two subsequent occasions by means of high pressure gas contained in bottles mounted at the ends of the solar panels (see Fig 2.1). Pointing stability was in fact being lost for the final time after expenditure of the gas, at the termination of the project.

The scientific payload consisted of three high-energy astrophysics instruments. The primary instrument was the cosmic ray detector, built by the University of Bristol and sealed "on top" of the spacecraft body. The two X-ray instruments were mounted on the sides of the spacecraft, viewing along the major (spin) axis and down the side of the

TABLE 2.1

ARIEL-6 SPACECRAFT AND ORBITAL PROPERTIES

MEAN ORBITAL PERIOD	1 ^h 36 ^m 56 ^s
ALTITUDE	625 km
ECCENTRICITY	0.003
INCLINATION	55 ^o .02
SPACECRAFT MASS	154 kg
BODY HEIGHT	1.3 m
BODY DIAMETER	0.96 m
SOLAR PANELS (TIP TO TIP)	2.7 m



Thermal blankets not shown in complete form

Fig 2.1 Ariel-6 Spacecraft (Orbital Configuration).

cosmic-ray sphere. One instrument consisted of two X-ray telescopes sensitive in the 0.1 - 2 keV energy range built by a joint Mullard Space Science Laboratory/Birmingham University collaboration. The second X-ray instrument was built by the University of Leicester and provided timing and spectral studies in the 1 - 50 keV energy band.

The cosmic-ray sphere had a field of view of 4π steradians and therefore no "preferred" pointing direction for the spacecraft. Consequently the X-ray instruments were free to point at any sources which were within $\pm 45^\circ$ from the anti-sun. This restriction on pointing direction was imposed by the limited power available from the spacecrafts solar panels at large anti-sun angles.

Ariel-6 remained in operation for ~ 1000 days, the project being terminated on 12th February 1982 when the instruments were commanded off.

2.1.2 Power Supply

The total power requirement of the three astrophysics instruments was 10.5 watts. This was supplied by $\sim 1 \text{ m}^2$ of solar cells arranged on the four booms extended co-planar to the base of the spacecraft (see Fig 2.1). The solar cells were designed to be capable of supplying ~ 60 watts over the entire range of satellite pointing angles ($\pm 45^\circ$ from the anti-sun direction) after two years degradation in orbit.

During the $\sim 66\%$ of the orbit that the satellite was in sunlight the solar panels were used to charge twelve, 6Ah, Ni-Cd cylindrical cells. These were then used to power the instrumentation during the subsequent satellite eclipse.

2.1.3 Attitude Determination and Control

Real-time satellite attitude was determined by the use of two independent groups of sensors, each consisting of two Sun and one Earth albedo sensor. These sensors were of a type that had been used successfully on the earlier X-3 mission.

Each Sun sensor consisted of a semi-circular slit with a field of view of $180^{\circ} \times 1^{\circ}$, behind which was a centrally mounted photo-diode. The slit on one of the sensors was aligned with the satellite spin axis (the "meridian" sensor), whilst the second (the "tilted" sensor), was inclined at 35° to the first. The intersection of the two fields of view was situated on the satellite equator, (Fig 2.2).

In operation the Sun transits the field of view of each slit once per satellite revolution, thereby enabling a determination of the spacecraft spin period. Similarly the time delay between the detection in the meridian and tilted sensors, combined with the knowledge of their angular separation, provided the solar aspect angle.

Earth albedo sensing was by means of a silicon detector, with a 1° field of view, operating at visible wavelengths. Detections of both edges of the bright Earth were made and the phase of these detections relative to the output from the meridian sun sensor was recorded. With the knowledge of the satellite spin period the Earth-satellite-Sun angle could be calculated.

The older X-3 sensors were supplemented by four purpose-built devices. These consisted of two linear solar aspect sensors which were identical in all respects apart from output, one having digital output (Array Sensor Digital - ASD) whilst

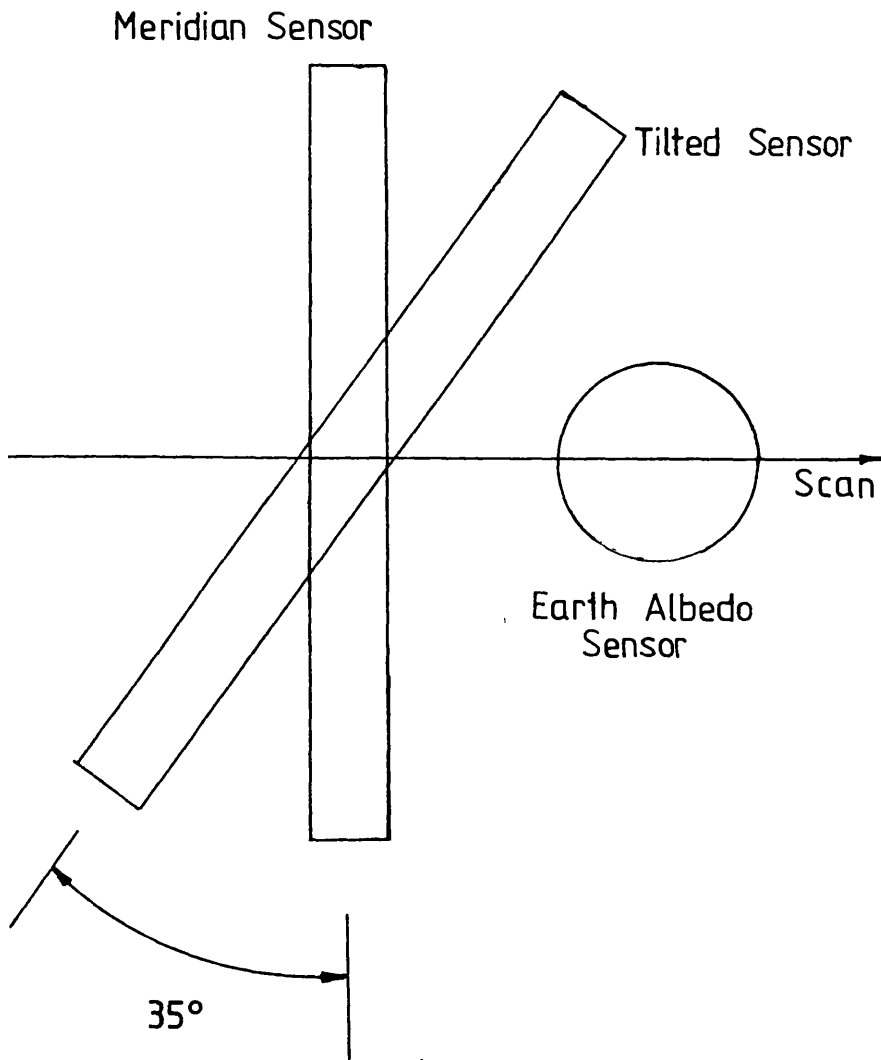


Fig 2.2 Ariel-6 Attitude sensing equipment (Not to scale).

the second was an analogue device (Array Sensor Analogue - ASA). These two sensors were simply an array of photo-diodes mounted behind a slit. Output could be obtained either in coarse, $\sim 2^\circ$, or fine ~ 0.4 steps and consisted purely of an output voltage which was directly proportional to the solar aspect angle.

The third new device was the Crossed Slit Sensor which was used to provide an independent measure of the spin period and a very accurate determination of the solar aspect angle when combined with the output from a Coning Angle Sensor (CAS). Which, as its name implies, accurately measures the offset between the satellite's major and spin axis'. In operation the CAS was similar to the meridian/tilted sensor arrangement. The final pieces of information required to determine the satellite's pointing position; its latitude, longitude and height above the Earth, were provided by NASA's mini-track network.

Control of the attitude was by a magnetic torque system which consisted of two 0.76 m diameter coils of aluminium wire located in the base of the spacecraft. When a current was passed through the coils a turning moment was generated, due to the surrounding magnetic field of the Earth, thereby altering the spacecraft attitude. The degree of manoeuvrability achieved by this method was dependent upon the current spin rate of the satellite but was typically $\sim 15^\circ$ per day.

During the passes of the satellite over the ground station at Winkfield the magnetorquing system was programmed with the time at which a manoeuvre was to commence and its duration. After acquisition of a target the magnetorquer was used for

"trimming" the attitude to allow for the ~ 0.5 per day drift due to the satellite attempting to align along the Earth's gravitational field.

2.1.4. Onboard Data Storage, Telemetry and Commanding

Each instrument had associated with it a limited amount of memory which acted as a buffer between the instrument and the satellites two tape recorders. The recorders used 4-track tape, each track of which had a maximum capacity of 800 minutes of data, thereby giving a total onboard storage capacity well in excess of 24 hours. Data was received from the instruments by a low speed encoder and placed on the tape at a rate of 64 bit s^{-1} .

During the five or six passes per day; each of ~ 10 minutes duration, that the satellite made over the ground station the tape was replayed and the information transmitted to the ground at a rate of $\sim 2k \text{ bit s}^{-1}$. The telemetry was arranged such that when the satellite was over a ground station the information from the different instruments' memories could also be dumped directly by using a high speed encoder (HSE). Scientific data could be obtained at a rate of $\sim 2k \text{ bit s}^{-1}$ using the HSE without any onboard buffering.

Control of both tape recorders, the astrophysics instruments and the satellite systems was all performed by a unit called the "Programmer". This contained a command decoder that interpreted up-linked telemetry which the "Programmer" then used to control the spacecraft.

Each of the scientific instruments had a variety of modes of operation which were controlled by their own "Command Registers", these "registers" were loaded via the "Programmer".

2.1.5 Timing

All timing was derived from one of two spacecraft clocks (one reserve clock) which ran at a nominal 2^{20} Hz (1.048576 MHz). Two divider chains on each clock provided timing for the high- (HS) and low-speed (LS) encoders, these were the HS-clock and the LS-clock respectively. The HS-clock was also used for timing the commencement of an observation whilst the LS-clock organised the acquisition of data and the management of the storage local to each instrument.

The two clocks ran at slightly differing rates, however timing to within a millisecond was technically possible without undue difficulty.

2.1.6 The Cosmic Ray Gas Scintillator

The purpose of this instrument was to measure the charge and energy spectra of galactic cosmic rays with a particular emphasis on the ultra-heavy component, that is primary rays with $Z > 30$. Similar instruments to that on Ariel-6 had been used with success on earlier balloon flights, however with the flux of the heaviest primaries being $\sim 0.5 \text{ day}^{-1}$, the increased exposure provided by a satellite based instrument was essential.

The instrument was a combined Cerenkov/Scintillation radiation detector consisting of two concentric spherical shells, the innermost shell being made of an acrylic plastic which emitted Cerenkov radiation during the transit of a primary. This radiation was detected by eight pairs of photomultipliers equidistantly spaced on the surface of the outermost sphere. Scintillation radiation was generated when

the primaries passed through the Argon, Nitrogen and Helium mixture contained within the spheres. The scintillation radiation was detected by the same photomultipliers as the Cerenkov emission but the two could be distinguished by the differing rise-times of their output pulses.

Since the emitted light was directly proportional to the charge on the detected primary the production of a charge spectrum was not difficult. It was possible to obtain a crude energy spectrum due to the highly inclined orbit of Ariel-6 which subjected the instrument to varying degrees of geo-magnetic shielding (high over equatorial regions and low towards the poles).

2.1.7 The Low Energy X-ray Instrument

This collaborative instrument was built to provide low energy $\sim 0.1 - 2.0$ keV spectral and spatial observations of known and suspected soft X-ray sources. As the instrument was non-imaging the mapping of extended sources or the soft X-ray background required either repeated scans across an area of sky or several pointed observations.

The instrument consisted of four detectors, with a total geometric area of $\sim 100 \text{ cm}^2$, mounted in diametrically opposing pairs viewing along the spacecraft main axis. Each detector consisted of a gold coated grazing-incidence-parabaloid reflector beyond the focus of which was a thin window proportional counter. Between the counter and reflector was situated a variable aperture disc, which allowed the counters' field of view to be varied between the limits $\sim 0.1^\circ$ FWHM and $\sim 1.8^\circ$ FWHM. A further disc contained a calibration source, a

boron filter (to modify the low energy response) and a blanking portion for determining the particle rate in the counter. The background in each counter was monitored and reduced by the use of extensive anti-coincidence grids.

In order to obtain a high efficiency to soft X-rays the counter windows were very thin ($\sim 1 \mu\text{m}$ carbon covered polypropylene). This, inevitably, meant that the propane filling gas would be lost by diffusion through the detector windows. To overcome this restriction in detector lifetime each pair of detectors had a reserve of ~ 0.25 kg of liquid propane. This was fed into the counters through a very accurate pressure sensitive switch, which maintained the gas pressure to within $\sim 1\%$ of the nominal value.

2.1.8 The Medium Energy Instrument

a) Instrument Description

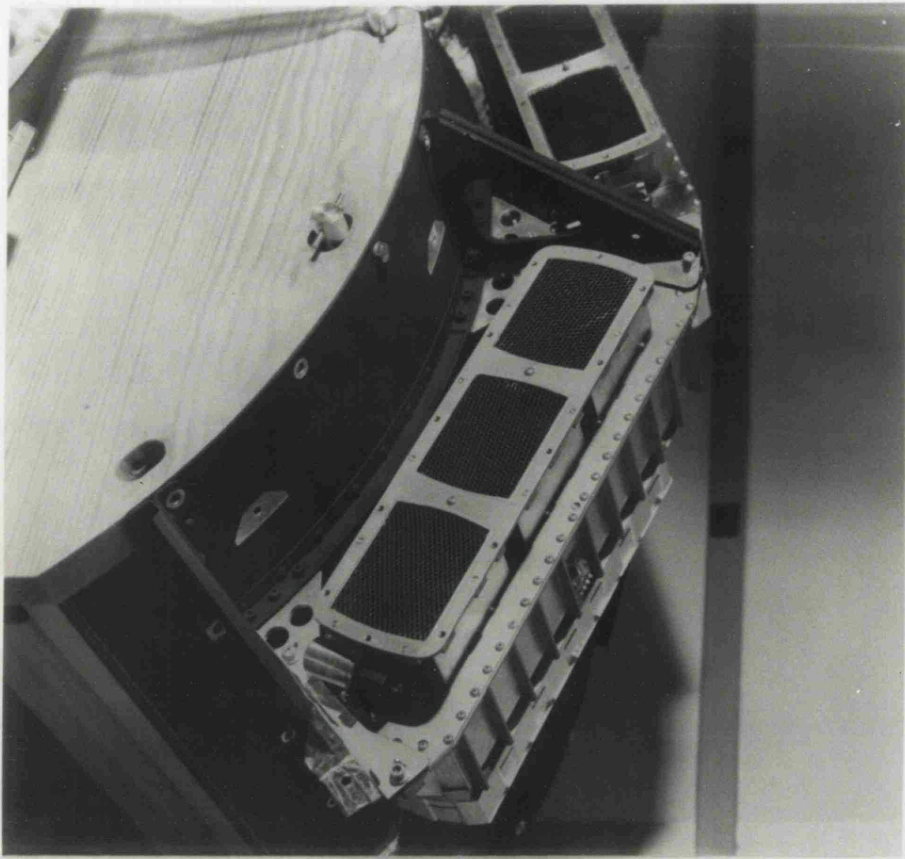
Four medium energy detectors were mounted in pairs between the two groups of low energy telescopes on the sides of the spacecraft body. Plates 2.1(a) and (b) show the detector orientation and their mounting to the spacecraft. The detectors were multi-wire proportional counters filled with a Xenon/Methane gas mixture at a pressure of ~ 1.5 atmospheres at 0°C . Subdivision of the detectors electronically, by a plane of cathode wires, provided two active volumes. The "front" section, directly beneath the window, had a depth of ~ 1.0 cm and provided most of the X-ray absorption at energies ~ 10 keV. The use of thin ($\sim 32 \mu\text{m}$) Beryllium windows enabled the 20% efficiency points of this "low-energy" section to be extended down to ~ 1.2 keV, whilst the corresponding

Plate 2.1

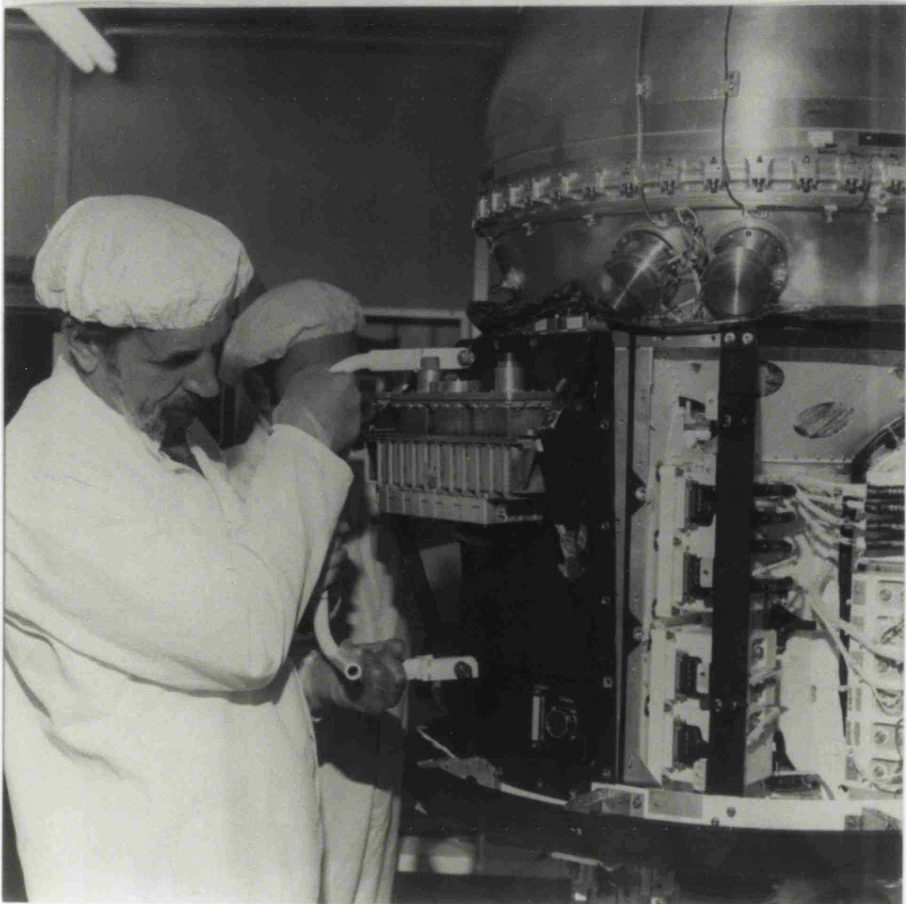
- a) Two of the four Ariel-6 medium energy detectors, the honeycomb collimators and the calibration device are clearly seen.

- b) Two detectors during mounting to the spacecraft. The detectors view towards the top of the Plate. (Protective covers are in position over the collimators.)

a



b



upper point was at ~ 20 keV. Incoming X-rays of energy ~ 10 keV were preferentially absorbed in the rear, or "high-energy" compartment, up to a maximum effective energy of ~ 50 keV, see Fig 2.3. The detector characteristics are given in detail in Table 2.2, whilst Fig 2.4 shows the detector construction.

Front and rear sections were isolated from each other by a cathode plane, they were also surrounded on three sides by guard detectors which were similarly isolated. Pulses that occurred from any two of the independent sections within $\sim 5 \mu\text{s}$ of each other were most likely to be due to the detection of a particle and were therefore vetoed from the data stream. A background monitor was incorporated to count such events thereby allowing data acquired in regions of high particle background to be flagged. In total the anti-coincidence guards rejected $\sim 90\%$ of the particle induced background.

Honeycomb collimators were mounted in front of the Beryllium windows, the individual hexagonal elements of the collimator being deliberately misaligned to provide an approximately circular ~ 3.0 FWHM field of view. The total geometric effective area of the four detectors was $\sim 400 \text{ cm}^2$.

Inflight calibration of each detector was by the use of two radioactive sources mounted in a turret and attached to each detector body (see Fig 2.4). The radioactive sources used were Fe^{55} and Cd^{109} which produce characteristic line radiation at energies of 5.9 keV and 22.4 keV respectively. Normally the sources were pointing away from the detectors, however during calibration the turrets were rotated to expose the detector to the sources. The relative energy of the

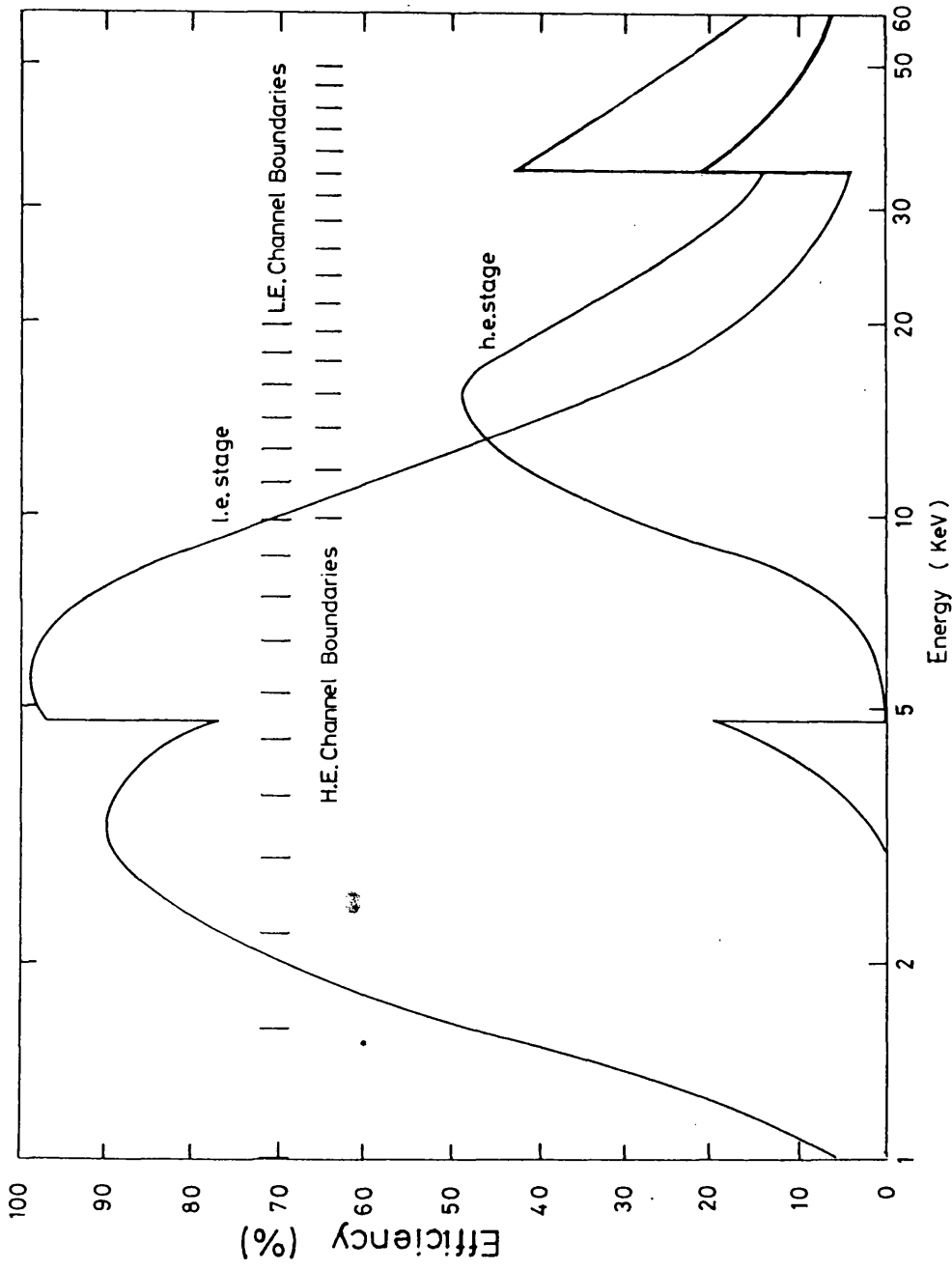


Fig 2.3 Detector efficiencies for the low- and high-energy systems. Also shown are the PHA channel boundaries.

TABLE 2.2

MEDIUM ENERGY INSTRUMENT DETECTOR CHARACTERISTICS

ENERGY RANGE (20% TRANSMISSION - LOW ENERGY SYSTEM)	1 - 20 keV
ENERGY RANGE (20% TRANSMISSION - HIGH ENERGY SYSTEM)	10 - 50 keV
GAS MIXTURE	XENON/CH ₄
GAS PRESSURE	1.45 atmospheres
Be WINDOW THICKNESS	32 μ m
GEOMETRICAL AREA	400 cm ²

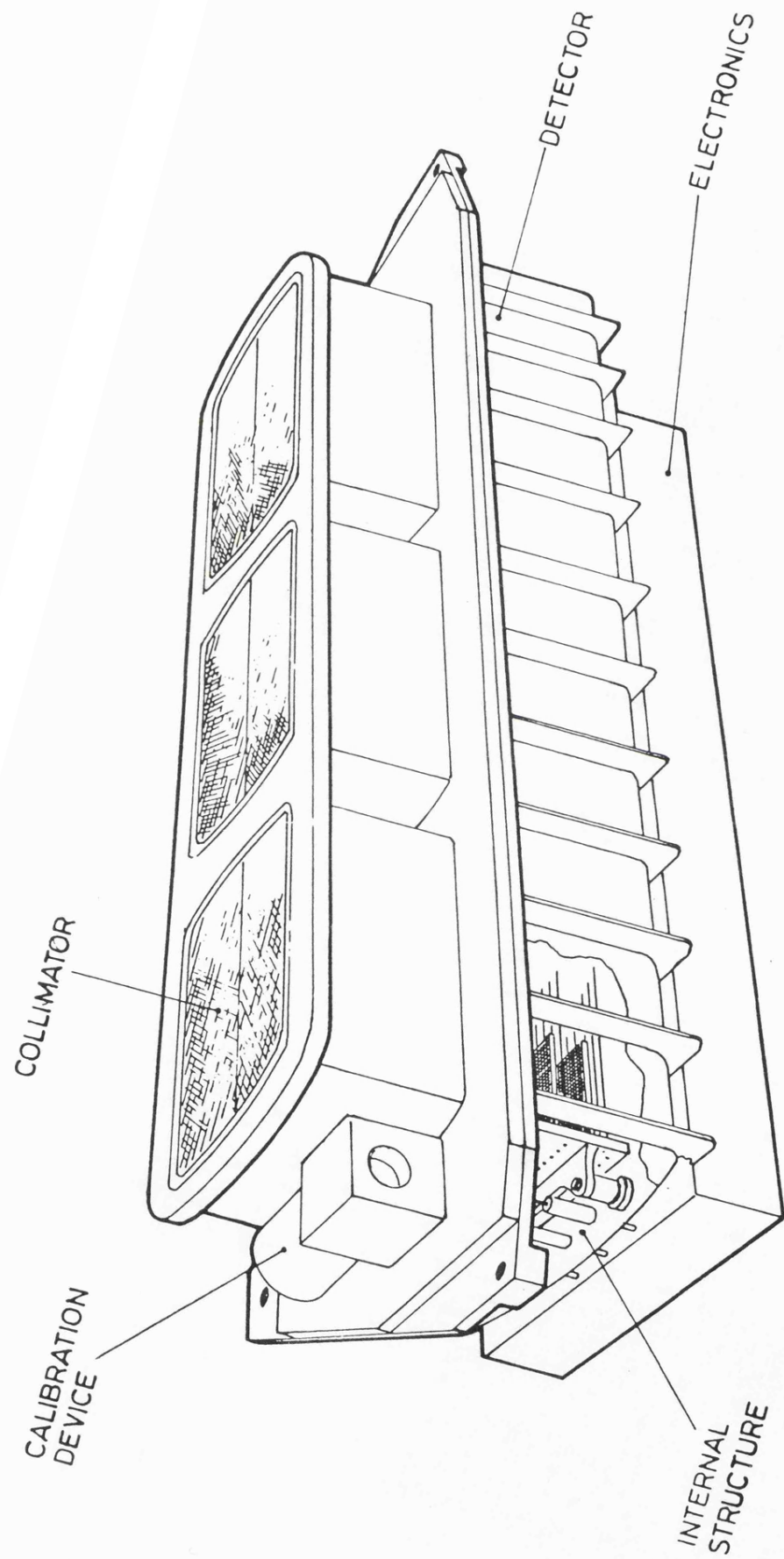


Fig 2.4 The major components in one of the Medium Energy Instruments' four detectors.

appropriate photopeak enabled the detector gains to be determined.

Each of the detectors incorporated its own high voltage (HT) supply and whilst this was nominally operated at 2 - 2.5 kV three different voltage steps were available. The associated pre-amplifiers for both low- and high- energy systems were also fully adjustable to provide intermediate steps in the gas gain between those produced by varying the HT supply. The HT supplies and pre-amplifiers were packaged together in an electronics module which was attached to the base of each detector assembly (see Fig 2.4).

Output signals from low and high energy systems were processed independently by two pulse height analysers (PHA) which were designed with non-linear characteristics such that the width of a PHA channel, at a particular energy, corresponded to the theoretical resolution of the detector at that energy. Ground calibration had shown that the resolution obeyed the energy (E) relationship:

$$\text{FWHM}(E) = \text{constant} \cdot E^{-\frac{1}{2}}$$

and that the resolution at ~ 6 keV was $\sim 23\%$. The dynamic ranges of the PHA's were divided into 16 approximately logarithmic energy channels.

Electronically down stream from the detector output and the PHA's were two single channel analysers (SCA), one per system. Their purpose was to restrict the energy range of the data output from the instrument.

Due to its highly inclined orbit Ariel-6 spent approximately one third of its life in regions of high particle

background, such as the South Atlantic anomaly. Very high count rates were anticipated from these regions and to prevent degradation of the detectors a background protection system was included in the electronics. The number of events recorded in ~ 64 ms by the background counter were monitored and the detector HT's automatically switched off if the count was greater than 256, the HT's would then remain off for a preset duration of ~ 2 minutes. The detectors would cycle through this on/off loop until the count rate in the background monitor dropped to < 256 , at which time normal operation would resume.

b) Data Storage and Modes of Operation

Incorporated within the medium energy instrument was a semi-conductor data store of 64 kbits capacity. This was organised into 8k bytes of 8 bits each, every 256 bytes forming one record (or page) of memory. This store provided buffering and reformatting of the data between its collection by the detectors and its subsequent copying to tape. The size of the buffer allowing data collection and copying to proceed at vastly different rates, the transfer of data from store to tape progressing at ~ 0.5 records per minute (64 bit s^{-1}).

Input to the store from the PHA's or SCA's was by two random access, one page long, input buffers. Whilst one was filled with data the other was being copied to the store. The interchange from one buffer to the other occurred at regular intervals which were determined by the mode of data acquisition. Transfer of the whole of one input buffer to the main store required ~ 64 ms and this therefore set the upper-limit on the data collection rate.

The natural storage unit was one byte and the maximum count that could be accumulated was therefore 256; should higher count rates be anticipated however two bytes could be combined to give double precision accuracy and a maximum acceptable count of 65 535; though obviously this reduced the capacity of the store by a factor of two.

The manner in which the store was addressed was dependent upon the instruments' mode of operation (i.e. the time resolution, the number of PHA channels required and whether double precision was to be used). Due to the limited physical size of the store the above criteria also determined the duration of an observation. For example the acquisition of a 32 PHA channel spectrum every minute with single precision count rates would fill the store in ~ 64 minutes, at which point the observation would terminate. Similarly, with double precision and collecting a 32 PHA channel spectrum every second, the entire observation would last a mere 32 seconds.

Since the copying of the instrument store to tape required ~ 64 minutes, observations were normally scheduled to optimise temporal and spectral resolution during those portions of the orbit that had low background and where the source was not occulted. One of the most important aspects of the medium energy instrument was its capability to maximise the "available science" by trading off between time resolution, number of PHA channels and the observation duration.

If, for example, high time resolution was of high priority and spectral information not required, then, as an alternative to decreasing the observation duration to a few seconds, the store could be output directly to the telemetry using the high speed encoder (see Section 2.1.4). Using this method the

TABLE 2.3 OBSERVING MODES

<u>MODE</u>	<u>DESCRIPTION</u>
E \emptyset	Intensity samples with no energy information but providing the highest time resolution of those modes that had no onboard processing. The energy band over which the intensity samples were accumulated was controlled by the SCA.
E2	Eight broad pulse height channels were available, (each one consisting of four intrinsic PHA channels), covering the energy range 1 - 50 keV. The time resolution was a factor of 8 less than that of the E \emptyset mode.
E3	The time resolution was identical to that of the E2 mode, the energy information consisted of eight narrow (intrinsic) PHA channels selected from either the low- or high-energy systems by means of the SCA.
E4	Full 32 PHA channel spectral information with the individual detectors identified.
PULSAR	Incoming data were overlaid at a preset period in the instrument store. The periods could be preset to an accuracy of ~ 1 part in 10^6 thereby minimising the smearing of the pulse profile. The pulsar mode was used in conjunction with E \emptyset , E2 or E3 modes to provide some energy information.

TABLE 2.4

POSSIBLE TRADE-OFFS BETWEEN OBSERVATION DURATION (THE TIME REQUIRED TO FILL THE INSTRUMENT STORE) AND THE AVAILABLE TEMPORAL AND SPECTRAL RESOLUTION

E ϕ	TIME RESOLUTION* MODE ⁻¹		PULSAR	OBSERVATION DURATION
	E2/E3	E4		
512 μ s	4 ms	64 ms	16 s	4 s
1 ms	8	128	32	8
2	16	256	64	16
4	32	512	128	32
8	64	1 s	256	1 m
16	128	2	512	2
32	256	4	1 ms	4
64	512	8	2	8
128	512	8	2	8
128	1 s	16	4	16
256	2	32	8	32
512	4	1 m	16	1 h
1 s	8	2	32	2
2	16	4	64	4
4	32	8	128	8
8	64	16	256	16
16	128	32	512	32

* For the double precision option the time resolution figures were double the quoted values.

instrument count rate could be sampled at ~ 2 ms intervals.

It was possible to command the instrument into several "modes" of operation, these "modes" subdivided naturally into two types, those that were simply raw count rates and those that had undergone some onboard processing and in which the original count rates had been lost. Table 2.3 details the main modes of operation, whilst a summary of the possible trade-offs between time resolution, data precision and spectral information are outlined in Table 2.4.

Commanding of the instrument's modes was only possible during one of the five or six ground station passes per day. This would have severely restricted the instrument's flexibility and therefore a 'Deferred Command Store' (DCS) with a capacity for 32 separate instructions was included into the electronics module. The DCS was loaded with the required mode changes via the "Programmer" (see Section 2.1.4), from the DCS the instructions were loaded into the instruments Command Register (CR) which then organised the store according to the mode requested. The time at which instructions were loaded into the CR from the DCS, and hence the observation start time, was controlled by the Delayed Start Timer (DST). By using the DST it was possible to commence observations only when the satellite was in areas of low particle background, thereby maximising the data of good quality that were obtained. Short periods of low background were used for higher time-resolution observations whereas the long periods were useful for obtaining spectral information.

A further use of the DCS and DST was for timing the commencement and duration of magnetorquing (see Section 2.1.3) during manoeuvres when the spacecraft was out of ground contact.

2.2.1 Data Handling

Data from all instruments, either from the tape recorders or direct dumps of the instrument store contents, were received at the Rutherford Appleton Laboratory (RAL), Slough. The scientific data was combined with housekeeping information, such as spacecraft temperatures and attitudes and reformatted onto a "Master" tape, which then had the direct store dumps inserted into the correct locations, producing a sequential file of the day's observations. The information relevant to, or requested by an institute was then copied from this onto a "sub-master" tape which was internally divided into arbitrary units called orbits. At the commencement of each orbit a data block was written to the tape containing the relevant housekeeping information, such as the orbital elements and the current spacecraft clock calibration.

The submaster tape produced at RAL consisted of blocks of 720, 6-bit characters on 7-track tape. The information on these tapes was transmitted to Leicester University over a GPO Datel Link between the PDP-8e computer at RAL and Leicester's PDP-11/34. One of the first requirements at Leicester was to dispose of the "orbit" segregation of data and to subdivide it into a more natural unit of "observations", where an "observation" corresponded to one filling of the instrument store. Also it was essential to remove the time delays introduced into the data stream by its buffering in the instrument memory. This delay between the time at which the data was acquired and the time it was copied to the tape recorders was in the range

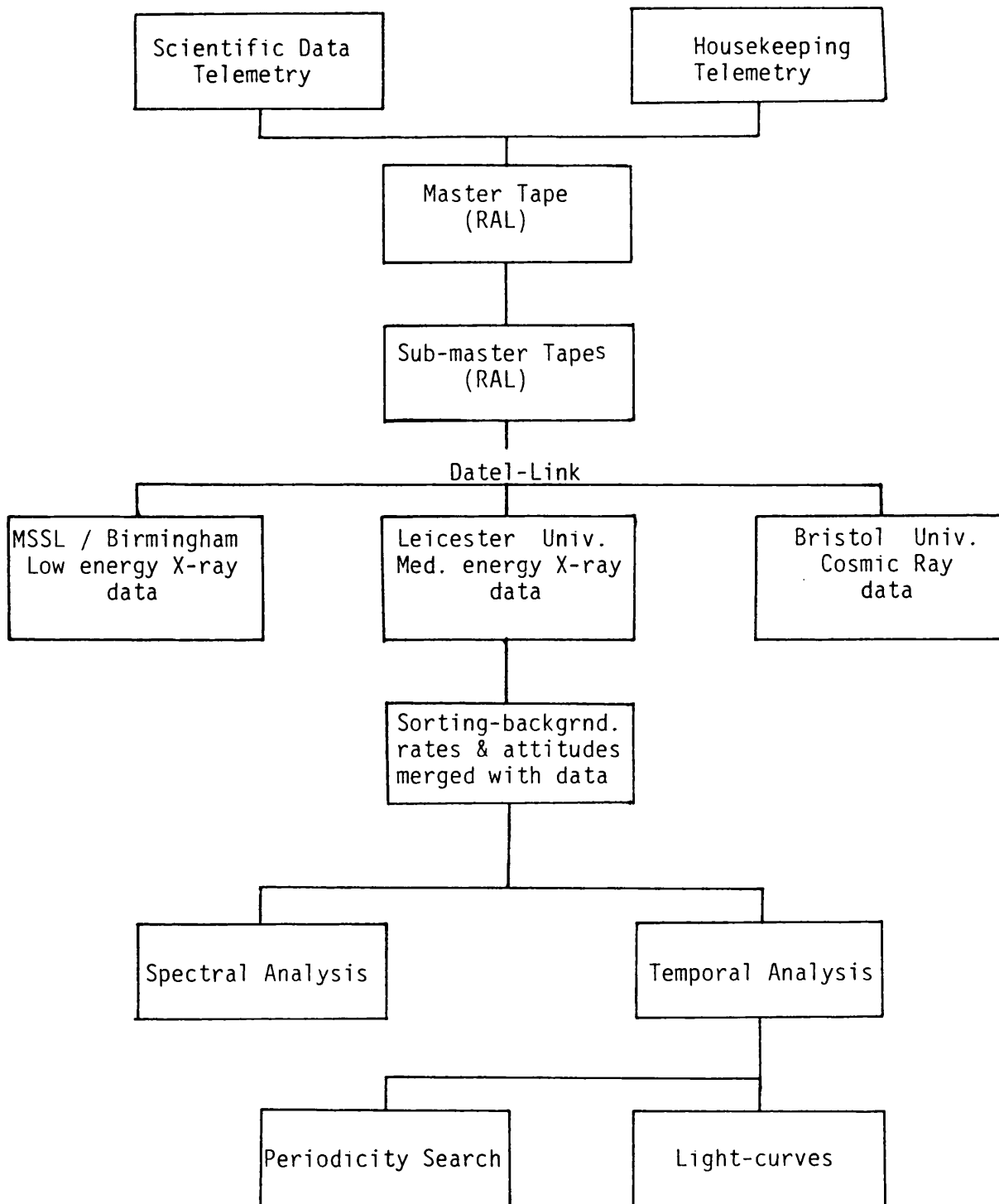


Fig 2.5 An overall view of the Ariel-6 data handling and analysis system.

128 - 4096 s, typically being towards the lower limit of this range.

Repeated transmissions of the same data had to be compared to find which had been transmitted from the satellite with the lowest telemetry error rate. Further, it was necessary to associate the background monitor count rates, the clock calibration and correct attitude solution to the appropriate data records.

The sorting program required to convert the raw data into a usable, direct access file format was written by Dr Clive Page and all subsequent scientific analysis was based on the use of this sorted data file. A diagrammatic representation of the Ariel-6 data analysis system is shown in Fig 2.5.

2.2.2 Temporal Analysis

Generally the search for periodicities in the data followed one of two possible paths. Observations of the known X-ray pulsators were searched over a limited dynamic range of periods using the maximum- χ^2 technique, whilst periodicity searches in other sources were made using Fourier power spectral analysis.

In the maximum χ^2 technique the data were folded over a range of trial periods and the resulting "binned" data set compared to the mean of the data by means of the χ^2 test. The hypothesis was made that when folding the data at the "true" period the χ^2 would be a maximum and at all other trial periods any periodic structure would be smeared out.

Periods derived by either technique were refined by folding a number of independent data sets at the estimated period and

then matching the phases of the sets to a mean template. Between each data set there was a whole number of cycles, which meant that the period could be refined and if a large number of data sets were available a value for the period derivative also determined.

2.2.3 Spectral Analysis

The observed X-ray spectrum was the sum of both source and background spectra convolved with the detector characteristics. A direct deconvolution of the source spectrum was complicated by the less than perfect response of the detectors. Firstly there was possibly some irreducible background, which may have been time dependent, secondly the incoming X-rays had poorly determined energies and finally there existed the possibility that some of the energy of the incoming X-ray might be lost. This latter factor was of great importance for X-rays with energies greater than ~ 35 keV where the absorption of the X-ray may be followed by the emission of a K-shell photon from the Xenon. Approximately 60% of K-shell photons were lost from the detectors.

The spectral analysis system employed used model input spectra which were folded through the detector characteristics to generate a "predicted" spectrum which was then compared to the observed (background subtracted) data by means of the χ^2 test. A satisfactory model was denoted by a reduced $\chi^2 \sim 1$. Spectral fitting was a multi-stage process, the components being contained in six separate programs, these are diagrammatically illustrated in Fig 2.6.

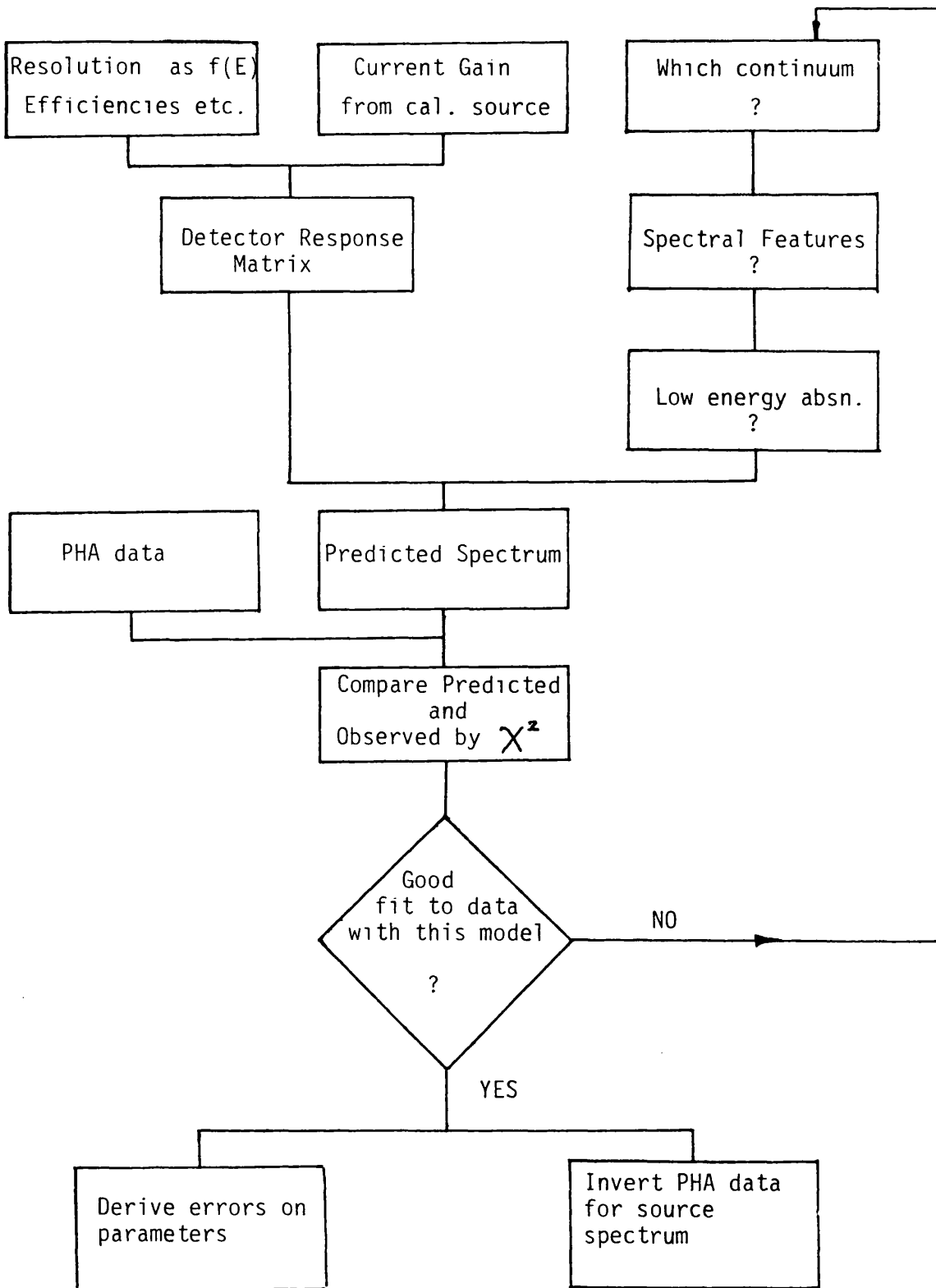


Fig 2.6 The spectral analysis procedure used on Ariel-6 PHA data.

The information required to describe the detector characteristics consisted of the gas gains, resolution as a function of energy, effective areas and the losses due to fluorescence effects. This data, obtained from both ground and inflight calibration, was combined into a "detector matrix". Essentially this was the response of the detectors to an input at a given energy compiled for a range of input energies. Generally the "detector matrix" consisted of the response at ~ 130 and ~ 170 input energies spaced at ~ 0.1 FWHM(E) steps in the low and high energy systems respectively.

The required spectral model was generated and folded through the appropriate "detector matrix" producing a "predicted" spectrum. Several models were available and could be thought of as consisting of two components; the "continuum" and spectral "features" such as lines and absorption edges. The following models were available.

a) Power Law

$$\frac{dN}{dE} = A \cdot E^{-\alpha} \text{ photons}/(\text{keV cm}^2\text{s})$$

where A is a normalisation factor

α is the photon number index

E is the input energy

Fitted parameters were A and α .

Some spectra show evidence for a cut-off at high energies, this was modelled by a modified power law spectrum of the form:

$$\frac{dN}{dE} = A \cdot f \cdot E^{-\alpha} \text{ photons}/(\text{keV cm}^2\text{s})$$

where $f = 1$ for $E < P$ keV

$$f = \exp\left(\frac{E - P}{R}\right) \text{ for } E > P \text{ keV}$$

P and R represent the cut-off position (in keV) and cut-off rate (keV) respectively. P and R were for modelling purposes only and bear little relation (if any) to the physical process(s) generating the cut-off.

Fitted parameters were A, α , P and R.

b) Thermal Bremsstrahlung (Optically thin plasma)

$$\frac{dN}{dE} \approx A \cdot g \cdot \exp\left(\frac{E}{kT}\right) \cdot E^{-1} \quad \text{photons}/(\text{keV cm}^2\text{s})$$

where A is a constant

g is the Gaunt factor

k is the Boltzman constant

T is the temperature (keV)

The energy dependence of the Gaunt factor was approximated by:

$$g \approx \left(\frac{1}{kT}\right) \cdot E^{-0.4} \quad \text{Holt (1980)}$$

The model used was therefore:

$$\frac{dN}{dE} \approx B \cdot \exp\left(\frac{E}{kT}\right) \cdot E^{-1.4} \quad \text{photons}/(\text{keV cm}^2\text{s})$$

where B is a new constant.

Fitted parameters were B and T.

c) Black Body Spectrum (Optically thick plasma)

$$\frac{dN}{dE} \approx A \cdot \frac{E^2}{\left(\exp\left(\frac{E}{kT}\right) - 1\right)} \quad \text{photons}/(\text{keV cm}^2\text{s})$$

where the variables are as defined above.

Fitted parameters were A and T.

In addition the observed continuum was usually deformed by the presence of a low energy absorbing column of cool material. This was modelled by an additional factor.

$$\text{Attenuation (E)} = \exp(-\sigma(E) \cdot N_H)$$

where $\sigma(E)$ is the energy dependent cross section of a gas consisting of elements at solar abundances (Brown and Gould 1976, Fireman 1978).

N_H is the Hydrogen column density.

Fitted parameter was N_H in units of 10^{22} cm^{-2} .

Spectral Features

a) Lines were modelled by a simple gaussian (centred at the line energy) whose integrated area corresponded to the equivalent width of the feature. The fitted variables were the line energy and equivalent width, both in keV.

b) Absorption Edges

The only absorption features available, independent of the low energy "continuum" absorption were those of Iron at energies > 7.1 keV.

$$\text{Cold Fe (E} > 7.11 \text{ keV)} \quad \sigma(E) = A \cdot E^{-2.73}$$

$$\text{He-like Fe (E} > 8.8 \text{ keV)} \quad \sigma(E) = B \cdot E^{-2.67}$$

$$\text{H-like Fe (E} > 9.3 \text{ keV)} \quad \sigma(E) = C \cdot E^{-2.67}$$

where A, B and C were different constants. The approximations to the energy dependent cross-sections (i.e. $E^{-2.67}$) were from Tucker (1978). The attenuation was given by:

$$\text{Attenuation (E)} = \exp(-\sigma(E) \cdot N_{Fe})$$

where N_{Fe} is the iron column density. The fitted parameter was N_{Fe} in units of $10^{17.6} \text{ cm}^{-2}$, (the iron

column associated with a Hydrogen column of 10^{22} cm^2 , assuming solar abundances).

The "predicted" spectra were generated for a range of either one or two parameters. Comparison of the predictions to the observed spectrum was then made by means of the χ^2 test, the minimum χ^2 in the " χ^2 -grid" enabling improved model parameters to be determined. When several parameters were required to obtain a satisfactory fit they were varied in pairs until a χ^2 was obtained that could not be further decreased by the variation of any other parameter.

Associated uncertainties on the "best fitting" parameters were determined using the prescription of Lampton, Margon and Bowyer (1976). Within the range of the parameters in a χ^2 -grid, the region that defines the degree of confidence in a one parameter grid is given by:

$$68\% \text{ confidence } (\sim 1\sigma) \quad \rightarrow \quad \chi^2 \text{ (minimum)} + 1$$

$$90\% \text{ confidence } (\sim 2\sigma) \quad \rightarrow \quad \chi^2 \text{ (minimum)} + 2.3$$

and for a two parameter grid:

$$68\% (1\sigma) \quad \rightarrow \quad \chi^2 + 2.3$$

$$90\% (2\sigma) \quad \rightarrow \quad \chi^2 + 4.6$$

In this work χ^2_{ν} denotes the reduction of the χ^2 by the number of degrees of freedom during the fit.

Throughout this work the quoted errors on spectral parameters are all 68% confidence ($\sim 1\sigma$), unless otherwise stated.

The inversion of an observed spectrum to obtain the "source" spectrum was not possible, for the reasons given above. However, for the best-fitting model spectrum, where the χ^2 was sufficiently small that the model could be taken as being a good representation of the data, it became possible to produce an "inverted" or "source" spectrum by a re-distribution of the observed count rates about the model spectrum, in an identical manner to that in which they were distributed about the prediction. Essentially this was the calculation of PHA channel dependent efficiency factors on the basis of the best fitting model. The validity of this technique was therefore totally dependent upon the quality of the spectral fit. All "source" spectra in this work have been obtained in this manner.

Chapter 3

In-flight Performance and Calibration

57

Faults that became evident in the Ariel-6 satellite following launch led, to some extent, to the project being "written off" by the scientific community. It is the primary aim of this chapter to place into context these faults, attempt to explain their causes and to indicate the steps which were taken to ensure that X-ray observations of a high quality were still made.

A detailed study of, or search for, spectral variability is obviously limited by the knowledge one has of the in flight detector characteristics. The latter part of this chapter discusses the inflight calibration of the instrument with both the onboard sources and observations of the Crab nebula.

The determination of the detector background spectrum is also discussed.

3.1 In Flight Performance

It was immediately apparent following launch that several acute problems existed with the Ariel-6 satellite. All of the scientific instruments were seriously affected by a series of defects in the spacecraft's design and manufacture. An outline of the major defects is given below.

3.1.1 Spurious Command Reception

The spacecraft continually received spurious commands, typically several times a day, especially when passing over areas with powerful radio and radar transmitters such as North America, Europe and the Near East. These commands affected many of the systems on the spacecraft, most seriously when they resulted in:-

- i) switching off the HT supplies to the medium energy detectors;
- ii) commanding tape recorder replays (thus erasing any collected data and increasing tape wear);
- iii) randomly switching from main to reserve spacecraft clock (which ran $\sim 0.3\%$ slower), thereby losing synchronisation on the read out of the instruments' store to tape and adding a large uncertainty in the timing of events observed before the clocks could be switched by ground command;
- iv) the switching of magnetoquer modes so that the spacecraft was manoeuvred to the wrong position with the consequent delay of subsequent observations.

The specific cause of the problem was not established because attempts to simulate these effects on the flight spare modules were not successful, but it is thought that the following features of the satellite design were responsible.

- i) The antennae pattern was greatly affected by the projection of the four solar panels. In fact the transmitted signal was so deeply modulated at four times the satellite spin rate that the ground stations, used to switch the instruments HT's back on, were unable to use their auto-track systems for Ariel-6 and were forced instead to point their antennae to the predicted path of the satellite. It seems probable that the satellite was sensitive to command signals similarly modulated.
- ii) One of the command receivers was almost certainly oversensitive as the radio noise alone over Europe was

sufficiently high enough to switch the receiver into its command acceptance mode.

- iii) Whenever the telemetry link command wave was received by the satellite, above a certain intensity, a reset pulse was sent to the command decoder circuits in the Programmer. When the carrier level subsequently fell below this level a different pulse was sent out to clear any of the "command enable" latches which might have been set. It was feasible therefore that the accidental reception of radio signals just above this threshold resulted in the transmission of reset and clear pulses at a high frequency which had unintended side-effects.

Since it was impossible to switch off the command receivers the only means of alleviating the problem was to request that all ground stations that had contact with the satellite leave their carrier wave on for the whole time that the spacecraft was above their horizon. To facilitate this action as many NASA ground stations as possible and the Italian ground station at San Marco were used. As well as providing screening from spurious commands the ground stations were used to reset the instrument into a useful observing mode and to obtain tape recorder replays as often as possible.

3.1.2 High Spacecraft Temperatures

Due to precession of the highly inclined orbit of Ariel-6 the satellite moved into continuous sunlight for periods of ~ 5 - 10 days about four times a year. During each of these "all-sun" periods the internal temperatures increased rapidly

causing several modules to become hotter than their designed limits. These higher temperatures degraded the performance and the lifetime of both the battery and the tape recorders. The cause of the large temperature rise was not certain since the spacecraft thermal model could not explain the observed results even when all the known uncertainties were pushed to their limits.

The principal action taken to avoid damage was to manoeuvre to a position offset from the anti-sun by 60° - 65° . This cooled the battery and tape recorders but warmed up the cosmic ray detector and consequently increased its contamination by outgassing. Whilst these large manoeuvres considerably disrupted the observing program they increased the area of sky and hence the number of X-ray sources, that the instruments could view.

3.1.3 Battery Failures

Shortly after eclipses recommenced at the end of each "all-sun" period the battery voltage dropped below its safety threshold and all non-vital load was shed. This switched off not only all of the instruments but also the tape recorders, which then proceeded to erase all stored data when restarted. It was thought at first that a cell had suffered a large drop in capacity from the repeated over-heating, since the observed behaviour could be induced in the flight spare battery at temperatures not much greater than those on the spacecraft. Further investigation, however, suggested that the battery charging circuitry was faulty.

A computer model of the Ariel-6 battery characteristics, including the charge/discharge history with faulty circuitry was capable of predicting the observed cut-outs; even assuming the battery to be in perfect condition. Also, the charge characteristics of the Ariel-6 battery had not been measured before launch so that the actual charge level of the battery when "fully" charged was unknown. This may well have been a contributing factor to the problems. The main effects of the battery problem were that only one of the three instruments could be supported at a time and that the manoeuvre rate was decreased.

3.1.4 Tape Recorders

One of the two recorders failed intermittently on playback and was out of use for over half of the satellite lifetime. The other recorder alone had insufficient capacity when dumped only at the Winkfield ground station and therefore other ground stations were used, but with a corresponding increase in tape wear. The error rate actually increased noticeably over the project duration and some sections of tape obviously had a severe loss of oxide.

3.1.5 Coning Angle

The coning angle achieved was $\sim 1.1^\circ$ which was greater than anticipated and actually outside the spacecraft specification. This had the consequence of reducing the effective area of the medium energy detectors by $\sim 25\%$ (see Fig 3.1) and of modulating the signal from the source, when not situated at the centre of the instruments field of view.

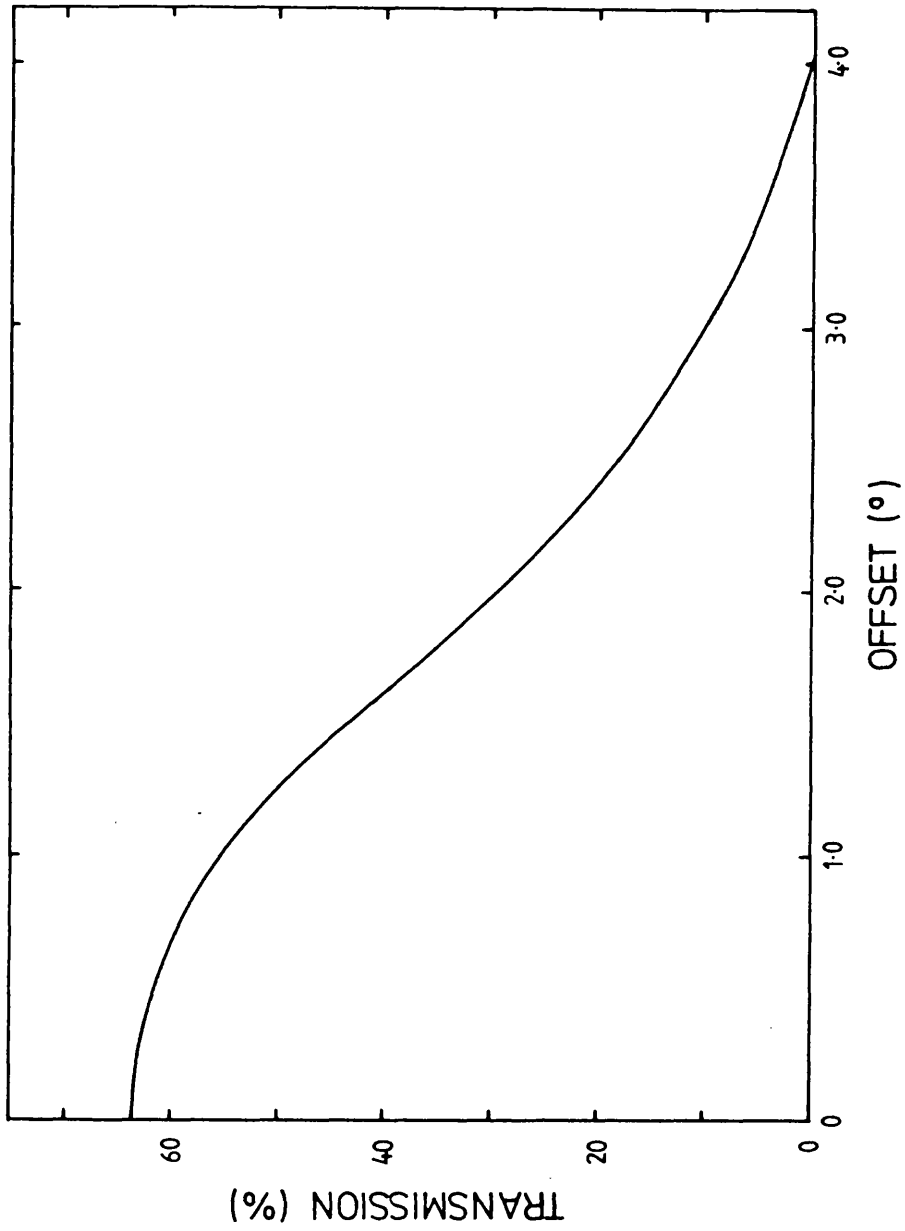


Fig 3.1 The collimator transmission as a function of offset angle from the satellites spin axis.

For strong sources, however the spin-modulation was useful in enabling an independent estimate of the attitude to be made.

3.1.6 Timing

A fault in the RAL data processing software that produced master tapes arose from the expectation that the spacecraft clock would be subject only to very slow drifts; it therefore carried out integrations over a day or more, in an effort to obtain a more precise clock rate. With the random switching between the two clocks this long integration had the effect of making the conversion rate from spacecraft clock time to UT in error for up to a day at a time. Several hundred clock transitions occurred during the duration of the project which introduced errors of up to a minute in the specified timing of events.

3.1.7 Attitudes

Before launch it was anticipated that the spacecraft attitude would be determined to $\sim 0.2^\circ$. Many problems were created by the results from the two groups of sensors disagreeing by $1^\circ - 2^\circ$ systematically in the same direction. Similarly the quoted attitudes from RAL suggested variations around the orbit as large as 4° . Faults in the RAL software were able to account for some of these discrepancies; for example the large coning angle ($\sim 1.1^\circ$) was not correctly allowed for until several months after launch, also large attitude 'glitches' were evident when the software changed from one algorithm to another.

The effect of the poor attitude solution was that the instruments were frequently pointed in the wrong direction and when attitude "trims" were made they were just as liable to move the instrument "off" source as "on". To overcome this difficulty the spacecraft was sometimes steered so as to maximise the count rate in the primary X-ray instrument. This solution had inherent difficulties, particularly in crowded regions of sky such as the galactic plane.

In the following chapters the fluxes quoted were derived using source offsets determined by a technique that utilised the modulation (at the satellite spin period) introduced into the data by the large coning angle of the spacecraft, for sources that were not exactly centred in the instrument's field of view. The spin modulation technique involved folding the X-ray data at the satellite spin period and comparing this to models generated by using the known collimator profiles and different assumed source offsets. This technique was only useful for bright sources where a good signal to noise was obtained. For sources near the centre of the instruments' field of view the derived attitudes were accurate to $\pm 0.1^\circ$ whilst for sources at the edge, where the collimator transmission was not as well known, the uncertainty could be $\sim 0.5^\circ$.

3.2 Instrument Calibration

3.2.1 Calibration Source

Each of the four medium energy detectors had a calibration source mounted in a turret on the detector body (see Section 2.1.8). Rotation of the turret enabled the source to radiate into the active volume of the detector. The radioisotopes in the source produced characteristic line radiation at ~ 5.9 and ~ 22.4 keV, there being a total of $\sim 30\,000$ counts per second in each feature. The instrument electronics were arranged so that the calibration source cycled in and out of the detector, thereby enabling associated background measurements to be made.

After background subtraction the position of the line was determined and a comparison made with the laboratory data obtained prior to launch, it was then possible to accurately determine the current gain of the detectors. The measured gains for a typical calibration are shown in Fig 3.2, here expressed as the energy of the top boundary in both the low- and high-energy PHA's as a function of orbital phase. This data was acquired over ~ 10 orbits.

A modulation was readily apparent in the data, the depth of which varied with the duration of the satellite eclipse. Similarly the phase of the peak corresponded to the satellite entry into occultation. There was, however, no correlation between the gain and the detector body temperatures. During some of the "all-sun" periods (Section 3.1.2) no modulation was discernable, whilst in others it was clearly present.

The cause of the modulation was not known and therefore frequent calibrations were performed during observations. For

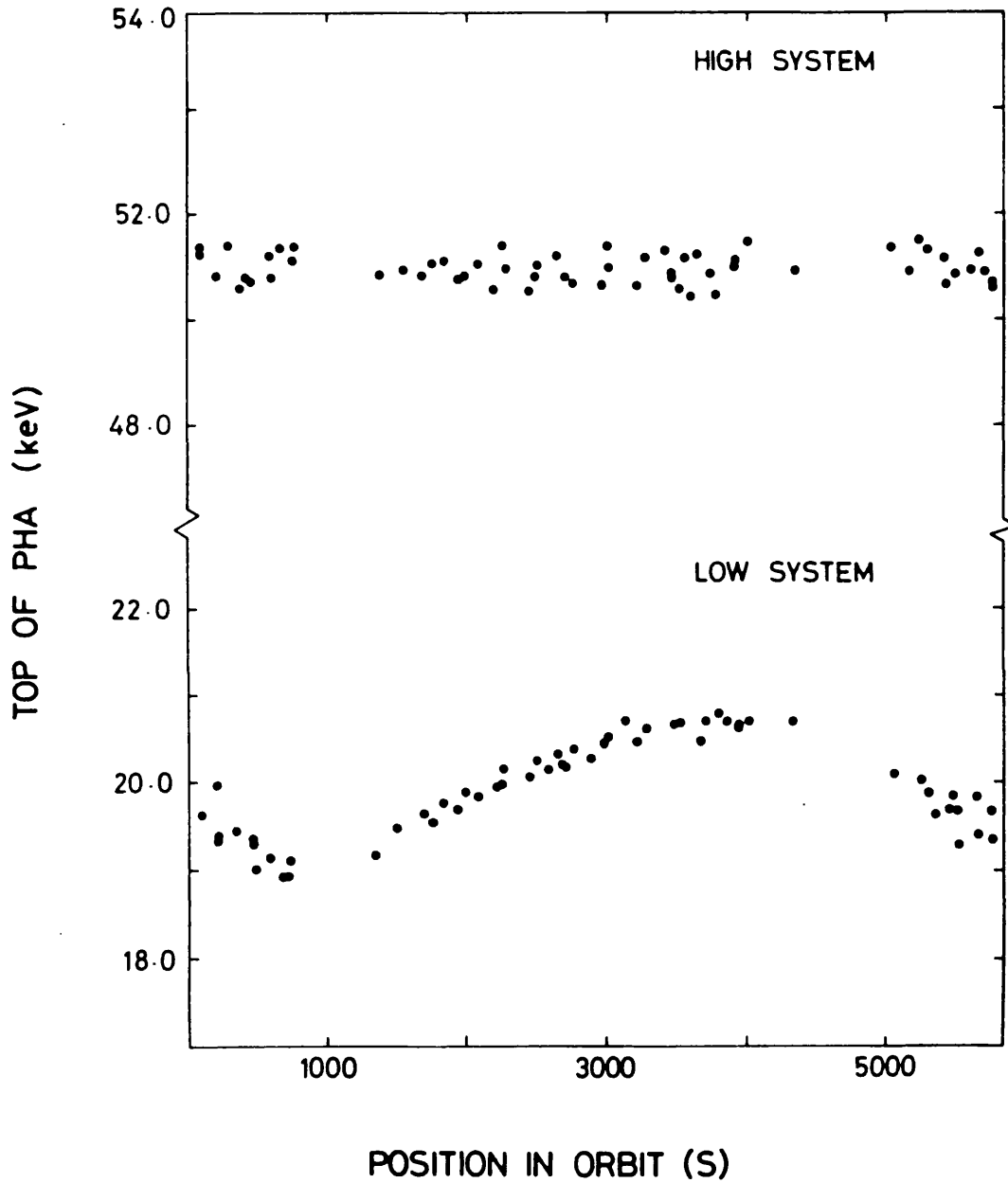


Fig 3.2 The energy of the top boundary of the PHA for low- and high-energy systems as a function of orbital phase.

all spectra presented in this work the gains were determined by concurrent calibration.

3.2.2 Detector Background Spectrum

An accurate determination of the detector background was essential, particularly for the study of weak sources such as the active galaxies.

The observed detector background spectrum consisted of contributions from the diffuse X-ray background, cosmic rays and the interaction of particles trapped in the Earth's magnetic field with the detectors (the latter two being classed for convenience as the particle background).

In order to study the detector background all of the available data acquired in the instruments E4 mode (see Table 2.3) up to day ~ 750 of the satellite life were used. For each pointing position the detector field of view was overlaid onto an Aitoff plot of the sky containing all reported (pre-Einstein) X-ray sources. The theoretical 0.5% collimator transmission contour was taken as being the edge of the instruments field of view; this corresponded to $\sim 4^\circ$ FWHM. Those fields containing any known sources (other than Extreme Ultra Violet) were excluded from further analysis. The remaining data were subdivided into two groups according to their galactic latitude, the discriminator being $b_{II} = 10^\circ$, those fields with $b_{II} \gtrsim 10^\circ$ are shown in Fig 3.3.

One effect that had been anticipated before launch and was clearly observed, was the large variation in background count rate, as monitored by the guard counters, around the orbit. The measured guard count rates are shown in Fig 3.4

SELECTED BACKGROUND REGIONS

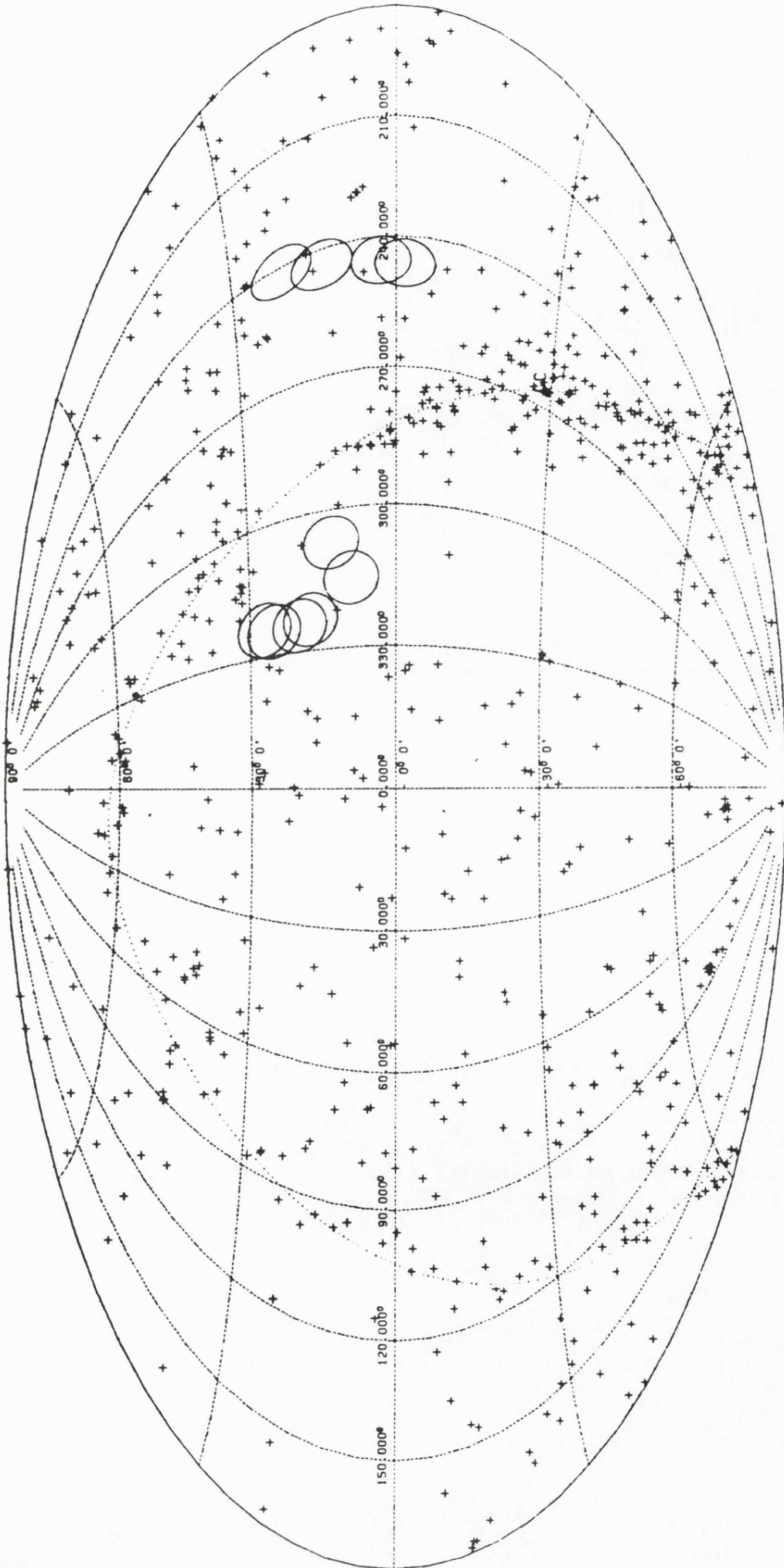


Fig 3.3 An Aitoff projection of the sky showing all known (pre-Einstein) X-ray sources. The fields selected for background analysis are also shown.

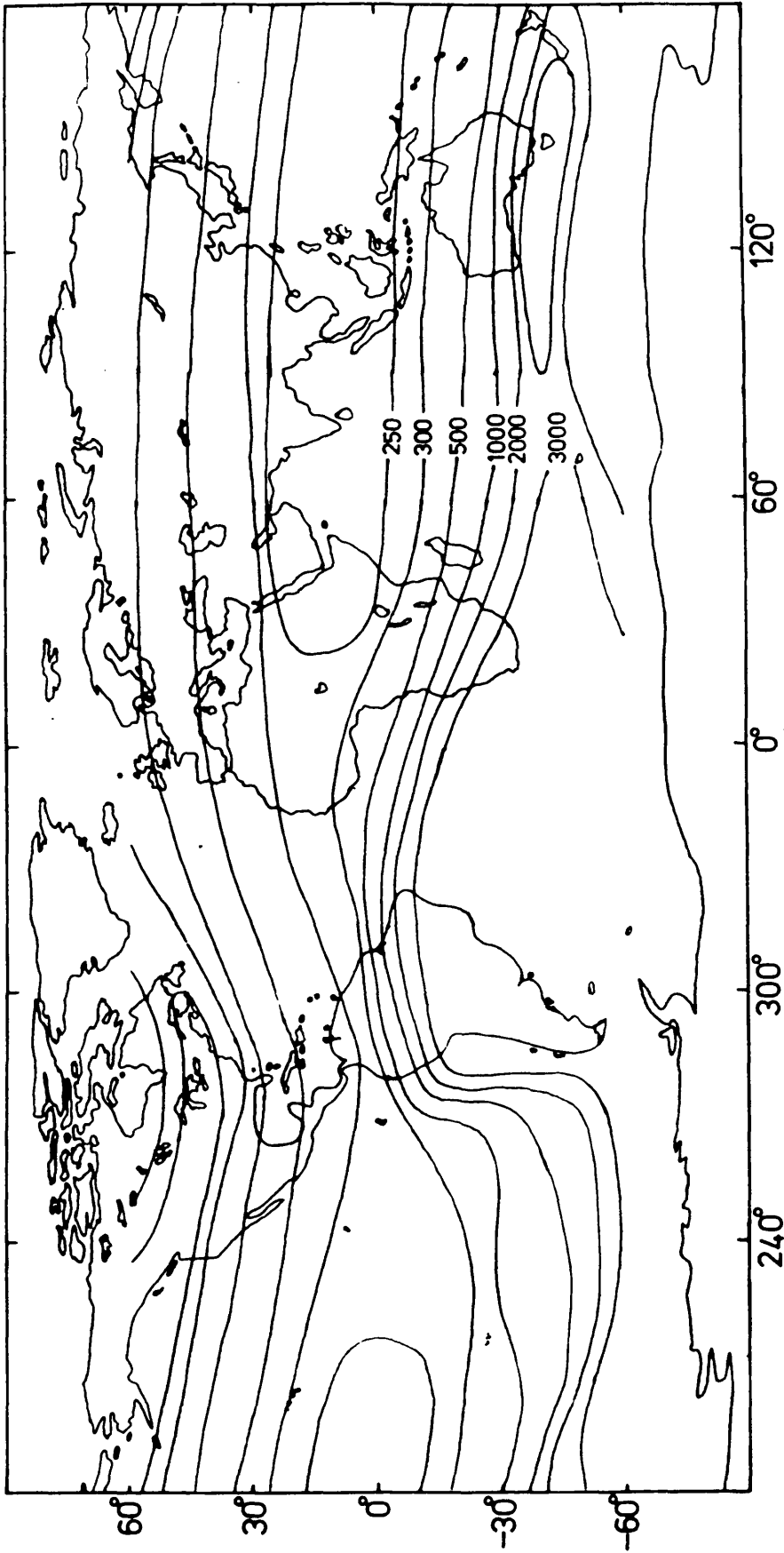


Fig 3.4 The longitude and latitude dependence of the detector guard count rates.

overlayed onto a map of the Earth. The large extent of the South Atlantic Anomaly is clearly seen as are the effects of the decreased magnetic shielding of the Earth at higher latitudes.

The large variation in guard count made it essential to define the correlation, if one existed, between the "accepted" or "qualified event" count rate in the detectors and the guard count rate. Fig 3.5 shows a series of plots of qualified event rate versus guard counter rate for six of the 32 PHA channels available. The numbering system used was PHA channel 1 - 16 for the low energy system and 17 - 32 for the high energy system.

The qualified events in the high energy system appear to be relatively stable as a function of guard count with only a slight gradient being discernable. In the low energy system however there is a significant gradient and an increase in the scatter of the qualified event rate when the guard counter rates are in excess of $\sim 300 \text{ s}^{-1}$.

It was necessary to define a limit at which the qualified event rate was not dependent upon the guard rate and therefore variations in the source count rate or spectra would become questionable. To accomplish this the data were sub-divided into six bandwidths, corresponding to the guard count rates $270 - 280 \text{ s}^{-1}$, $280 - 290 \text{ s}^{-1}$ etc., throughout the $270 - 330 \text{ s}^{-1}$ range. The mean qualified event rate and the reduced χ^2 statistic were determined for each bandwidth. For qualified event rates $> 290 \text{ s}^{-1}$ the mean detector count rate was no longer representative of the sample at the 99% confidence level and therefore this was defined as the upper limit to

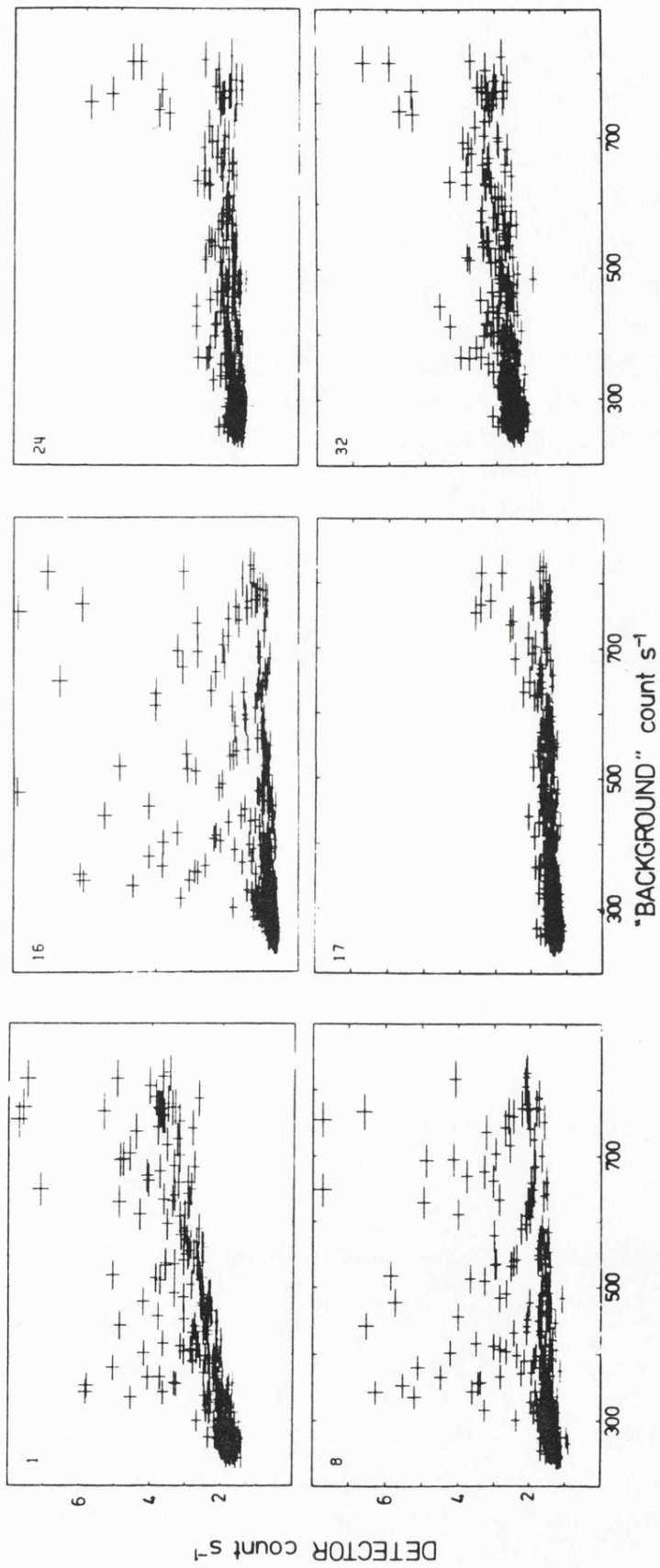


Fig 3.5 The qualified event rate as a function of guard count rate.

useful data. All of the available data with guard rates $< 290 \text{ s}^{-1}$ ($= 2 \times 10^4 \text{ s}$) were summed to provide the detector background spectrum, Fig 3.6a.

With identical selection criteria a limited amount ($\sim 3 \times 10^3 \text{ s}$) of data was available with $b_{II} \lesssim 10^0$. There was no discernable difference between the two summed spectra.

As stated above the detector background spectrum consisted of two components, the X-ray and the "Particle" background (XRB and PB respectively). If it was possible to accurately determine the PB then a direct method of obtaining the XRB spectrum became plausible. The XRB has generally been represented as a two component power-law spectrum with indices of ~ 1.4 and ~ 2.4 , the break occurring at $\sim 20 \text{ keV}$, Zambech (1980). One of the main disadvantages of earlier work had been the limited dynamic range of the instrumentation. The HEAO 1-A2 detectors did not suffer from this handicap however and their results suggested that the XRB was more accurately represented by a single thermal bremsstrahlung spectrum at a temperature of $\sim 40 \text{ keV}$ over the dynamic range of $4 - 60 \text{ keV}$ (Marshall et al. 1981).

During periods of source occultation our detected spectrum consisted of two components; (i) atmospheric fluorescence, and (ii) the particle background spectrum. Since the XRB spectrum is time invariant and we had established that the particle background spectrum remained constant providing that the guard rate $< 290 \text{ s}^{-1}$, there was the possibility that if the soft fluorescence component could be removed a direct subtraction of detector and PB spectra would yield the XRB spectrum.

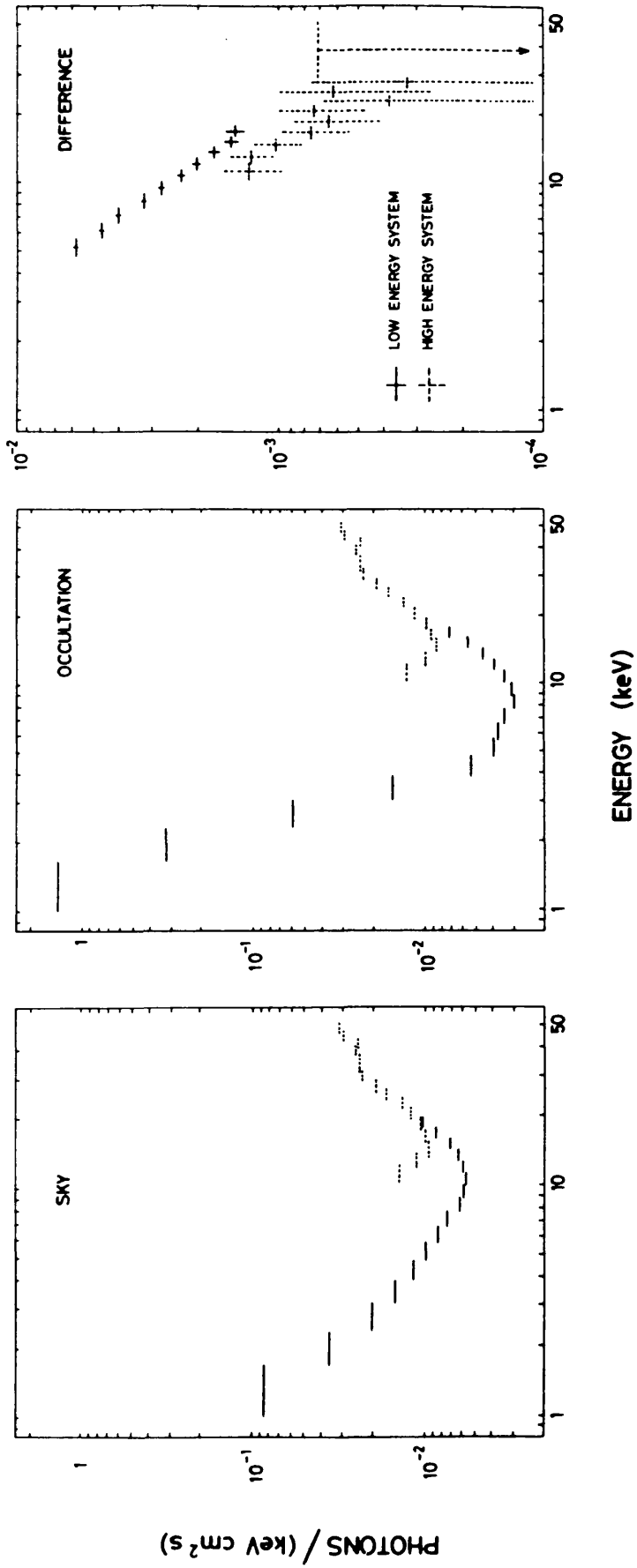


Fig 3.6 Spectra for: a) The detector background
 b) During occultation
 c) a - b for $E > 4.5$ keV

All spectra were inverted using E^{-1} for convenience.

Fig 3.6b shows the summation of $\sim 10^4$ s of occultation data with guard rates $< 290 \text{ s}^{-1}$.

A soft component can be clearly seen. By neglecting those PHA channels which were below $\sim 4.5 \text{ keV}$ the fluorescence was effectively removed leaving the PB spectrum. The difference spectrum, produced by the subtraction of the detector and PB spectra, is shown in Fig 3.6c. This should correspond to the XRB spectrum, but it was immediately obvious that there existed a large discontinuity between the low- and high-energy systems.

The atmospheric fluorescence spectrum was very steep, having a photon number index, $\alpha \sim 5.2$, for a simple power-law model (see Section 2.2.3) with a normalisation of $\sim 400 - 500$ at 1 keV . By using the data of Grader, Hill and Seward (1968), on X-ray airglow, we find that the predicted count rate at $\sim 0.5 \text{ keV}$ was $\sim 10^5 \text{ s}^{-1}$. Since the low energy PHA has a lower limit of $\sim 0.9 \text{ keV}$ this was not evident in Fig 3.6b. The lowest energy accepted by the SCA, which encompassed the PHA, was $\sim 0.1 \text{ keV}$, therefore any detected events were actually being processed by the detector electronics though not registering in the PHA. The window transmission at $\sim 0.25 \text{ keV}$ was $\sim 1\%$ suggesting an influx of several thousand events per second.

A possible interpretation of the 'glitch' in the difference spectrum was that the low energy events, which did not register in the guard count rates, increased the probability of the (in this case) desired particle events being vetoed by anti-coincidence. A second possibility was that the low energy photons created an almost d.c. like signal in the electronics, thereby increasing the output voltage from a valid particle event. This would have had the effect of increasing the low

energy count rate during occultation as it was a falling spectrum and decreasing the higher energy count rate as it was a rising spectrum, resulting in the difference spectrum for the low energy system being harder and having a higher normalisation than desired. The high energy system was unaffected by the low energy events as the signals were processed independently.

It would be naive to expect that either effect was acting in isolation and the observed discontinuity is most probably due to the presence of both processes.

3.2.3 The Crab Nebula

Two observations of the Crab nebula were made by Ariel-6 for periods of ~ 8 and ~ 6 days during 1980 and 1981 respectively. The spectrum obtained from a brief, $\sim 10^3$ s exposure during 1980 is shown in Fig 3.7, following inversion using the best fitting power law model. The best fitting model parameters and those reported by other observers are given in Table 3.1. Spectral parameters determined by Ariel-6 are in very good agreement with the values previously reported. There was no discernable change in the Ariel-6 spectrum between the two observations, showing the long term stability of the medium energy detectors.

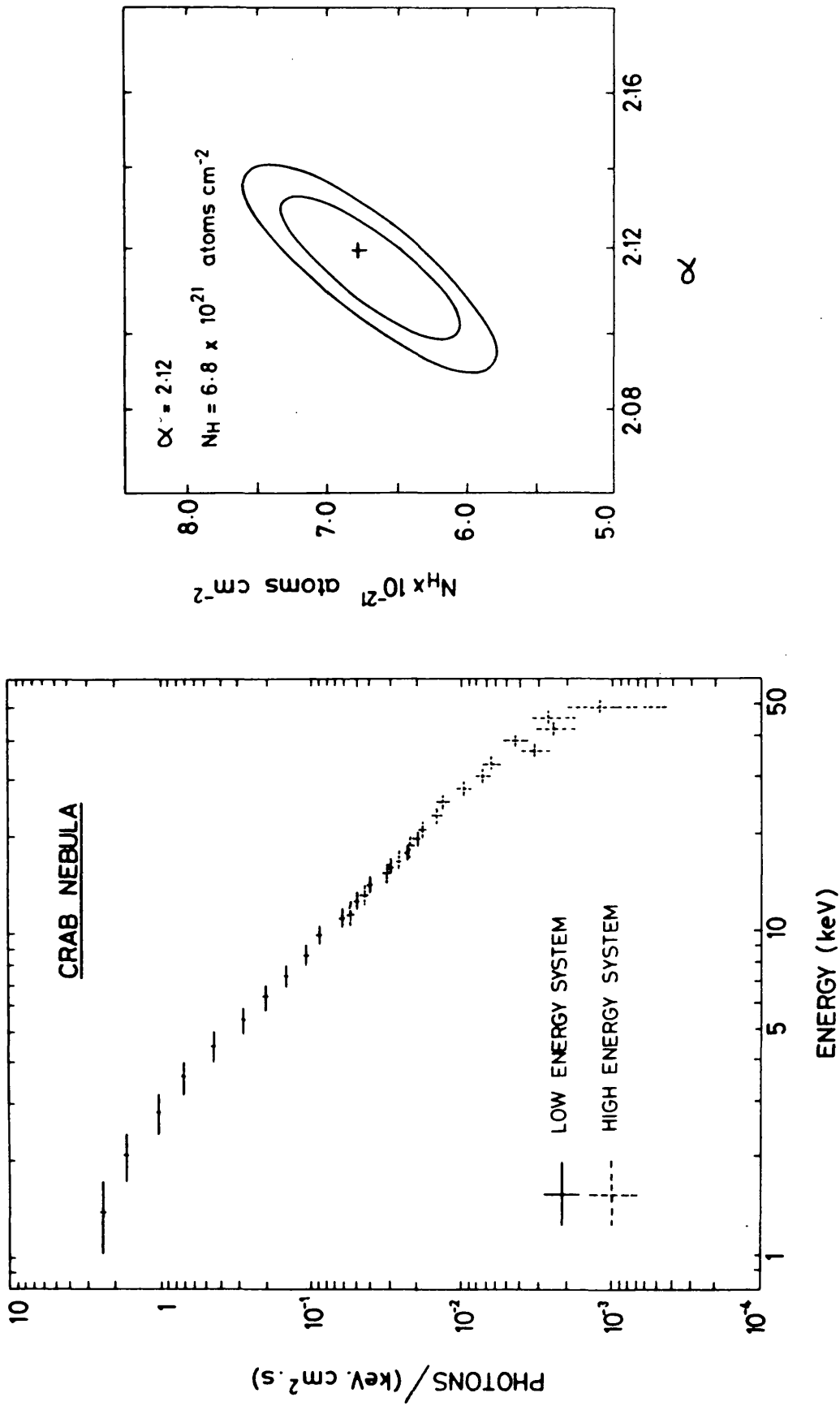


Fig 3.7 Ariel-6 spectrum of the Crab nebula.

TABLE 3.1 Spectral Parameters of the Crab nebula

		Normalisation (photons $\text{cm}^{-2} \text{s}^{-1} \text{keV}^{-1}$)	$N_{\text{H}} \times 10^{-21} \text{cm}^{-2}$
Ariel-6 (This work)	2.12 ± 0.02 2.12 ± 0.03	9	6.8 ± 0.8 6.8 ± 1.0
OSO-8 (Pravdo and Serlemitsos 1981)	2.10 ± 0.01	6.87 ± 0.15	2 (Fixed)
OSO-7 (Clark et al. 1973)	2.11 ± 0.05	9.8	5
Rocket (Toor and Seward 1974)	2.1 ± 0.03	9.7	-

90% Confidence error estimates

Chapter 4

Ariel-6 Observations of

Galactic Sources

4.1 Introduction to the X-ray Pulsators

The first of the X-ray pulsators, Cen X-3, was discovered during 1971 (Giacconi et al. 1971). Since their discovery the class has swelled to ~ 21 members, which exhibit a range of pulse periods from ~ 0.06 to $\sim 10^3$ s. The observed pulse profiles from the different sources range from those that are approximately sinusoidal to those which are highly peaked and cannot be explained by an isotropic emission region. To account for the observed beaming the most likely and widely accepted candidate is the accretion of material onto the magnetic pole of a highly magnetised $B \sim 10^{12} - 10^{13}$ G neutron star. Pulses are then seen to occur naturally through some misalignment between the magnetic and rotational axis (i.e. Lamb, Pethick and Pines 1973, Basko and Sunyaev 1975).

From the relationship between the rate of change of the pulse period and the X-ray luminosity it is most likely that the majority of pulsators are in disc fed systems (Ghosh and Lamb 1979, Savonijie 1980); though the region in which there is interaction between the neutron stars' magnetic field and the disc, the transition zone, is not yet fully understood. In particular the process by which the accreting material departs from the Keplerian dynamics of the disc and threads itself onto the magnetic field lines is unknown (see for example Ghosh and Lamb 1979, Anzer and Bauer 1982).

Once into the region of magnetospheric flow the material accretes onto the magnetic pole, the free fall temperatures generated being of the order $\sim 2 \times 10^4$ keV (Holt and McCray 1982).

Conversion of the gravitational potential energy into X-rays is yet another area in which further theoretical work

is required. The review of Joss and Rappaport (1982) sites the deceleration of the material and thermalization of the infall energy in one, or more, of the following ways.

- i) Deceleration of the particles and ions by radiative pressure within the optically thick medium of the accretion column, which rises above the pole of the neutron star (see Basko and Sunyaev 1976). The infalling electrons are decelerated by photon interactions, such as inverse compton scattering and they in turn decelerate the incoming ions.
- ii) Free falling material undergoes deceleration during nuclear or coulomb collisions beneath the surface of the neutron star. The problems associated with this hypothesis are that the particles can only penetrate a very short distance into the neutron star surface before it is impossible for the emitted radiation to escape transversely. Alternatively, if the radiation escapes back up through the column then the resulting radiation pressure is sufficient to prevent further accretion, even for very low X-ray luminosities (Lamb, Pethick and Pines 1973, Meszaros 1982).
- iii) A shock above the surface of the neutron star decelerates the infalling material. Following the loss of the majority of its kinetic energy in the stationary shock matter settles slowly onto the neutron star pole, cooling as it does so

(Basko and Sunyaev 1976, Langer and Rappaport 1982).

Assuming that the X-ray emission has been generated in one, or more, of the above ways, it has still to escape from the optically thick accretion column, producing as it does the observed pulse profiles and spectra. Much theoretical effort has been directed towards an understanding of the radiative transfer in the accretion column (e.g. Pravdo and Bussard 1981, Meszaros 1982, Langer and Rappaport 1982 and Wang and Welter 1981). As yet, however, the models are not sufficiently accurate to enable viable comparisons to be made to the observational data. In the majority of cases even the X-ray beaming mechanism is not clear, there being confusion between pencil- and fan-beam emission processes (see Fig 4.1 and also Basko and Sunyaev 1976, White et al. 1982).

Ariel-6 was used to make observations of several X-ray pulsators, two of which, 4U0115 + 63 and GX1 + 4 are presented here. The data obtained are interpreted in terms of the currently available models.

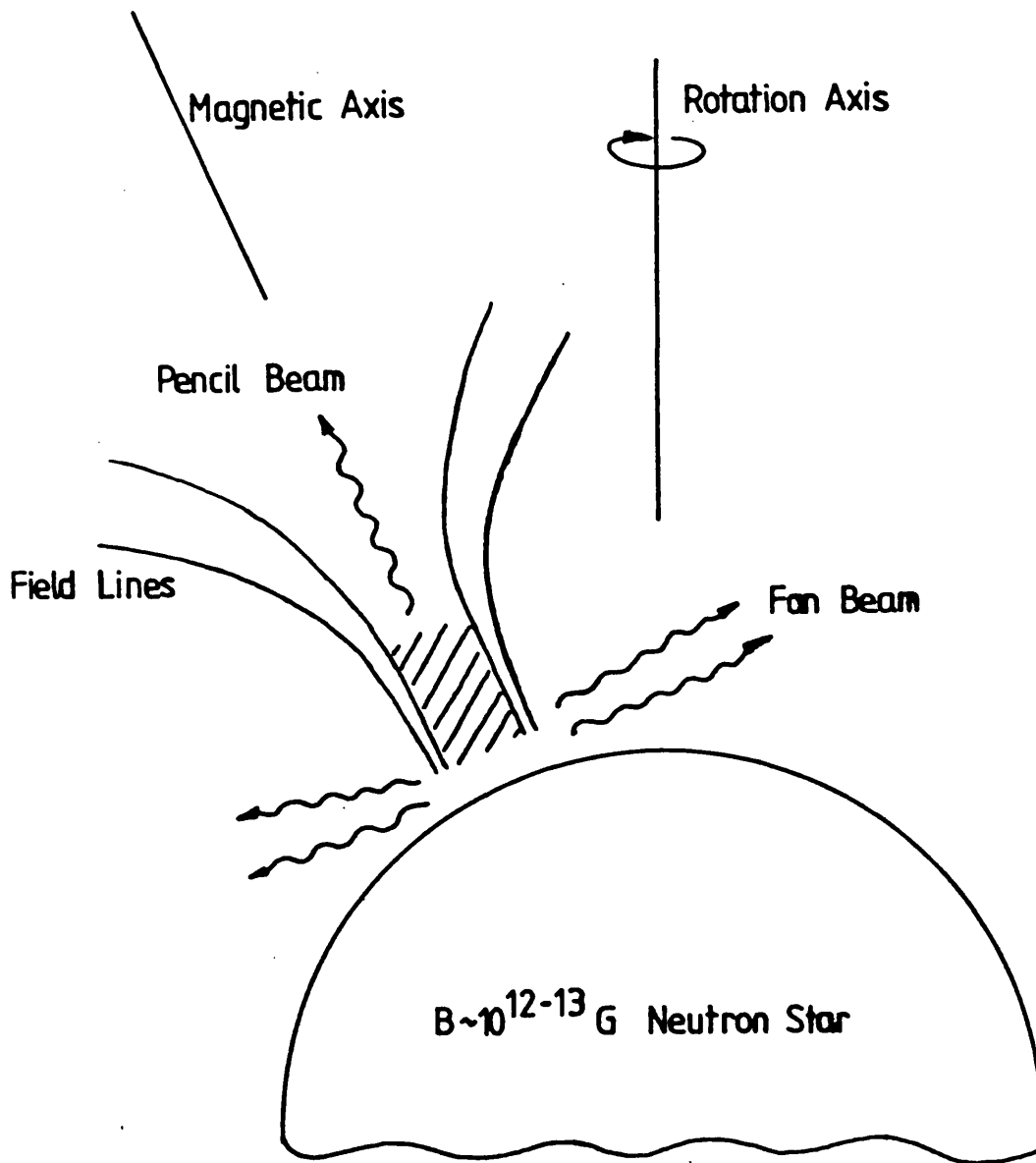


Fig 4.1 X-ray beaming, the pencil and fan-beam patterns.

4.2 4U0115+63

During early 1971 the transient nature of 4U0115+63 became apparent when the Uhuru satellite observed a flux increase to ~ 70 mCrab in ~ 20 days and subsequent decay over several months to a persistent level of ~ 10 mCrab (Forman, Jones and Tananbaum 1976). The source was found to have a hard X-ray spectrum with photon number index, $\alpha \sim -0.1$ (Jones 1977).

In December 1977 - January 1978 a second outburst was detected by both the Ariel-5 All Sky Monitor (Holt and Kaluziensky 1978) and also by SAS-3 (Clark and Cominsky 1978). The source reached a peak 3-6 keV flux of ~ 300 mCrab and the emission was seen to be pulsed with a period of ~ 3.61 s (Clark and Cominsky 1978).

Analysis of pulse arrival times in SAS-3 data enabled the determination of the orbital period, $p \sim 24.3$ d, eccentricity ~ 0.34 and projected semi-major axis ~ 140 light seconds (Rappaport et al. 1978). The derived mass function showed the companion to be $\gtrsim 5M_{\odot}$. Cyclotron features have been reported in the X-ray spectrum by Wheaton et al. (1979) and White, Swank and Holt (1982) and these constrain the magnetic field of the neutron star to $\sim 1.2 \times 10^{12}$ G.

Following accurate positions determined by the SAS-3 and HEAO-1 instruments (Cominsky et al. 1978, Johnston et al. 1978) an optical candidate was identified. The optical counterpart has $m_V \sim 16$, a featureless continuum (except for strong H_{α} emission) and ~ 5 magnitudes of extinction (Johns et al. 1978). The companion is classed as a Be star and the

absence of features other than H_{α} are consistent with its rapid rotation (Hutchings and Crampton 1981). The large orbital separation suggests that the predominant means of mass transfer during the outbursts was the ejection of mass from the equatorial regions of the companion due to its high rate of rotation (Rappaport and van den Heuvel 1981).

Optical observations over the period August 1980 - February 1981 showed the companion to have brightened from $m_V \sim 16.3$ to $m_V \sim 14.5$ (Kriss et al. 1980 and Middleditch et al. 1980).

4.2.1 The Ariel-6 Observations

Observations of 4U0115+63 were made with Ariel-6 between 17 - 31 December 1980, MJD 44 589.5 - 44 603.5. Data with spectral resolution were not obtained prior to MJD 44 592. A variety of instrument modes were used to observe the source, details of which are given in Table 4.1. After MJD 44 592 the majority of the data were acquired in the instrument's pulsar mode in which the data were folded over a preset period into 15 phase bins before telemetry (see Section 2.1.8). The period used was determined during the first two days of observations. Minor inaccuracies in the folding period were evident by a gradual phase shift of the pulse peak in the data from sequential orbits. However as the data sets were only integrated for ~ 2 minutes any smearing of the spectra or profiles was negligible.

4.2.2 The Outburst

The lightcurve of 4U0115+63 during the observation is

TABLE 4.1 Data Collection modes

Energy Range (keV)	Number of PHA channels (MODE)	Time resolution (s)	Exposure (s)
Variable	1 (E \emptyset)	0.125, 0.25, 0.5	1.2 x 10 ⁴
1.0 - 7.8			
3.0 - 11.2)	8 ^b (E3)	0.25 ^a	5.3 x 10 ⁴
)			
5.5 - 16.2)			
)			
10.3 - 26.5)			
1 - 50	8 ^c (E2)	0.125, 0.25 ^a	1.6 x 10 ⁴
1 - 50	32 (E4)	1.0, 32.0	5.2 x 10 ³

a - approximate time resolution for one 'pulsar' mode phase bin (see text).

b - narrow (intrinsic) PHA channels.

c - groups of four intrinsic PHA channels.

presented in Fig 4.2a, the data points were aspect corrected using the spin modulation technique (Section 3.1.7). It is apparent from this that the outburst commenced just before our observations on MJD 44 599 with a rise time of ~ 6 days to a maximum, 2 - 10 keV, flux of ~ 180 mCrab, followed by a decay with an e-folding timescale ~ 50 days. In contrast the 1977-78 outburst had a rise time of ~ 10 days, decay of ~ 20 days and peaked at ~ 300 mCrab (Rose et al. 1979). The 1980 X-ray outburst occurred ~ 60 days after the associated optical brightening (Kriss et al. 1983). Using this delay Kriss et al. have ruled out accretion in a stellar wind during the outburst and suggest instead the presence of an accretion disc in the system.

There was no evidence for variability of the pulse-phase averaged spectrum during the observation. Modelling of the overall X-ray spectrum was by a power-law, with low energy absorption by a column of cool gas along the line of sight and a high energy cut-off (see Section 2.2.3). Simple thermal bremsstrahlung and black-body models were also considered; however these gave totally inadequate fits to the data. Whilst the power-law did not give a statistically acceptable fit (hence the best fitting parameters are quoted without errors), the correct spectral shape was reproduced. The best fitting spectrum is shown in Fig 4.3. Failure to obtain a statistically satisfactory fit is perhaps not surprising since the spectrum is an average of many different spectra.

The hardness of the spectrum is apparent, along with the sharp cut-off at energies $\gtrsim 9$ keV. This spectrum is similar to those presented by Rose et al. (1979) for the 1977-78

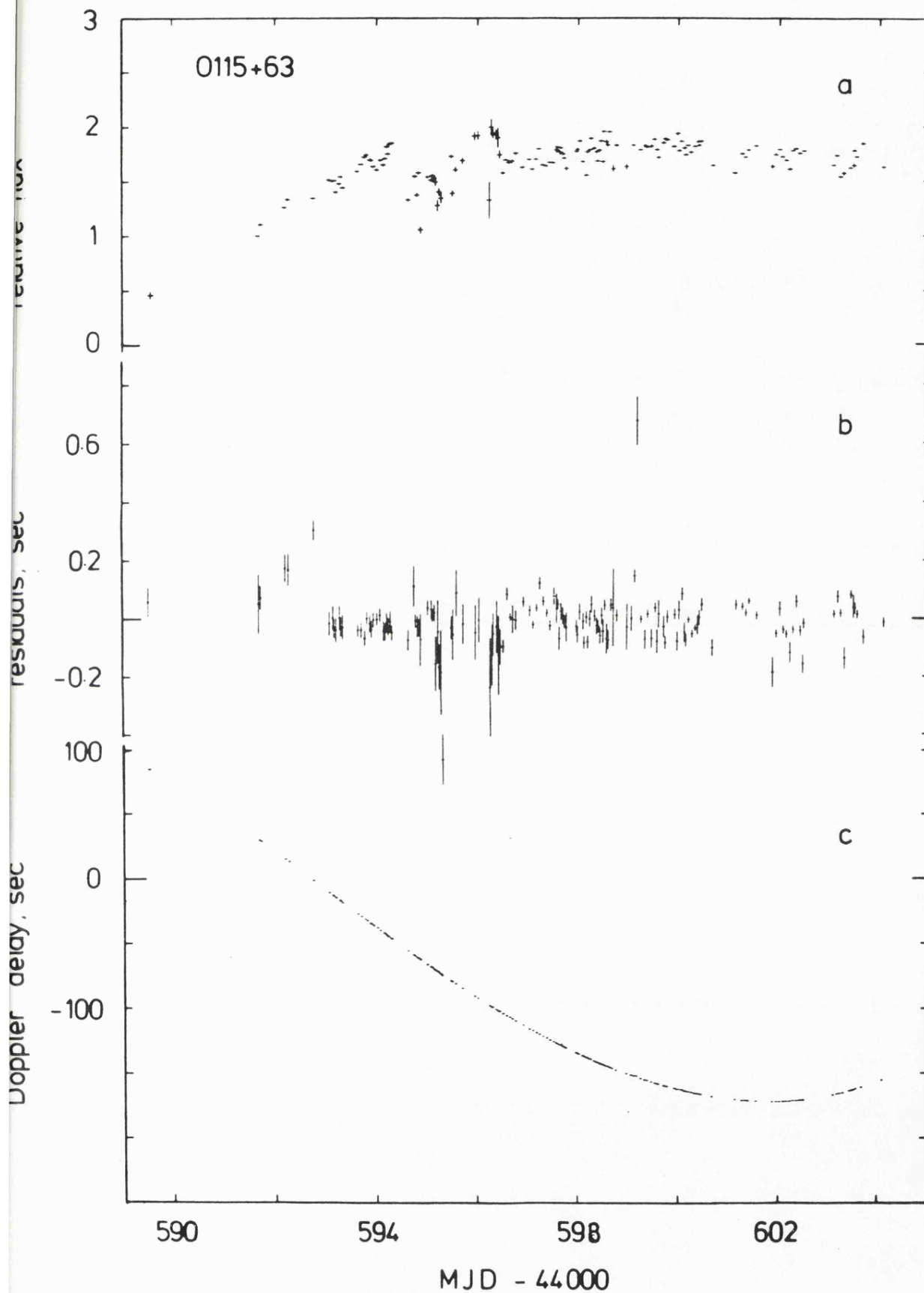


Fig 4.2

- a) The X-ray flux for 4U0115+63 corrected for offset, the scale is ~ 100 mCrab per unit.
- b) Residuals from the best fit to the orbital elements.
- c) Dopler delay plot for same points as in (b).

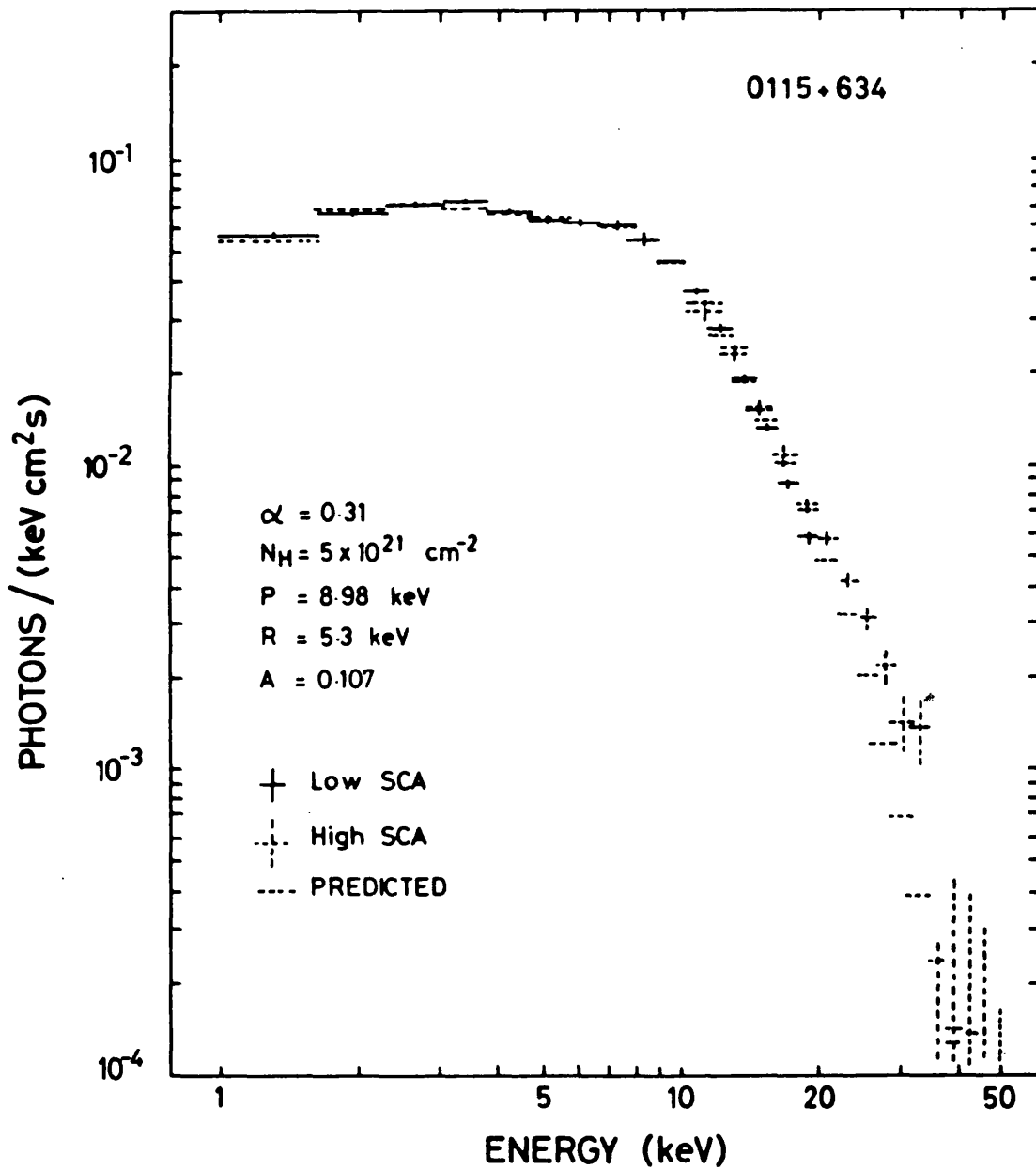


Fig 4.3 4U0115+63 : the pulse phase averaged spectrum.

outburst. We estimate the mean flux (1 - 13 keV) to be $6 \times 10^{-9} \text{ erg cm}^{-2} \text{ s}^{-1}$.

4.2.3 Pulse Timing Analysis

From each data set a phase reference point was determined by fitting a template to the data folded into 16 phase bins. The template was produced by folding one of the longest data sets at the pulse period as determined using the maximum χ^2 test (see Section 2.2.2). The phase error, between template and data, was estimated from the variation in χ^2 with the phase of alignment and was typically ~ 100 ms (see Fig 4.2b).

After barycentric correction and an initial fit to the orbital elements of Rappaport et al. (1978), it was possible to unambiguously assign numbers in the pulse train to each reference point. The Ariel-6 observation spanned only ~ 0.6 of the orbit and therefore the orbital period was fixed at that value derived from SAS-3 data (Rappaport et al.) For the remaining parameters required to define the orbit, the pulse period, its rate of change, the projected major axis of the orbit, the orbital eccentricity and the longitude of periastron passage, the χ^2 was minimised whilst allowing each to vary. For the best fit to the data the doppler delays in pulse arrival times and residuals are shown in Fig 4.2b and c. The minimum χ^2 value found for fitting to our ~ 150 data points was ~ 820 , so the single parameter confidence limits (see Section 2.2.3) were determined after reducing the χ^2 values by a factor:

$$\chi^2_{\min} / (\text{Number of points} - \text{Number of parameters}).$$

Values for the fitted parameters are given in Table 4.2, together with the results of previous determinations using Uhuru and SAS-3 data.

From the value of the longitude of periastron passage, ω , during 1977 - 78 we find that $\dot{\omega} = -0.58 \pm 0.27 \text{ yr}^{-1}$. This is opposite in sign to that generally expected (see Kelley et al. and references therein) and therefore a more conservative limit on the rate of periastron advance, using only the error on $\dot{\omega}$, is $\dot{\omega} \lesssim 0.5 \text{ yr}^{-1}$ (99% confidence). The analysis of Kelley et al. (1981) was based upon a value $\dot{\omega} \lesssim 2.1 \text{ yr}^{-1}$ and we may then adapt their results for this new, lower, limit. In particular this results in a new, lower, limit on the mass of the companion, $M_c \lesssim 35 M_\odot$ if the Be star were not spinning and a limit of $M_c \lesssim 20 M_\odot$ if the spin rate was the maximum allowed without Roche lobe overflow (see Kelley et al. 1981).

The spin rate, (\dot{P}/P) , during the 1980 observation was a factor ~ 8 greater than that observed in 1977 - 78. From the end of the earlier outburst to the beginning of this observation (\dot{P}/P) increased at $(9.0 \pm 0.2) \times 10^{-6} \text{ yr}^{-1}$. The value determined by Kelley et al. for the interval 1971 - 77 was $-(2.6 \pm 0.8) \times 10^{-6} \text{ yr}^{-1}$, but this was based on a fixed value of p for the earlier, 1971, outburst. Thus the decrease in the pulse period during the off-state may have been masked by the spin up during the outburst. If we have in fact observed the onset of the X-ray outburst then the value of (\dot{P}/P) that we have calculated for the interval, 1978 - 1980, will accurately represent the "off-state" value.

TABLE 4.2 4U0115 + 63 Orbital Parameter Measurements

Instrument	Uhuru*	SAS-3**	Ariel-6
Date (MJD)	40 586	43 540	44 589
p(s)	3.61464 ± 0.00002	3.614574 ± 0.000001	3.614664 ± 0.000001
\dot{p}/p Interval (yr^{-1})	-	$-(2.6 \pm 0.8) \times 10^{-6}$	$(9.0 \pm 0.2) \times 10^{-6}$
\dot{p}/p Observed (yr^{-1})	-	$-(3.2 \pm 0.8) \times 10^{-5}$	$-(27.2 \pm 0.7) \times 10^{-5}$
Orbital Period (d)	24.3149 ± 0.004	24.309 ± 0.021	-
Longitude of Periastron (w)	-	47.66 ± 0.17	47.08 ± 0.21
\dot{w} (yr^{-1} , 90%)	-	<2.1	<0.5

* Uhuru data is from Kelley et al. (1981)

** SAS-3 data is from Rappaport et al. (1978)

4.2.4 Pulse Profiles

Using the pulse period and orbital elements calculated above to determine epochs for the individual data sets we were able to combine the whole of our data and obtain the pulse profiles shown in Fig 4.4. The profiles are similar to those observed in the 1977 - 78 event (Johnston et al. 1978, Wheaton et al. 1979 and White, Swank and Holt 1982) but show a more clearly defined peak than in the 1971 event (Kelley et al. 1981), though this may be due to the softer energy response of the Uhuru detectors. We find no evidence for deviations from the mean pulse profile in any energy band over the ~ 14 days of our observations.

Reference to Fig 4.4 shows that below ~ 4 keV there is a distinct change in the shape of the pulse profile. Whether this corresponds to a broadening of the main pulse, or to the presence of a second pulse at a phase ~ 0.25 later, is uncertain. Above ~ 4 keV the profile appears to be energy independent. This is in contrast to other rapidly rotating pulsators in which phase reversals with energy are observed, e.g. Her X-1 and 4U1627-67 (McCray et al. 1982, White, Swank and Holt 1982). In 4U0115+63 the predominant differences at higher energies are the increasing modulation depth, from ~ 0.2 at ~ 8 keV to ~ 0.5 at ~ 50 keV and that the increase in flux from the pulse minimum commences earlier at higher energies (compare the 4-8 keV profile with that for the range 37 - 50 keV in Fig 4.4). We find no evidence for a phase shift of the peak between low and high energies, as reported by Wheaton et al. (1979), from a comparison of HEAO - A2 and A4 data, during the 1977 - 78 outburst.

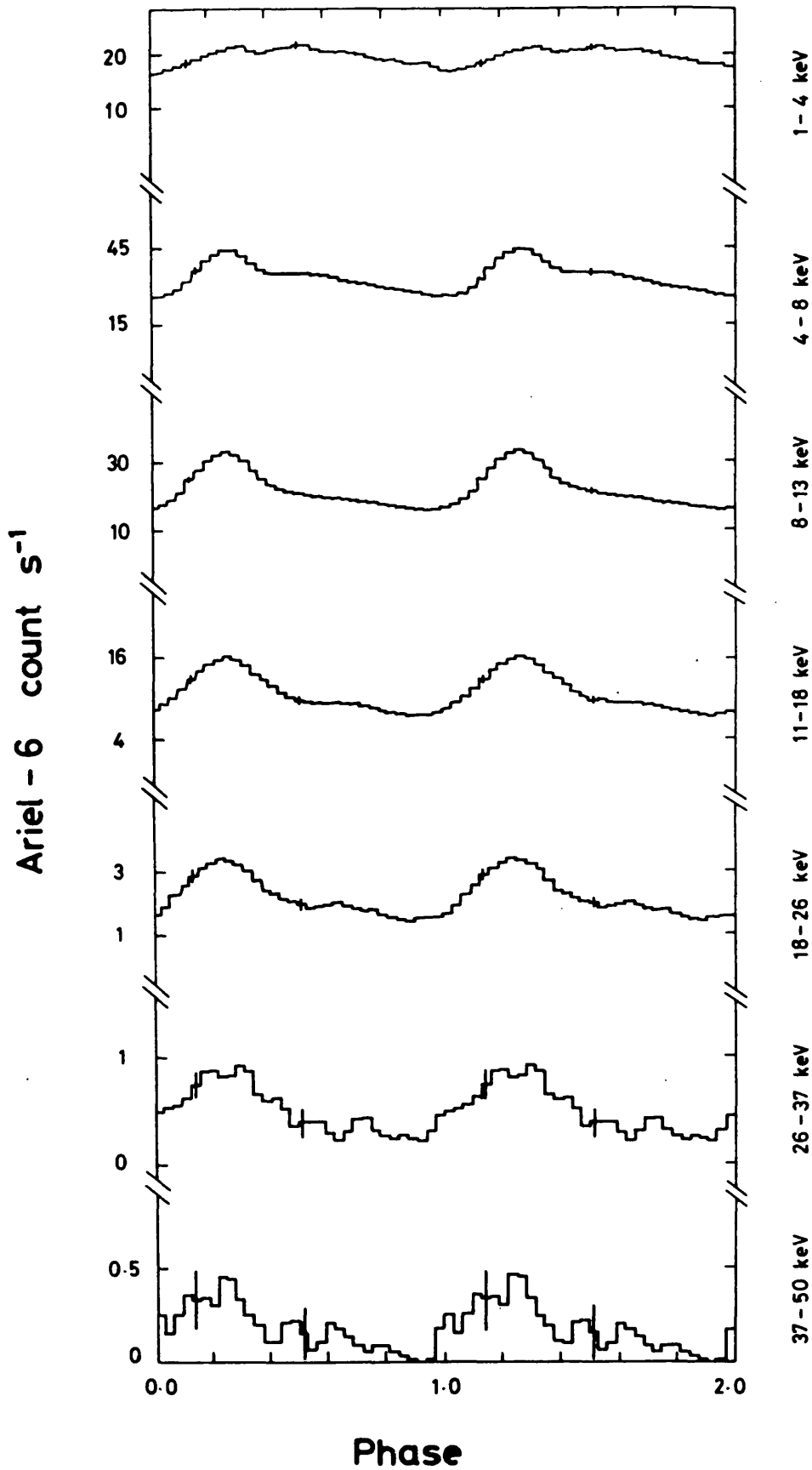


Fig 4.4

4U0115+63 : pulse profiles in seven energy bands, the data were folded at the pulse period. 1σ error bars are shown.

4.2.5 Pulse Phase Spectroscopy

Absence of variability in the phase averaged spectrum throughout the observation allowed the combination of those data sets which covered a reduced energy (grouped in Table 4.1) to provide improved statistics over the 1 - 26 keV energy range. The data were folded at the pulse period, rebinning into 16 equal phase bins.

The ratio of the spectrum at pulse peak to that at the pulse minimum was found in an effort to confirm the reported cyclotron features (White, Swank and Holt 1982). The derived spectral ratio gave an upper limit of ~ 0.25 keV (90% confidence) on the equivalent width of any feature at ~ 23 keV and we found no evidence for an ~ 12 keV feature. Our data suggest that such features, if present, were far weaker during 1980 than in the 1977 - 78 outburst when equivalent widths of $\lesssim 5$ keV and ~ 1 keV, were detected at 12 and 23 keV respectively.

Spectral fits were made to the individual phase bins using the model described above. Satisfactory values of χ^2 were obtained, other than in the phase range 0.06 - 0.25, where the addition of an iron line was required. The line energy was 6.6 ± 0.2 keV with an equivalent width of 120 ± 40 eV. This is not consistent with the HEAO A2 results which suggest a very broad line of equivalent width ~ 900 eV (Rose et al. 1979). Our derived parameters are shown in Fig 4.5 b-d along with the 1 - 26 keV pulse profile, Fig 4.5a. Fits to the 1 - 50 keV, 32 PHA channel data, are consistent with these results though the 1s time resolution only allows comparisons to be made at the pulse maximum and minimum.

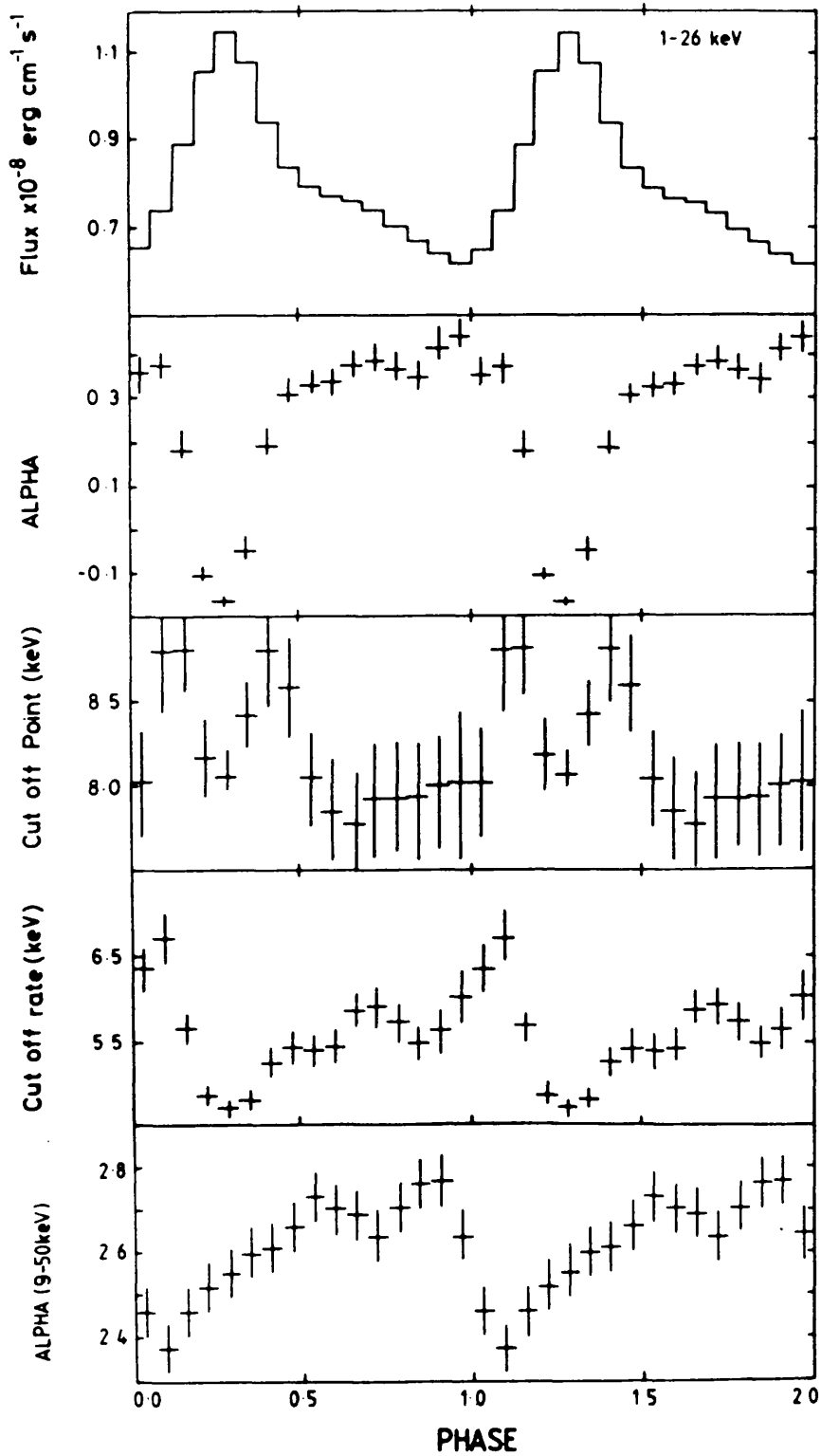


Fig 4.5

- a) 1 - 26 keV flux.
- b) Low energy power-law index for energies $< P$ keV.
- c) High energy cut off point, P keV.
- d) High energy cut off rate for energies $> P$, keV.
- e) Power-law index for 9 - 50 keV energy range.

The highly phase dependent nature of the spectral index, α , and its clear symmetry with respect to the pulse profile were not observed during the earlier outbursts. Rose et al. (1979) found little variation in α and no correlation with the pulse profile, whilst a re-analysis of the same data by White, Swank and Holt (1982) also shows little hardening of the pulse at maximum emission. The SAS-3 data for the 1977 - 78 outburst indicates slight spectral variability with a change in index, $\Delta \alpha = 0.18 \pm 0.05$ in contrast to which the Ariel-6 results which give $\Delta \alpha = 0.6 \pm 0.03$.

A possibility existed that the observed variations in the cut-off energy and rate (Fig 4.5 c, d) were simply an artifact of the fitting procedure. Therefore in order to search for high energy variability, power-law fits were made to the data with energy > 9 keV in each phase bin; the results of these fits are shown in Fig 4.5e. It is immediately apparent from the figure that the high energy (> 9 keV) spectrum hardens before the onset of the pulse (phase = 0). This effect was also seen in the pulse profiles above. The high energy spectrum is hardest before there is any evidence of a spectral change below ~ 9 keV, when this lower energy region hardens the high energy spectrum begins to soften.

4.2.6 Discussion

Rappaport and Joss (1977) have shown that the fractional rate of change in the pulse period (\dot{P}/P) can be expressed in terms of the absolute luminosity (L);

$$(\dot{P}/P) \approx - 3 \times 10^{-5} f (P/1 \text{ sec}) (L/10^{37} \text{ erg s}^{-1})^{6/7} \text{ yr}^{-1}$$

where f is a dimensionless constant and is expected to be ~ 1 .

Comparison of the derived parameters for the 1980 and the 1977 - 78 outbursts, (see Table 4.2) shows that $P_{78} \sim P_{80}$. Therefore

$$(\dot{P}_{78}/\dot{P}_{80}) \approx (L_{78}/L_{80})^{6/7}$$

and by using the values from the Table this implies that the X-ray flux during 1980 should have been a factor ~ 10 greater than that in 1977 - 78, if we assume that the relationship of Rappaport and Joss is strictly adhered to. Also that the accretion rate onto and the torque acting upon the neutron star scale approximately linearly. During 1977 - 78 the measured 1 - 60 keV flux was $\sim 9 \times 10^{-9} \text{ erg cm}^{-2} \text{ s}^{-1}$, Rose et al. (1979), whilst for the same energy band during 1980 the observed flux was $\sim 10^{-8} \text{ erg cm}^{-2} \text{ s}^{-1}$. This implication of an under-luminous outburst, at X-ray energies, during 1980 could account for the absence of strong cyclotron features, which are expected to be highly temperature dependent (Trumper 1979).

White, Swank and Holt (1982) have made comparisons between 4U0115+63 and Her X-1. They have interpreted the pulse phase dependent cyclotron features, detected during 1977 - 78, in terms of emission from a pencil beam (Basko and Sunyaev 1976, Meszaros et al. 1982) for the pulse peak and a fan beam (i.e. Nagel 1981) for the small interpulse. These comparisons with Her X-1 may not be valid, however, as the region of spectral hardening (interpreted as a view deep into the polar cone), seen in the Her X-1 pulse indicates a polar angle of $\sim 40^\circ$

//

(see Pravdo et al. 1978), whereas for 4U0115+63 our data require the angle to be $\sim 100^\circ$. The angles were simply calculated using the full width at half maximum of the region of spectral hardening in Fig 4.5b and that of Fig 1c in Pravdo et al.

It has been theorised that the X-ray spectra of the pulsators will harden at lower magnetic latitudes due to the dominance and angular dependence of the cyclotron-resonance cross section over that of Thomson scattering (Pravdo and Bussard 1981). The implication of this is that at the pulse peak we are seeing emission in a fan beam. This is clearly more easily reconcilable with the large angle over which the spectral hardening was seen, also the phase dependency of the spectra may then be easily interpreted as an effect of the observer's changing inclination to the magnetic field lines and hence the varying line of sight opacity.

Indeed if the increased \dot{P} implication of a higher accretion rate for the 1980 outburst is correct, then the optical depth in the polar cone may well have been > 1 , thereby inhibiting any beaming of the X-ray emission due to the enhanced scattering and giving the less well defined interpulse in our data. The implied transit of the polar cone across the observer's line of sight takes place at phase ~ 0.78 (180° after the phase of maximum spectral hardness) and is accompanied by minimal spectral changes, as one would expect.

The geometrical fan-beam models of Wang and Welter (1981) readily fit the observed pulse profile, the asymmetry of the

profile as a whole is explained by the differential rotation of the neutron star and the accreting plasma, accretion taking place primarily at the rear edge of the polar cone, for the case where the plasma velocity is higher than the neutron star velocity and at the front edge of the cone for the opposite case (see Wang and Welter 1981). Relatively sharp pulse peaks are obtained by postulating that the fans from opposing poles intersect near the magnetic equator.

In conclusion, it is found that the Ariel-6 observations of 4U0115+63 during the 1980 outburst may be understood in terms of emission in a fan-beam from the magnetic pole of a neutron star. The gross features of the pulse profile and the observed spectral hardening at pulse maximum are consistent with this interpretation. We have been able to provide a more restrictive limit on the mass of the Be companion star due to a new limit on the rate of periastron advance. The spin rate of the neutron star has been found to decrease between 1978 - 81, which implies that there had been little, if any, accretion. It is apparent from the complexity of the observed phase dependent spectra and the variable nature of the previously reported cyclotron features that further theoretical work is required to obtain a detailed, and satisfactory, explanation of the X-ray transfer mechanisms.

4.3 GX 1 + 4 (1728 - 247)

In observations made between 1971 and 1978 (Becker et al. 1976, Dofy, Hoffman and Lewin 1981, hereafter DHL) the period of the X-ray pulsar GX 1 + 4 was seen to decrease from ~ 135 s to ~ 117 s, thereby showing GX 1 + 4 to have the highest spin up rate of any of the known pulsators. Measurements by DHL have shown that the spin up was not uniform, probably due to a varying accretion torque on the neutron star. Their analysis of SAS-3 data showed that the modulation depth increased with energy without a change in the pulse profile. DHL also found a significant decrease in the flux below ~ 5 keV over a small phase range $\sim 180^\circ$ from the pulse peak, which they interpreted as being due to an increase in the low energy absorption.

The optical counterpart is an M6 giant, the only star of this type known to be associated with an X-ray pulsator (Glass and Feast 1973). Spectroscopic studies of the companion by Davidsen et al. (1977) found that it had a composite spectrum indicative of a symbiotic star. A strong H_α flux and other emission lines up to Fe X were present and were interpreted as being due to the photoionisation of gas surrounding the source by the incident X-rays.

The measured colours indicate a distance of ~ 10 Kpc and therefore an expected interstellar column of $N_H \sim 10^{22} \text{ cm}^{-2}$. Column densities as high as $4 - 10 \times 10^{22} \text{ cm}^{-2}$ have been seen (i.e. DHL, Becker et al. 1976), which indicates that the majority of the obscuring material is local to the X-ray source.

Two observations of GX 1 + 4 were made by Ariel-6 during

1979 July and 1980 April. In 1979 the observations spanned ~ 2.5 days, with good data being obtained on ~ 15 orbits, whilst in 1980 ~ 25 orbits were obtained during ~ 4 days on source. The dates of the observations and a summary of the different data collection modes used is given in Table 4.3/4.4.

4.3.1 The Pulse Period and Profile

The data, consisting of $\sim 10 - 20$ minute samples of the pulse train at intervals of ~ 90 minutes or more, were folded over a range of trial periods and the maximum χ^2 technique (see Section 2.2.2) used to determine the pulse period. For the 1980 data the χ^2 plot was sharply peaked, with only a single possible period value; however, the 1979 data showed two significant peaks, one at 112.0s and the other at 114.3s. The larger value, in addition to being of lower statistical significance, was ruled out on the grounds that it would require significant phase jitter of the pulse profile. The barycentric values for the derived pulse periods at the two epochs are given in Table 4.3.

Within the span of each observation the rate of change of the pulse period was checked by comparing the epoch of phase-zero in each data-set with that expected for the measured mean period. A least-squares fit to the differences gave values for $(\dot{P}/P) \sim -0.026 \pm 0.007 \text{ yr}^{-1}$ and $\sim -0.023 \pm 0.003 \text{ yr}^{-1}$ for the 1979 and 1980 observations respectively. This compares well with the mean value of $\sim -0.028 \text{ yr}^{-1}$ for the interval between the two observations. Depending upon the magnitude of any short term fluctuations,

TABLE 4.3 Observation dates and period determinations

Observation:	1979 July	1980 April
MJD range	44061.7 - 44064.2	44345.1 - 44348.8
Epoch for period	44063.	44347.
Barycentric Period	112.076 ± 0.003	109.668 ± 0.003
\dot{P}/P (per year)	$- 0.026 \pm 0.007$	$- 0.023 \pm 0.003$

TABLE 4.4 Data collection modes used on GX1 + 4

Energy Range	Time Resolution	Duration
keV	s	s
1 - 50	32	1 000
1 - 50	4	7 300
2.5 - 13(1979)	4	4 000
1 - 10	4	3 900
1 - 10	1	3 000

the 1979 - 80 decline rate may have been faster than that for the earlier years of the decade. Fig 4.6 shows all of the known period measurements.

From observations made at higher X-ray energies it has been reported that the fundamental pulse period consists of two of the ~ 100 s cycles. Koo and Haymes (1980) have found evidence for a period of ~ 4.3 minutes in 20 - 64 keV data obtained in 1974, whilst Strickman et al. (1980) observed differences between alternate two minute pulses in the energy range 20 - 75 keV. We folded the Ariel-6 data used for determining the period into 32 bins at periods twice those given in Table 4.3. Comparison of the pulse profiles in the two halves of the 1980 data yields a reduced $\chi^2 \sim 2.7$. The only differences greater than 1σ were among the six highest phase bins and these did not systematically differentiate the alternate pulses. For the 1979 data $\chi^2_{\nu} \sim 2.5$ and again large differences were only found in the bins of highest flux. Folding the data at three times the basic period showed there to be similar differences between pairs of the three pulses. Folding the 1980 data, for the energy range 26 - 50 keV, gave a flux ratio between alternate pulses of 0.96 ± 0.13 . Therefore we find that flux variations occur from one cycle to another at the peak of the pulse and that alternate pulses are indistinguishable. It is noted however that if the magnetic axis of the neutron star were in the spin plane then pulses from the two poles might normally appear identical, so the possibility of two pulses per spin period cannot be excluded.

The 1980 data from the eight broad band (E2 mode) PHA channels were collected over ~ 1 day and are shown in Fig 4.7

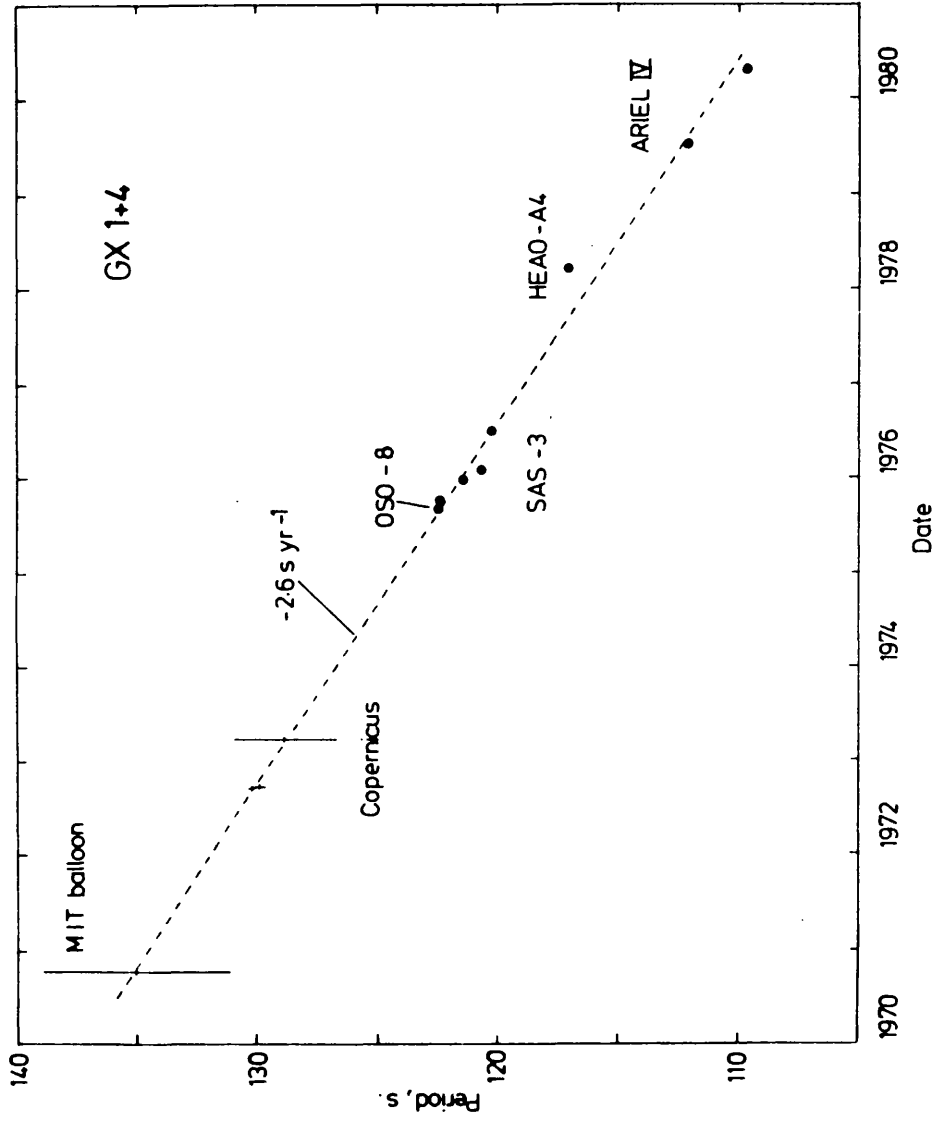


Fig 4.6 The pulse period of GX 1+4 for the period 1970 - 1980.

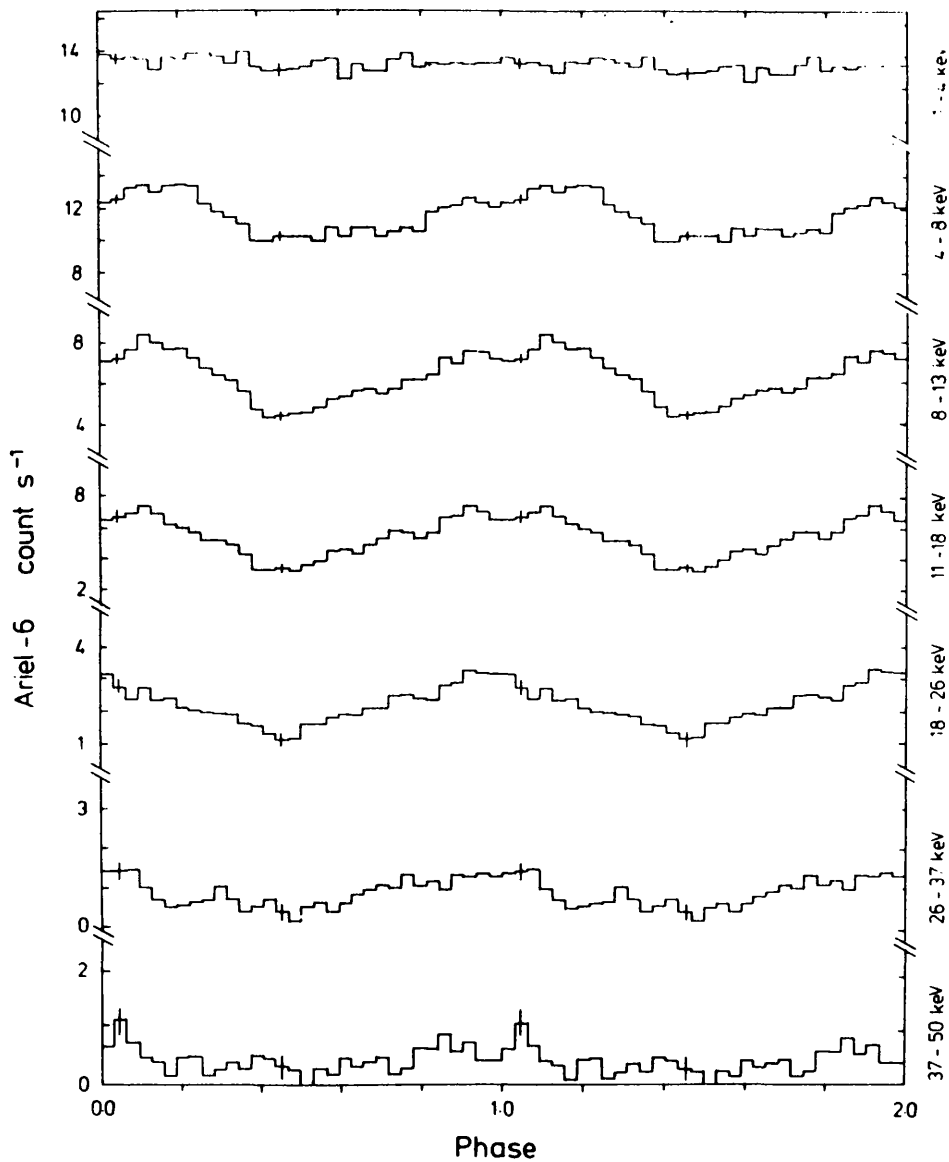


Fig 4.7

GX 1+4 pulse profiles in different energy bands obtained by folding the data at the pulse period.

folded at the pulse period into 32 phase bins. The modulation depth, defined as being (maximum - minimum)/mean, is seen to be zero for the 1 - 4 keV channel, ~ 0.5 for the 8 - 13 keV range and ~ 1.5 above ~ 26 keV. There was also an apparent lag in phase of ~ 0.1 between the high and low energy pulse profiles. Above ~ 26 keV the pulse shape was similar to that of 1976, see DHL; with peaks at phases ~ 0.8 and 1.0 while in the 4 - 8 keV energy range the peaks occur at phases $\sim 0.9, \sim 0.15$. An alternative to invoking a lag in phase is to introduce a low energy pulse at phase ~ 0.15 ; the profiles at different energies were not sufficiently similar to exclude this. For both the 1979 and the 1980 data the pulse profiles, for comparable energy ranges, are shown in Fig 4.8b, c and compared with that obtained during 1976 by DHL, Fig 4.8a, though the phase alignment here is arbitrary. The pulse profile below ~ 26 keV was much more sinusoidal during 1980 than in 1979 and in neither case was there any evidence for the low energy dip seen by DHL.

4.3.2 Spectra: The Continuum

The phase analysis of the spectrum was concentrated on the 1980 data, for which the statistics were better. Standard spectral models were considered and in the case of the power-law a high energy cut-off factor was included. The overall spectrum for two quarters of the period, centred on the peak and trough of the pulse profile, is given in Fig 4.9. Only the power-law and high energy cut-off model gave statistically acceptable fits for the 4 - 30 keV energy range, the spectral parameters determined for each eighth of the

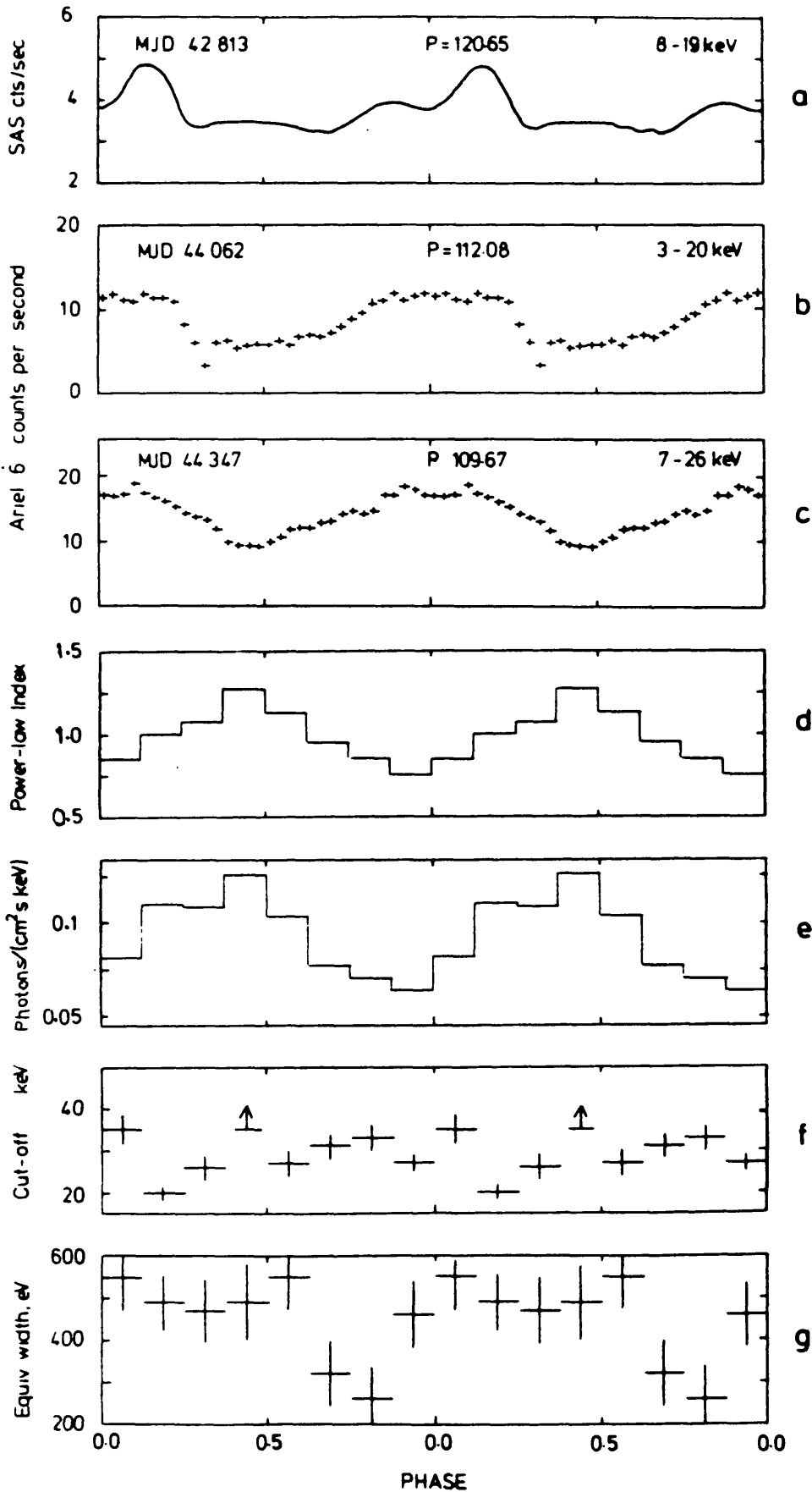


Fig 4.8 Pulse profiles:(a) 1976 (b) 1979 (c) 1980
 (d-f) α , A and the cut-off energy for the best fitting spectra.
 (g) Equivalent widths of the Iron line feature, eV.

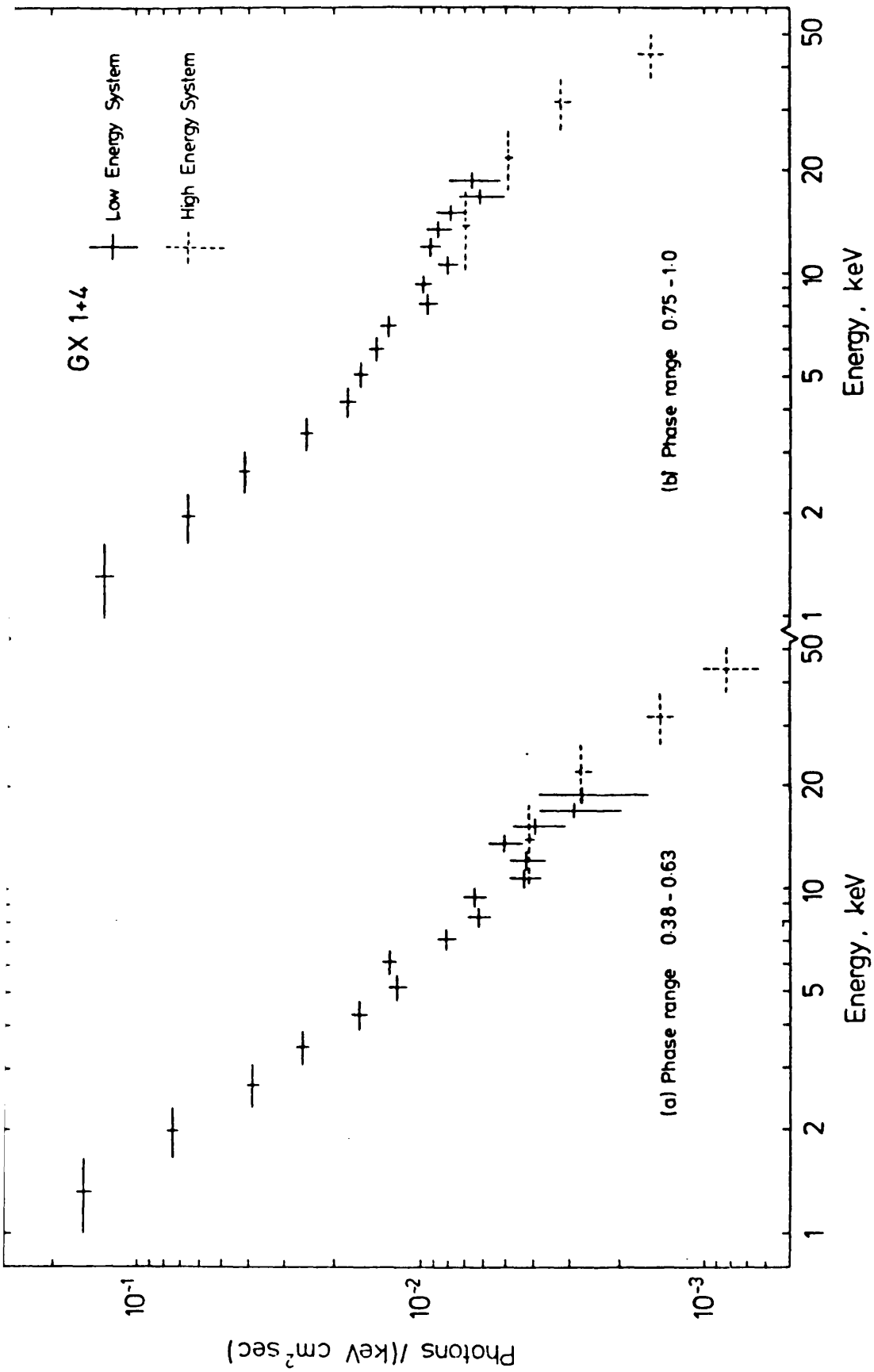


Fig 4.9 GX 1+4: X-ray spectra for two different phase ranges. High energy system data have been re-binned to improve statistics.

phase range are given in Fig 4.8 d - g.

The power-law index (Fig 4.8d) is almost symmetrical about phases 0.45 and 0.95, except that the phase range 0.13 - 0.25 shows a softer index and greater normalisation than the corresponding phase before the peak. This is a result of the excess flux at low energies for phases 0.1 - 0.3. Above ~ 30 keV most of the fits were improved by the inclusion of the high energy cut-off factor. The e-folding rate (defined as R in Section 2.2.3) was fixed at 20 keV whilst the energy at which the cut-off commenced was a free parameter; the results of this are shown in Fig 4.8f. Single temperature bremsstrahlung and black body spectra did not give a statistically satisfactory fit to the data, however the observed power-law could be the result of the combined emission from a range of black bodies, the maximum temperature (derived from fitting to the high energy cut-off) being ~ 7 keV.

Below ~ 4 keV, as seen in Fig 4.9, the data lie above the extrapolation from higher energies, but, since the hydrogen column could not be deconvolved the actual source spectrum may differ from that which we actually fitted. A power-law fit to this energy range gave a photon number index,

$\alpha = 0.8 \pm 0.15$ with $N_H = (0.4 \pm 0.2) \times 10^{22} \text{ cm}^{-2}$, whilst fitting to a black body spectrum gave a temperature of $\sim 0.75 \pm 0.1$ keV. During 1979, when the spectrum was only measured down to ~ 2.5 keV, it indicated a smaller excess over that fitted above ~ 4 keV.

The mean flux density in the 4 - 50 keV range was $(5.9 \pm \frac{1.8}{2.7}) \times 10^{-9} \text{ erg cm}^{-2} \text{ s}^{-1}$, whilst that below ~ 4 keV was

$\sim 0.6 \times 10^{-9} \text{ erg cm}^{-2} \text{ s}^{-1}$. The ratio of the 1 - 50 keV flux in 1980, to that measured in 1976 (DHL), is 0.7 ± 0.2 , the error being primarily due to the estimated instrumental uncertainties. So, the overall output from GX 1 + 4 in this energy range appears to be less, with a lower flux density above ~ 4 keV being partially offset by a greater output below ~ 4 keV.

4.3.3 Spectra: Iron Fluorescence

Interleaved with the broad band (E2 mode) data sets were those in the E3 mode, which provided a reduced energy range from the PHA (see Section 2.1.8). In order to obtain a satisfactory fit to the E3 data, in each of the eight phase bins, an iron line was introduced into the model. The significance of the feature can be seen from the fact that χ^2_{min} decreased from ~ 90 to ~ 4 , for the phase range 0 - 0.25 and from ~ 38 to ~ 2 , for phases 0.63 - 0.88, when a line was included.

Before the line was fitted, the data, excluding that region containing the line, were fitted by a power-law with attenuation by Iron absorption alone. This is as one would expect for emission from a hot plasma in which all elements, apart from Iron, were wholly or highly ionised. The purpose of including, or at least allowing for, this feature was to make it possible to very accurately determine the continuum emission, as a poor fit to this would affect the results of subsequent line fitting. The values found for the Iron column for the phases 0 - 0.875 were in the range $(0 - 3.2 \pm 2.4) \times 10^{18} \text{ cm}^{-2}$, whilst for phases 0.875 - 1.0 the value was $(8 \pm 2.4) \times 10^{18} \text{ cm}^{-2}$.

Equivalent widths derived as a result of line fitting are given in Fig 4.8g, the phase range 0.63 - 0.875 shows a width significantly below the mean value. The data for this phase range is compared in Fig 4.10 with that for phases 0 - 0.25, for which the power-law index was approximately the same. The minimum 90% confidence regions in equivalent width/line energy space are also shown. Considering the equivalent width alone the value for the phase range 0.63 - 0.875 is 310 ± 70 eV, compared with 500 ± 45 eV for the remainder of the cycle. Subdivision of the data did not reveal any significant variation of the equivalent width, either phase averaged, or between bins of the same phase range. With only two PHA channels covering the $\sim 20\%$ FWHM detector resolution at this energy, no significant broadening was observed.

Processing of the 1979 data was carried out in a similar manner, except that the initial fit was to the energy range 4 - 10 keV. The mean equivalent width found was 490 ± 50 eV, compared to the 1980 average of 450 ± 30 eV. No variation with phase was discernable, however, a fluctuation at the 1980 level would have been obscured by the poorer statistics.

4.3.4 Discussion

The phase-averaged continuum observed in GX 1 + 4 can be fitted by the Comptonised spectrum from a hot ($kT \sim 5 - 7$ keV) plasma. Compton scattering of the X-rays in a cool cloud, of temperature less than that of the radiation, produces a characteristic cut-off in the emergent X-ray spectrum at an energy $\approx (m_e c^2 / \gamma^2)$, where $m_e c^2$ is the rest mass energy of the

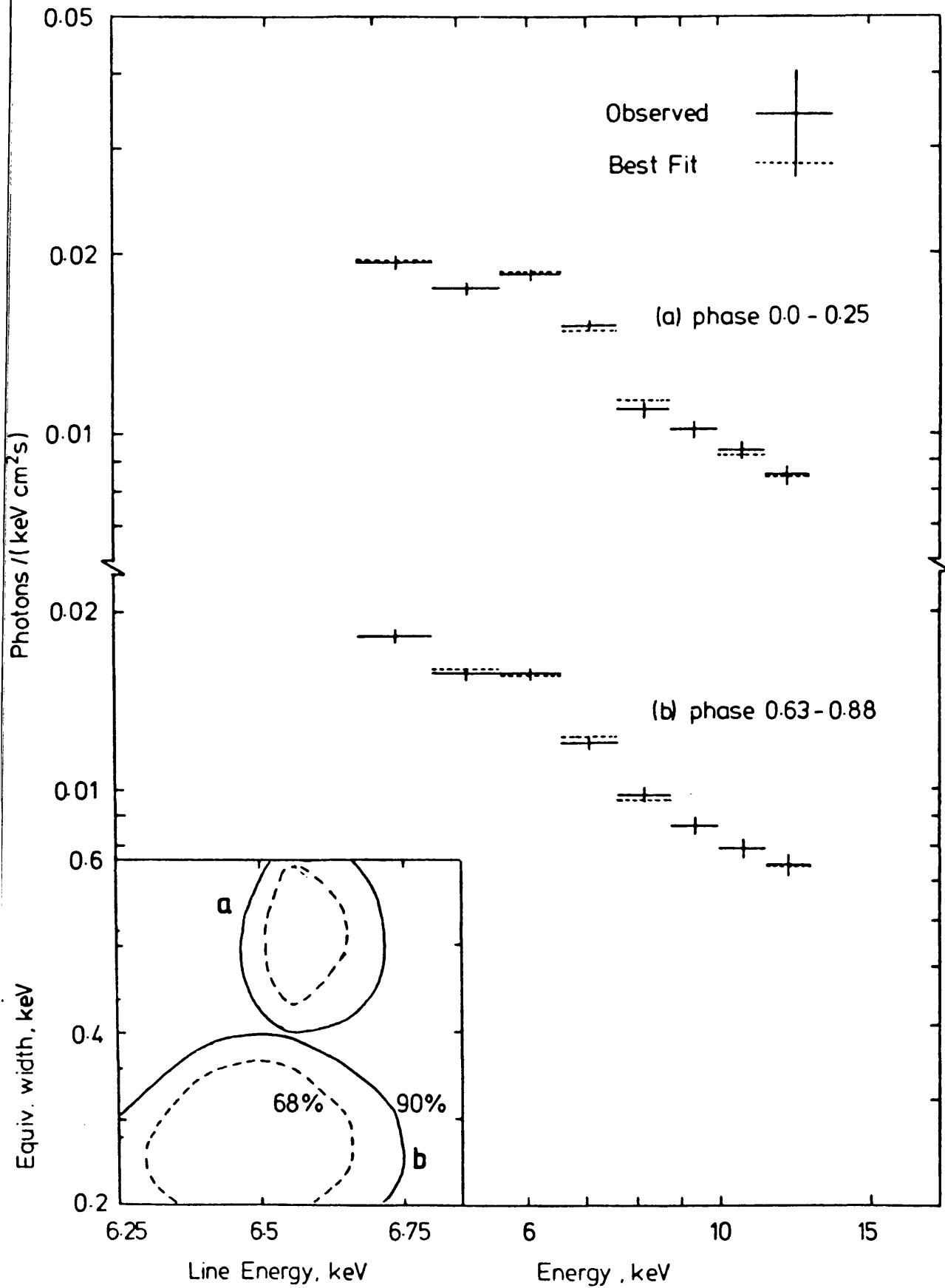


Fig 4.10 GX 1+4 E3 spectra showing the Iron line at different phases, the inset shows the confidence contours on the feature.

electron and τ the optical depth of the cloud (see Illarianov and Sunyaev 1972, Ross, Weaver and McCray 1978). For GX 1 + 4 the implied optical depth is ~ 7 .

Changes in the observed spectral index can be kinematically interpreted as being due to the varying opacity of the material through which the X-rays are escaping and the changing degree of scattering which they undergo, the hardest spectrum occurring when the emitting region is seen through the area of minimum opacity. In the case of GX 1 + 4 however, whether this corresponds to emission in either a fan- or pencil-beam and hence the transit of the neutron star magnetic equator, or pole across the line of sight, is uncertain, as accounting for the observed pulse profiles has proved a more intractable problem (see Rappaport and Joss 1977, Pravdo et al. 1979).

During 1976 GX 1+4 showed a double-peaked profile with the second peak dominating the first by a factor of two, but no discernable lag between high and low energies (DHL). In 1980 the profile was just resolvable into two peaks, also there was an apparent phase lag and a broader pulse in the 1 - 18 keV energy range compared with that in the 18 - 50 keV range. These characteristics are difficult to explain by either pencil- or fan-beam models.

The 1976 profile was similar to that of Her X-1 (Holt et al. 1974) which Pravdo et al. (1979) interpreted as a single pulse, in a pencil-beam, from the hot spot at the neutron star pole. This interpretation required two Thompson scattering regions in the line of sight, positioned asymmetrically with respect to the beam and with a maximum optical depth ~ 1 . The profile of GX 1 + 4 during 1979, which appears to be the reverse

of that seen in Her X-1, would require the accretion funnel to be curved in the opposite sense, i.e. in the direction of rotation at increasing radii. Consequently this data may be fitted by an asymmetric pencil-beam from a spread polar cap without any scattering, in the method of Wang and Welter (1981), although they did not specifically model GX 1 + 4 due to the ambiguity about the number of pulses per rotation period.

The 1980 data suggests a fan-beam interpretation, since the spectrum emitted by the accretion column is then expected to harden with increasing angle to the magnetic field (i.e. Pravdo and Bussard 1981), whilst the apparent lag still requires some asymmetry of the emission region with respect to the magnetic field. For the 1980 data the pulse is broad, as one would expect from a fan beam, but retains two peaks, albeit much less distinct, with the same phase separation as seen in 1976 by DHL.

Although a long-term trend of increased spin-up is noted, the value of (\dot{P}/P) measured in 1980 is significantly lower than that recorded by DHL during 1976 ($- 0.32 \pm 0.0015$) when the pulse profile was much narrower. Thus the broadening of the profile may be correlated with a lower accretion rate, implying a smaller optically thick region at the pole and allowing the implied fan-beam to extend to higher latitudes.

The Iron Emission line

The large mean equivalent width is most easily interpreted as fluorescence from a shell of material at the Alfvén surface. Following Hatchet and Weaver (1977) and Pravdo (1979), the ratio of the line strength to the number of photo-ionised

iron atoms is a measure of the photoionisation yield and the solid angle subtended by the fluorescing target.

$$N_{\text{LINE}} = \frac{\epsilon \Omega}{4\pi} \int_{7.1}^{20} \left(\frac{dN}{dE}\right) \left(\frac{7.1}{E}\right)^3 dE$$

where N_{LINE} is the number of line photons
 ϵ is the fluorescence yield (~ 0.34)
 $\frac{\Omega}{4\pi}$ is the solid angle of the target
 $\left(\frac{dN}{dE}\right)$ is the observed spectrum.

For the phase averaged line strength and spectrum we find, $\frac{\epsilon \Omega}{4\pi} \sim 0.24$, a value similar to those Pravdo (1979) gives for Her X-1 and Vela X-1; therefore, if the 7 - 20 keV spectrum we observed was typical of that seen by the fluorescing target a large fraction of the solid angle around the source is subtended, implying the disc and/or the Alfvén surface as the line generating region, rather than the surface of the giant companion star.

The phase range for which the equivalent width is lower overlaps that where a significant improvement in the continuum fit is made by including absorption by Iron. For the region $90^\circ \pm 45^\circ$ ahead of the pulse peak either the fluorescing material is obscured from view or the beam illuminates much less of the visible target area. The absence of strong Fe absorption above 7 keV indicates a reflecting target rather than a transmitting one (Langer et al. 1978); unless it is optically thin, which is unlikely due to the large optical depth inferred from the high energy cut-off in the X-ray spectrum. If illumination of the disc is concentrated in two regions near the magnetic poles, which themselves are not in

the plane of the disc, then the material accreting onto the nearer of the poles could hide part of the fluorescing target from view for some fraction of each period. It is possible that this may be analogous to the variation seen in the He II 4686 Å line of DQ Her by Chanan et al. (1978), where both the phase and amplitude of the line are variable and are interpreted as fluorescence from regions on the disc surface illuminated by the white dwarf. The cause of the amplitude modulation in this case was only speculated upon and could be due to obscuration by accreting material.

Finally, our observations of GX 1+4 during 1979 July and 1980 April have shown the pulse period to have decreased at a faster rate during 1978 - 80 than over the period 1970 - 78. Compared with that measured in 1976 the pulse profile was more sinusoidal, with an apparent phase lag of ~ 0.1 between the 4 - 8 keV pulse and that seen at energies > 25 keV. The 1 - 4 keV emission was not pulsed and was stronger than seen hitherto. The data suggested the presence of an iron emission feature whose equivalent width varied with pulse phase, this is the first such feature to be seen in the X-ray spectra of the pulsators and it is thought to have originated in material local to the neutron star. In the 1980 data there is a preference for a fan-beam interpretation, however the changes in pulse profile that occurred between 1979 and 1980 are not easy to reconcile with either pencil- or fan-beam models.

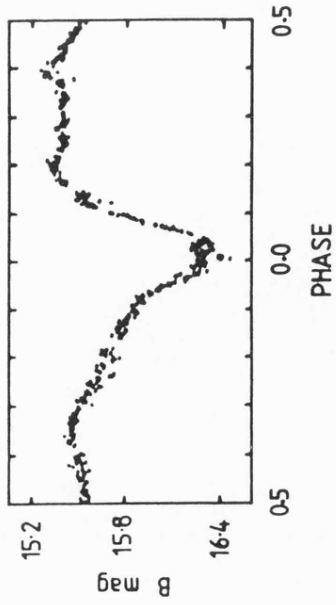
4.4 3A1822-371

Observations of 3A1822-371 with the HEAO-1 modulation collimators during September 1977 enabled the determination of an accurate source location, within an $\sim 1^\circ$ error box (Griffiths et al. 1978). A subsequent search of this error box using the Cerro Tololo Inter-American Observatory 1m telescope indicated an extremely blue, ~ 16 mag. star as the most likely optical counterpart (Griffiths et al.).

Photometry of this star over several months revealed a smooth modulation in the data with a period of ~ 5.6 hr (Seitzer et al. 1979, Mason et al. 1980). The period was stable with a variation in B from 15.4 to 16.4 mag., whilst there was no apparent phase dependent change in the colours, $\Delta(B - V) \lesssim 0.07$ mag. and $\Delta(U - B) \lesssim 0.14$ mag. Three predominant features were evident in the optical lightcurve (Fig 4.11), a large minimum commencing at phase ~ 0.66 , a small dip of duration ~ 0.1 , centred at phase zero by definition and a smaller secondary minimum at phase ~ 0.5 . It was suggested that the modulation was at the orbital period of the system as similar periods had been found in many cataclysmic variables (Mason et al. 1980). In contrast to the cataclysmics however there was no evidence for short timescale flickering in the data, implying that the source of the optical emission was extended.

An orbital period of ~ 5.6 hr implies that a normal main sequence companion would subtend an angle of $30^\circ - 40^\circ$ at the X-ray source. This is approximately the same width as the dip at phase zero and suggests that is the partial eclipse of the extended emission region by the mass donating star. The large

4.11



4.12

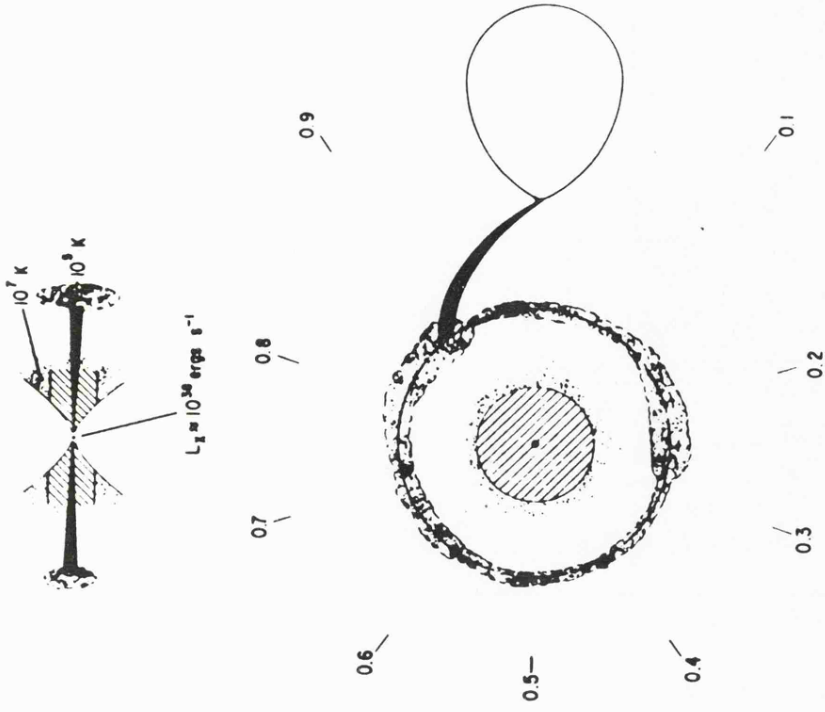


Fig 4.11 3A1822-371 : The folded B band data (Mason et al. 1980).

Fig 4.12 An idealised view of the 3A1822-371 system (from White and Holt 1982).

minimum, commencing at phase ~ 0.66 , was thought to be due to the presence of a gas stream in the system between the companion and X-ray star, alternatively, to a thickening at the edge of an accretion disc where it is intercepted by such a stream (Lubow and Shu 1976).

Optical spectroscopy revealed that the spectrum was dominated by emission lines, notably He II (Charles, Thorstensen and Barr 1980). They found that the observed UV lines were most likely to have been formed in the outer edges of an accretion disc by reprocessing of the incident X-rays. Not only did the optical emission suggest the presence of an accretion disc, but the large wings seen on the H_{α} line indicated that it was rapidly rotating.

Detection of the periodicity at X-ray energies was reported by White et al. (1981). X-ray observations by the HEAO-1 A2 instrument and the Monitor Proportional Counter (MPC) on the Einstein spacecraft, both clearly showed the modulation. The lightcurve was similar to that seen at optical wavelengths, with an $\sim 25\%$, almost sinusoidal, modulation combined with a smooth dip of short duration at phase zero. Absence of spectral variability around the orbital phase, combined with the width of the dip, shows the emitting region to be extended at X-ray energies.

The X-ray spectrum was characterised by a hard power-law, with a cut-off at high energies and a broad iron emission feature at ~ 6.5 keV (White et al. 1981). This suggested that the X-rays had undergone severe comptonisation during their passage out of the system. It was proposed that the X-rays were emitted from within an optically thick region surrounding

an accreting degenerate star and that the modulation seen was due to the presence of large scale structure at the edge of the accretion disc (see Fig 4.12). The width of the dip at phase zero was then interpreted as the partial eclipse of the X-ray source by the companion, which indicated that the optically thick region extended for $\sim 10^{10}$ cm. Further optical and UV spectroscopy (Cowley, Crampton and Hutchings 1982, Mason and Cordova 1982a, Mason et al. 1982), supported this idea of a structured accretion disc.

Mason and Cordova (1982a, b) found that the light-curve showed a smooth progression in shape from X-ray energies to the infra-red. They were able to successfully model the observed modulation over the entire 1200 - 12 500 Å range by considering an accretion disc with a profile identical to that shown in Fig 4.12, taking into account X-ray reprocessing and the emission from each surface of the disc as a function of orbital phase.

The presence of large scale structures at the edge of an accretion disc raises questions regarding their formation and stability, particularly for the secondary bulge at phase ~ 0.4 which was introduced on an ad-hoc basis by White et al. (1981) in order to model the X-ray modulation. At the present time however, there appears to be overwhelming evidence in support of the accretion disc coronae (ADC) model (see White and Holt 1982 and references therein, Fabian, Guilbert and Ross 1982).

4.4.1 Ariel-6 Observations

Ariel-6 was used to make observations of 3A1822-371 during 1980 April 20th - 24th. Data were acquired just prior

TABLE 4.5 Data collection modes used on 3A1822-371

Energy Range	Time Resolution	Duration
keV	s	s
2.3 - 10.1	0.25	2 300
1 - 50	0.5 and 1.0	1 400
1 - 7.7	4	4 900
1 - 50	32	5 400

to an all-sun period and losses were therefore reduced. A total of $\sim 1.4 \times 10^4$ s data were obtained, details of the instrument modes using being given in Table 4.5.

The discontinuity of the data was a major problem, as various phases of the orbital period were sampled during different cycles and at possibly differing offsets from the instrument's field of view. Source offsets were determined using the spin modulation technique (Section 3.1.7). It was possible to use this method for $\sim 60\%$ of the data, for which the time resolution was less than the spin period (fortuitously this data was scattered throughout the observation). The source remained offset from the axis of the instruments collimator by $1.3 - 1.7$ throughout the duration of the observation.

It was essential to ascertain whether the source, which was clearly variable, was in fact periodic. In context the Ariel-5 observations by Charles, Thorstensen and Barr (1981) had indicated the absence of any modulation at X-ray energies with an upper-limit of $\lesssim 3\%$. Simply folding the data at a range of periods close to the known period and using the maximum χ^2 technique was insufficient as so few samples were available that the folding might have induced an apparently periodic modulation into chaotic data. Comparisons of the data, in ~ 4 minute samples throughout the observation, showed there to be three high points. Dividing the time delay between successive high points by the orbital period (Cowley, Crampton and Hutchings 1982), indicated separations of 8.99 and 2.03 orbital cycles, positively identifying the periodic nature of the source during the Ariel-6 observation.

Data acquired in the 1 - 8 keV energy range using E2, E3 and E4 modes (see Section 2.1.8) were folded using the period and ephemeris: $P = 0.232108$ days, $HJD_{\min} = 2\ 444\ 105.673$ (Crampton, Cowley and Hutchings 1982). The non-aspect-corrected, folded, data are shown in Fig 4.13 and again in Fig 4.14 where they are compared to the previous X-ray light-curves obtained with the HEAO-1 A2 and Einstein MPC instruments.

The scatter on the light-curve noticeable mainly in the phase range 0.4 - 0.8 is within that expected due to the variations in the source offset angle. Our light-curve is in good agreement with that obtained during earlier observations, showing the stability of the profile, though at two phases there is clear evidence for variability. At phase ~ 0.2 (the 'shoulder' referred to by White et al. 1981) there is a considerable increase in the flux, though the only other data available at this phase was obtained during the HEAO-A2 scan, for which the exposure in this phase range is unknown. In the phase range 0.5 - 0.6 there is a second, slightly less significant increase, the data at this phase more clearly resembling that of the HEAO A2 scan data than that of the more recent MPC observations. The dip in flux at phase zero is not clearly seen in our data and we are therefore unable to refine the orbital period given by Crampton, Cowley and Hutchings.

Data acquired in E4 mode were subdivided into four phase ranges and spectral fits were then made to each data set. Power-law, black-body and thermal bremsstrahlung models were all considered. For the data in the phase range $\sim 0.65 - 1.5$ however, the best fit was to a simple power-law with a broad iron line feature at an energy of ~ 6.6 keV. In the phase

3A 1822-371

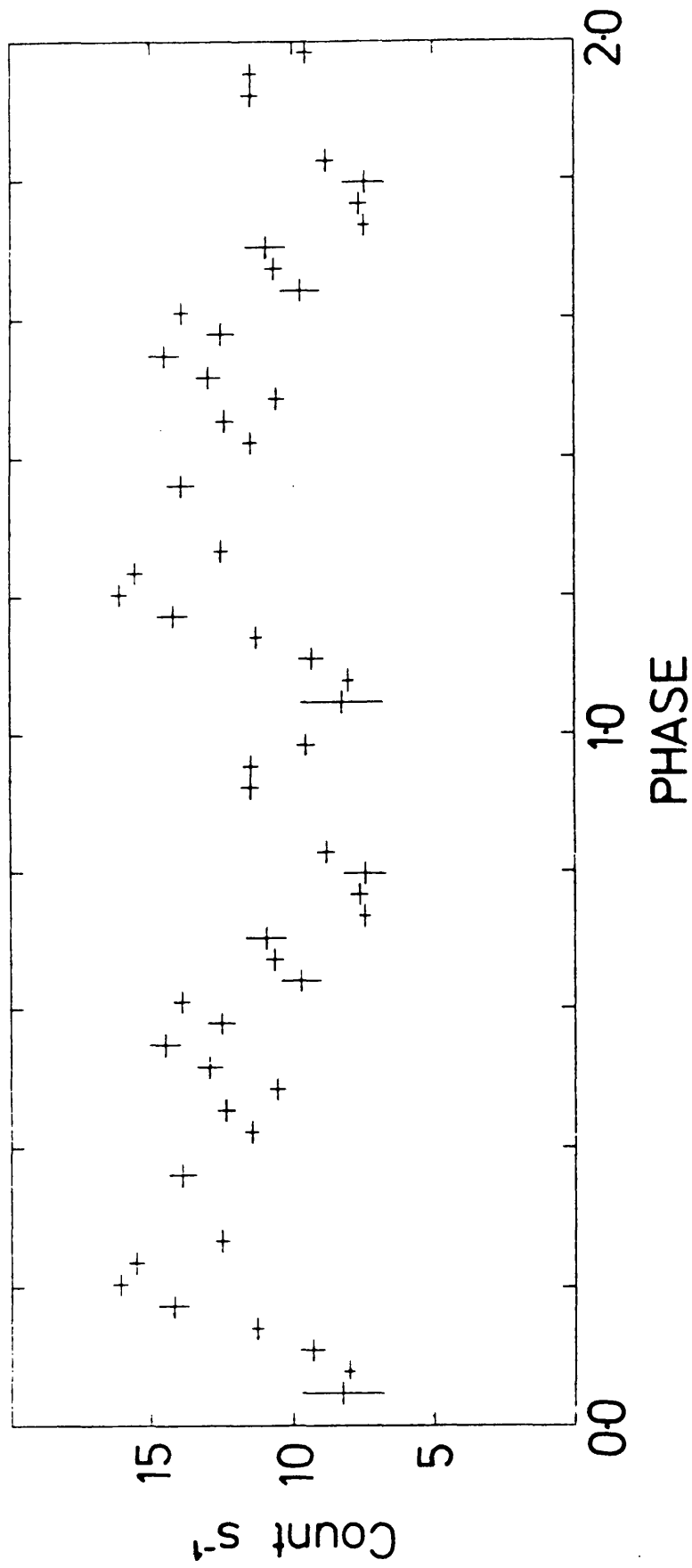


Fig 4.13 The Ariel-6 data folded into 32 phase bins at the orbital period given in the text.

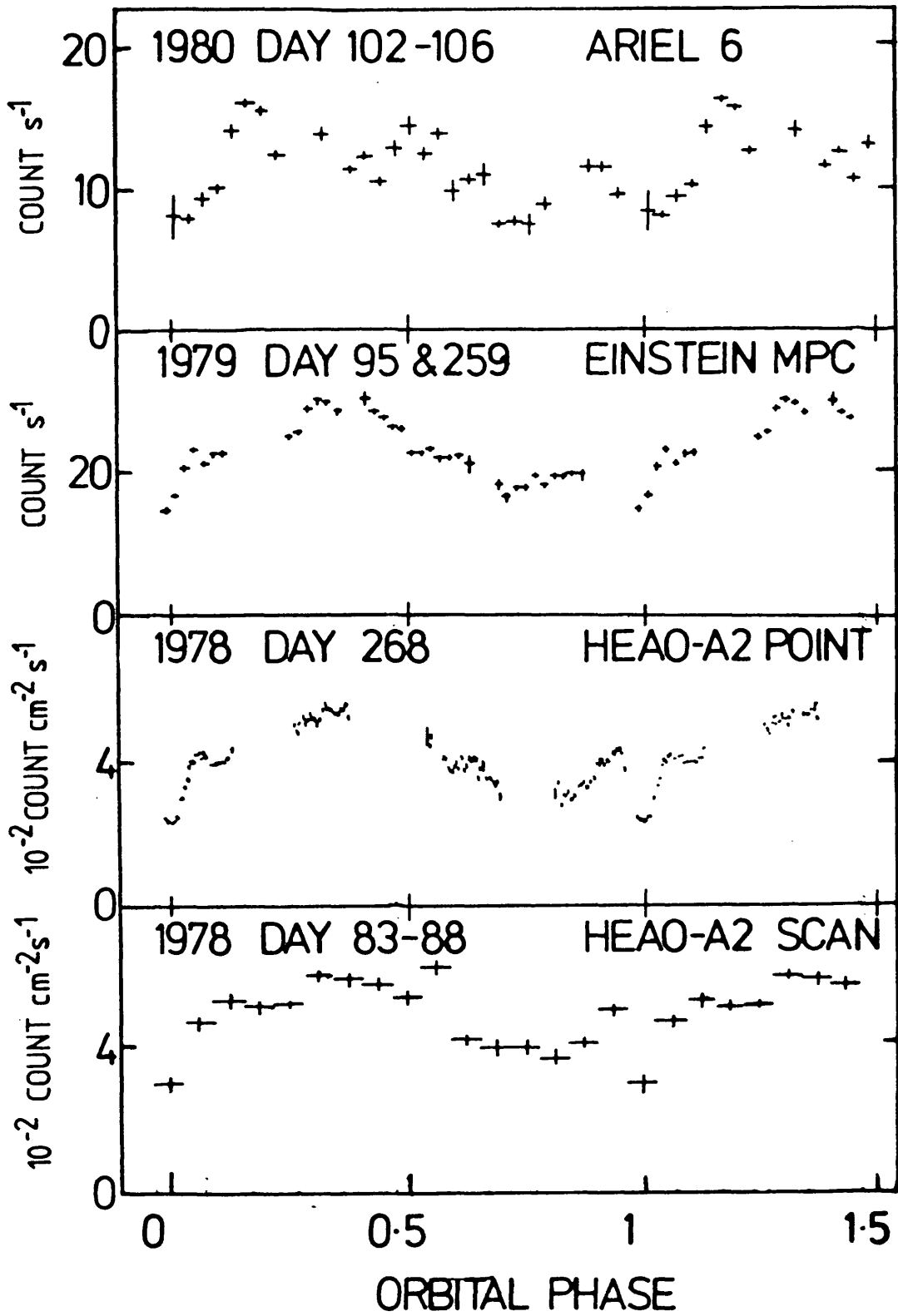


Fig 4.14 Folded lightcurves obtained by different instruments.

range $\sim 0.5 - 0.65$ the data required the model to have a softer power-law index with a corresponding increase in low energy absorption. A significant improvement to the fit at this phase was made by the addition of a broad iron line feature at ~ 6.5 keV and a cut-off in the spectrum at energies > 14 keV. The best fitting spectral parameters, for the two different phase ranges, are given in Table 4.6 and the source spectra are shown in Fig 4.15.

In both cases the models were required to contain broad iron lines, equivalent widths ~ 500 eV and there was no evidence for any variation in this equivalent width around the orbital phase. The statistics were not sufficient to enable a distinction to be made between a fluorescent (~ 6.4 keV) or thermal (~ 6.7 keV) origin for the line.

There was no requirement for, nor evidence of, a high energy cut-off in the harder (b in Fig 4.15) spectrum. The softer (a) spectrum for phases $\sim 0.5 - 0.65$ is in very good agreement with that seen by the HEAO A2 instrument (White et al. 1981). They report a flux of $\sim 1 \times 10^{-9}$ erg cm $^{-2}$ s $^{-1}$, whilst the average flux in the same energy band during the Ariel-6 observations was $\sim 2 \times 10^{-9}$ erg cm $^{-2}$ s $^{-1}$, assuming no correction for the source offset in the instruments field of view (which would be a 15 - 25% increase in flux).

Clearly the Ariel-6 data shows the X-ray lightcurve to have changed from that previously reported, also the observed spectral variability has not been seen previously.

TABLE 4.6 Results of spectral fitting for 3A1822-371

Spectrum:	(a)	(b)
Phase Range:	0.5 - 0.65	0.65 - 1.5
α	1.4 ± 0.09	1.22 ± 0.06
N_H ($\times 10^{-22}$ cm ²)	1.46 ± 0.46	0.58 ± 0.29
Normalisation	0.092	0.054
Line Energy (keV)	6.5 ± 0.3	6.65 ± 0.25
Equivalent Width (eV)	510 ± 180	500 ± 160
P (keV)	~ 14	-
R (keV)	~ 8	-
Flux in 1-20 keV band ($\times 10^{-9}$ eVg cm ⁻² s ⁻¹)	1.07	1.22

All errors are 90% confidence limits

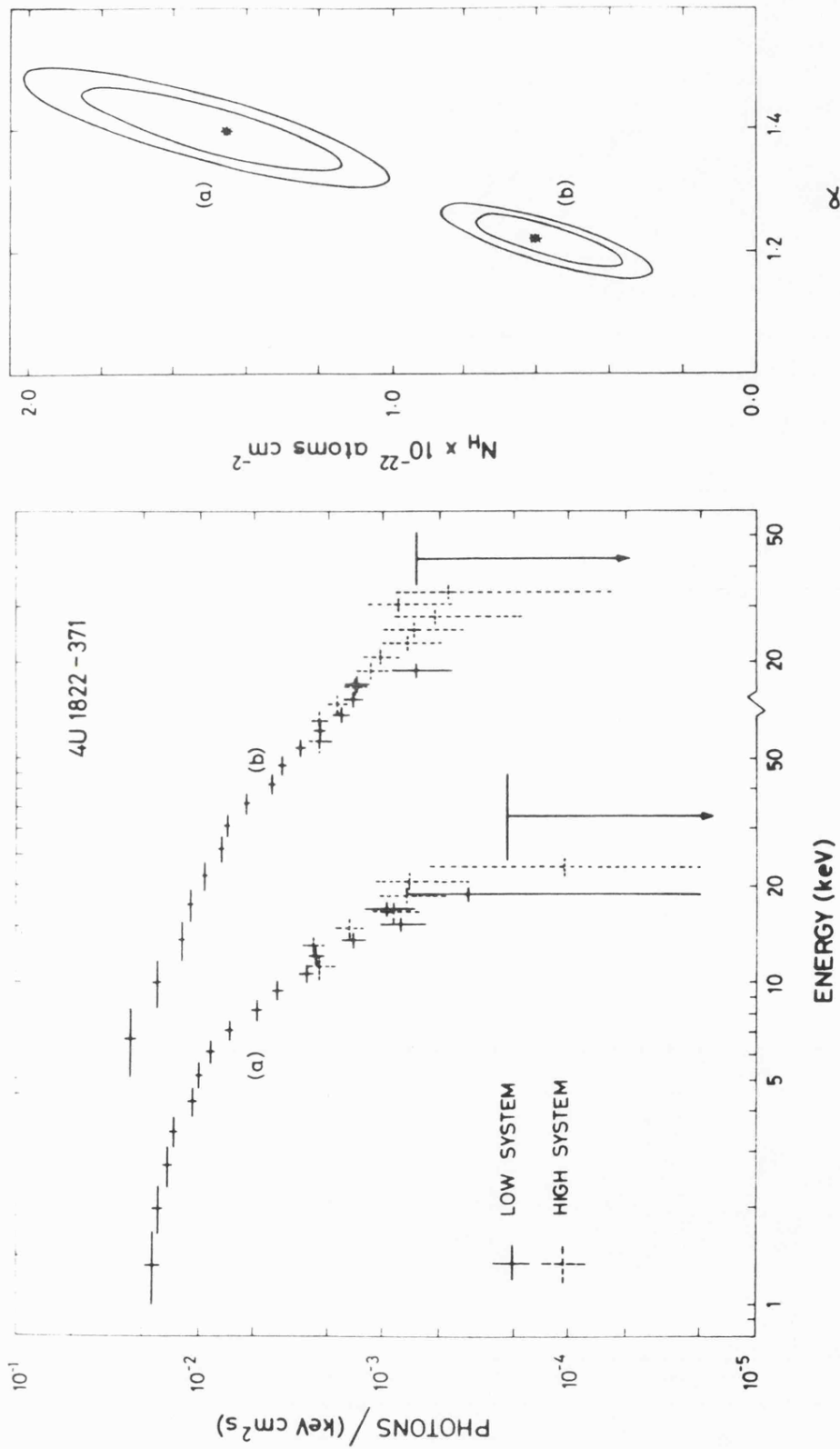


Fig 4.15 3A1822-371 : X-ray spectra for two different phase ranges.

4.4.2 Discussion

Since there appears to be overwhelming evidence in support of the ADC model from observations in several wavebands, it was essential to determine whether our data were compatible with an ADC. For the region of anomalously high flux, at phase ~ 0.2 , data were obtained on three independent orbital cycles, the fluxes being compatible within the expected scatter. This feature was used above to establish the periodic nature of the source during the Ariel-6 observation. The spectrum at this phase is consistent with that for the phase range $\sim 0.65 - 0.5$, which suggests, using the ADC interpretation, that there has been a decrease in the height of the edge of the disc at this phase and that we are viewing an increased fraction of the central source.

For the major part of the orbital phase the spectrum (b in Fig 4.15) was well fitted with $\alpha \sim 1.22$, which is harder than that reported by White et al. (1981), who found $\alpha \sim 1.35$ and that the spectrum was sharply cut-off at energies > 17 keV. The optical depth to Compton scattering of the material along the line of sight is related to the energy at which the cut-off commences, see (Section 4.2). If such a cut-off existed in our spectrum (b) then it must be at an energy $\gtrsim 35$ keV, the point at which we do not have a significant source detection, thereby implying that the optical depth was $\lesssim 4$, during the majority of our observation.

Fabian, Guilbert and Ross (1982) have modelled the X-ray spectrum of 3A1822-371 by means of the transfer of X-rays through a highly ionised, scattering medium. They find that a large fraction of the optical depth must reside within $\sim 2 \times 10^8$ cm

of the neutron star. In turn this is enclosed by a larger region of, $\sim 10^{10}$ cm diameter, which is required to account for the observed partial eclipse duration. Their model shows that the radius of the central optically thick region is dependent upon the X-ray luminosity (L_x), the optical depth (τ) and the ionisation state of the material (ξ),

$$R \propto L_x \cdot \tau^{-1} \cdot \xi^{-1}$$

- see Fabian, Guilbert and Ross.

During our observation the measured 1 - 50 keV flux was approximately twice that seen by White et al. (1981), who also reported that $\tau \sim 6$. An increase in the X-ray luminosity combined with a decrease in τ implies that either R , ξ or both, have increased. A study of the transfer of X-rays through a spherically symmetric gas cloud has shown that the ionization parameter, ξ , is required to have a value $\gtrsim 5 \times 10^3$ in order to account for the absence of an iron absorption edge in either the Ariel-6 or HEAO A2 data (Hatchet, Buff and McCray 1976). The line flux reported by White et al. (1981) was $(5.5 \pm 1.3) \times 10^{-3}$ photons $\text{cm}^{-2} \text{s}^{-1}$, whilst we detect $(3 \pm 1) \times 10^{-3}$ photons $\text{cm}^{-2} \text{s}^{-1}$. Reference to Fig 4 of Hatchet, Buff and McCray indicates that a reduction in the line flux by a factor ~ 3 corresponds to an increase in ξ of $\lesssim 60\%$, inferring, therefore, that the central optically thick region had expanded at some time prior to the Ariel-6 observations by a factor ~ 2 . Absence of spectral variability at phases other than $\sim 0.5 - 0.65$ during the ~ 4 days of our observation suggests that the ADC had reached a different equilibrium to that previously seen.

In the region of spectral softening, phases $\sim 0.5 - 0.65$, only one observation was available. The high energy cut-off in the spectrum (see Fig 4.15a), implies that at this time the optical depth, $\tau \sim 5 - 6$. If this was an orbitally phase dependent phenomenon then a decrease in flux at this phase would be anticipated, as the X-rays would then preferentially escape through the regions of lower optical depth. In fact what is observed is a slight increase in flux, implying that the whole of the source is encased in an extra layer of scattering material and that the observed softening is of a transient nature. Using our data it was not possible to accurately determine the timescale of the event, however, observations made ~ 3 hrs prior to the softening show no evidence for change from the harder, $\alpha \sim 1.22$ spectrum.

It would seem that changes in the accretion rate, \dot{m} (hence L_x and the corresponding ADC equilibrium), if sustained, allow a new equilibrium to be established, as shown by the stability of the harder X-ray spectrum in our data. Conversely, changes in \dot{m} occurring on shorter timescales, less than hours, do not require variations in the size or ionization state of the coroneae.

In conclusion, we find that our observations, whilst of a limited coverage, are consistent with the simple model of an ADC. On the basis that no short term phenomena have been previously reported we conclude that such events only occur when the source is in a high luminosity state and that they are accompanied by changes in the observed spectrum which reflect the varying opacity of the material surrounding the neutron star.

Chapter 5

Ariel-6 Observations of
Active Galaxies

It is not yet a decade since the publication of the third Uhuru catalogue and the detection of three extragalactic compact sources NGC 4151, 3C273 and NGC 5128 at X-ray energies (Giacconi et al. 1974). With the launch of the Ariel-5 satellite carrying the Sky Survey Instrument (SSI), the number of extragalactic X-ray sources reliably identified as active galaxies rapidly increased; culminating in the publication of the 3A high-latitude catalogue (McHardy et al. 1981). One of the most significant features of the Ariel-5 results was the frequency of source identification with members of the Seyfert class of galaxies. Observations with the SAS-3, OSO-8 and HEAO-1 satellites have further increased the number of active galaxies detected at medium energies to over 50 (Pounds 1980).

The outstanding feature of the active galaxies is the presence of a bright, active core, which for sources other than the QSO's is seen to be contained within a 'normal' galaxy. The optical emission from this nucleus is predominantly non-thermal (i.e. non-stellar) and is therefore suggestive of highly energetic processes occurring in the core of the galaxy. Association of the X-ray emission with the nucleus of the active galaxy, even since the earliest observations, is therefore not surprising; though at first the positional uncertainty in the location of the X-ray source did not specifically suggest this.

Initially source locations were within error boxes of, typically, a few arc-minutes to a few degrees square. In some cases however, this was still sufficient to exclude the stellar fraction of the galaxy and indicate the nucleus as the X-ray source, e.g. NGC 4151 and NGC 3227 (Griffiths et al. 1979).

More recently the Einstein satellite has used its High Resolution Imager (HRI) to locate the X-ray sources in several active galaxies to within $\sim 5''$ of the visible light nucleus (Tananbaum 1980). For these sources the HRI data were well fitted by a point source, with no evidence for the presence of any diffuse emission.

Elvis et al. (1978) found that the X-ray luminosity of the Seyfert type 1 galaxies was correlated with that of the non-thermal infra-red and optical continua; also with the luminosity in the broad H_{α} emission line. Further work showed that these correlations extended to the X-ray selected QSO's and Seyfert type 2 galaxies, suggesting that the same physical processes were acting in each class of objects over a wide range of intrinsic luminosity (see Kriss et al. 1980, Wilson 1979).

The greatest observational constraint placed on the possible energy generating mechanisms has been the detection of X-ray variability on very short time-scales. The variability has been observed on time-scales ranging from months to flares lasting no more than a few days (Marshall, Warwick and Pounds 1981). By light-travel-time arguments this implies that the emitting region is $\sim 10^{15-16}$ cm. No spectral information was available during the flares, however it is highly unlikely that the observed variability was simply due to the changing hydrogen column density as suggested by Barr et al. (1977), since subsequent spectral observations of many of these sources reveals little, if any, intrinsic low energy absorption (Mushotzky et al. 1980, Hayes et al. 1981). The high signal to noise possible with the Einstein HRI has enabled detection of variability on ~ 6000 s time-scales, thereby further reducing the dimensions

of the emitting region to $\lesssim 10^{14}$ cm (Tananbaum 1980). There have been two reports of variability on shorter timescales, Tananbaum et al. (1978) observed ~ 700 s flaring in NGC 4151 though further extensive observations have failed to confirm this. (Mushotzky et al. 1978); similarly Tennant et al. (1982) detected variability over ~ 500 s in NGC 6814, though the remainder of their sample of 31 active galaxies showed no such characteristics and it is possible that a different mechanism is responsible.

5.2 Energy Generation

Many theoretical models have been proposed to account for the vast quantities of energy generated within the small volumes associated with the X-ray sources in active galactic nuclei. Accretion onto a central massive black hole is the most likely candidate (Rees 1980). Simple radial infall of material is not capable of producing the observed X-ray emission since the gravitational energy of the accreting matter is not released. This difficulty can be circumvented in two ways however, either by assuming that the material has some angular momentum, in which case it may form an accretion disc (see Lynden-Bell 1969, or Shakura and Sunyaev 1973); or alternatively, there may be shocks present in the infalling material, hence raising its temperature whilst at the same time being capable of producing the relativistic electrons which are required to generate the observed non-thermal radio, infra-red and optical fluxes (Blandford 1977). The reviews given by Fabian and Rees (1978), Fabian (1979) and Rees (1980) provide a satisfactory overview of the proposed energy generating and spectral formation processes, the following is therefore a somewhat condensed version of their discussion.

Doppler broadened lines indicative of mass motions at velocities $\sim 0.03 c$ have been observed in the optical filaments present in the nuclei of several Seyfert galaxies. Collisional shocks between two or more such filaments are quite capable of heating the gas to temperatures of $\sim 10^8$ K and hence radiating predominantly at X-ray energies by the thermal bremsstrahlung process. These same shocks also produce high energy electrons if there is a magnetic field present in the nucleus. Very rapid variability, such as that reported by Tennant et al. (1982) is

difficult to account for with a thermal cooling time as it would require the particle density to be $\gtrsim 10^{13} \text{ cm}^{-3}$, hence producing a high optical depth to electron scattering. The resulting, comptonised thermal emission would be in a Wein spectrum extending to γ -ray energies (Lightman, Giacconi and Tananbaum 1978).

An alternative to a thermal emission mechanism is the comptonisation of a source of soft, optical or infra-red photons. Very rapid variability may be produced in this model, providing that the initial radiation density is high, $\sim 10^5 \text{ erg cm}^{-3}$. Such high values may be anticipated however as we are considering regions of $\approx 1.5 \times 10^{13} \text{ cm}$ which have total optical/infra-red luminosities of $\sim 10^{45} \text{ erg s}^{-1}$. The spectrum emitted by the plasma will extend from the input energy of the photons to that of the maximum energy of the electron distribution. A disadvantage with this pure comptonisation model is that it requires the electron energy to be $\sim m_e c^2$ in order to produce the observed X-ray spectrum, this would seem unlikely within the chaotic volume of galactic nucleus where rapid energy loss would be anticipated. Alternatively if the source of soft photons lies outward from the high temperature region this problem does not arise. One observable consequence of this model is that the soft X-ray photons will diffuse out of the emission region faster than the hard X-rays, this effect may have been detected in NGC 6814, though the results are only marginally significant (Tennant et al. 1982).

A third process which has been considered is the inverse scattering of the soft photons by relativistic electrons. The observation of variable non-thermal radio, infra-red and optical

emission, which in some cases is highly polarised, has been taken as a fingerprint for the presence of relativistic electrons and synchrotron radiation. Upscattering of the synchrotron photons is by the very electrons which spawned them, the process being named the Synchrotron Self Compton mechanism (SSC). Not only is variability on very short time-scales possible but a further advantage is that high initial radiation densities are not required. A possible problem with the SSC model is that unless the electron distribution is truncated at high energies the photons undergo multiple scattering and the emission peaks in the γ -ray region.

It would be naive to suppose that any of the physical processes described above were acting in isolation, however it is clearly plausible that one mechanism might dominate the X-ray emission of, say, the Seyfert's, whilst a different one would be evident in the BL Lac's. Discrimination between alternatives might therefore be possible, even with X-ray spectral observations obtained over a limited dynamic range.

5.3 Ariel-6 Observations

Poor satellite attitudes have made it impossible to produce useful light curves for any of the observed active galaxies as the flux from even the brightest source, NGC 4151 was insufficient to enable the spin modulation technique (Section 3.1.7), to be used. For each of the four sources observed their offset in the instrument's field of view, due to the poor attitude, was such that a significant detection could not be made in the useful data collected per orbit, except for NGC 4151. At the present time the most useful estimate is that the sources were offset from the centre of the instrument's field of view by $1^{\circ} - 2^{\circ}$, this value has been used in determining the fluxes quoted in the remainder of this chapter.

Simultaneous optical and infra-red monitoring was available for the observation of III Zw 2; whilst γ -ray observations of MCG 8-11-11 were fortuitously made just prior to our own. Absence of accurate fluxes and lightcurves has prevented detailed modelling of the emission processes, however comparisons with the results obtained by other instruments have been used to infer the most probable mechanisms.

5.3.1 Seyfert Galaxies

Two distinct classes of Seyfert galaxy are commonly referred to, being defined by the nature of their optical emission lines. Several Seyferts however, have properties which lie at points between the two extremes (Osterbrock 1977). Weedman (1977) defined certain characteristics which he used for classifying the Seyferts¹, these were:

Seyfert type 1: broad Balmer and permitted lines with a typical FWZI $\sim 10^4$ km s⁻¹ and also narrow forbidden lines.

Seyfert type 2: all lines are narrow, FWZI $\lesssim 10^3$ kms⁻¹.

The simplest explanation for these differences is that in the Seyfert type 1 galaxies the broad and narrow lines originate in different regions. The broad line region (BLR) lying within the narrow line region. Weedman also suggested that the width of the broad lines indicated a higher proportion of very dense gas in the nuclei of type 1 Seyferts than in type 2's. He also found that the gas in type 1's was very inhomogeneously distributed and that their nuclei strongly resemble those of the QSO's. The Seyferts observed by Ariel-6 were all type 1's, though it has been suggested that NGC 4151 might more accurately be classified as a type 1.5 (Osterbrock 1977).

NGC 4151

This is the 'local' member of the Seyfert 1 class and whilst its X-ray luminosity, $\sim 6 \times 10^{42}$ erg s⁻¹ Lawrence (1980), is towards the lower end of the observed distribution, Marshall, Warwick and Pounds (1981), its proximity gives it the highest observable flux. The X-ray flux has been found to be highly variable on a time-scale of days, with one report of a factor ~ 6 increase in $\lesssim 700$ s (see Elvis 1976, Mushotzky et al. 1978, Tananbaum et al. 1978 and Lawrence 1980). The nature of this variability has been discussed by Lawrence in terms of a shot-noise model in which the emission is characterised by repeated flares which have rise times of ~ 0.5 days and decay over 2 - 4 days. This behaviour contrasts strongly with the stability observed at optical and infra-red wavelengths and suggests that

the X-ray emission arises in a physically different region (Lawrence et al. 1981).

Two observations of NGC 4151 were made by Ariel-6 during January and February 1980, the observations were of ~ 10 and ~ 7 days respectively, being separated by ~ 20 days. Specific details of the observation dates and the instrument modes used are given in Table 5.1.

Due to the stability of the detector background (Section 3.2.2), we had the capability to detect short term variability on time-scales $\sim 10^3$ s. We have systematically searched our data for variability by subdividing the ~ 20 minute observation made per orbit into ~ 5 minute samples (each an $\sim 3\sigma$ detection), a χ^2 -test was then used to detect variations from the mean within the 4 or 5 samples. There was no evidence for any variability that could not be accounted for by counting statistics alone, we are therefore unable to confirm the reported short timescale variability.

The data within each of the two observations were summed; upon comparison of the two spectra there were no discernable differences and the data were therefore merged in order to improve statistics. Spectral fitting was by a range of power-law models with a low energy cut off due to absorption by a column of cool gas. Inclusion of an Iron line into the model gave an improved and statistically satisfactory fit with a reduced $\chi^2 \sim 1.2$. The best fitting spectral parameters are given in Table 5.2 and the source spectrum is shown in Fig 5.1.

The values of N_{H} and α obtained from our data are in very good agreement with those found during 1977 June by OSO-8 (Mushotzky et al. 1978). Features in the spectrum of NGC 4151

Table 5.1 Ariel-6 Observations of Active Galaxies

Source	Date	Exposure* (s)
NGC 4151	1980 Jan 8 - 20 Feb 6 - 16	10 ⁴
MCG 8-11-11	1979 Nov 18 - 21	3 200
III Zw2	1979 Sep 27 - Oct 5	1.3 x 10 ⁴
Mkn 421	1980 Jan 1 - 3 Jan 23 - 31	4 000

* Useful spectral data.

Table 5.2 Active Galaxy Spectral Parameters

Source	A (photons/keV cm ² s)	α	$N_H \times 10^{-22}$ (cm ⁻²)	Line Energy (keV)	Eqv. Width (keV)
NGC 4151	0.038	1.51 ± 0.15	8 ± 1.8	6.75 ± 0.3	0.47 ± 0.18
MCG 8-11-11	0.018	2.15 ± 0.4 0.6	< 3.5	6.2 ± 0.5	1.6 ± 1.2 1.3
III Zw 2	0.004	1.72 ± 0.5 0.6	< 3.6	-	-
Mkn 421	0.043	2.9 ± 0.4	< 0.6	-	-
	(0.052)	3.4 ± 0.4			
	(0.004)	1.0 ± 0.8			

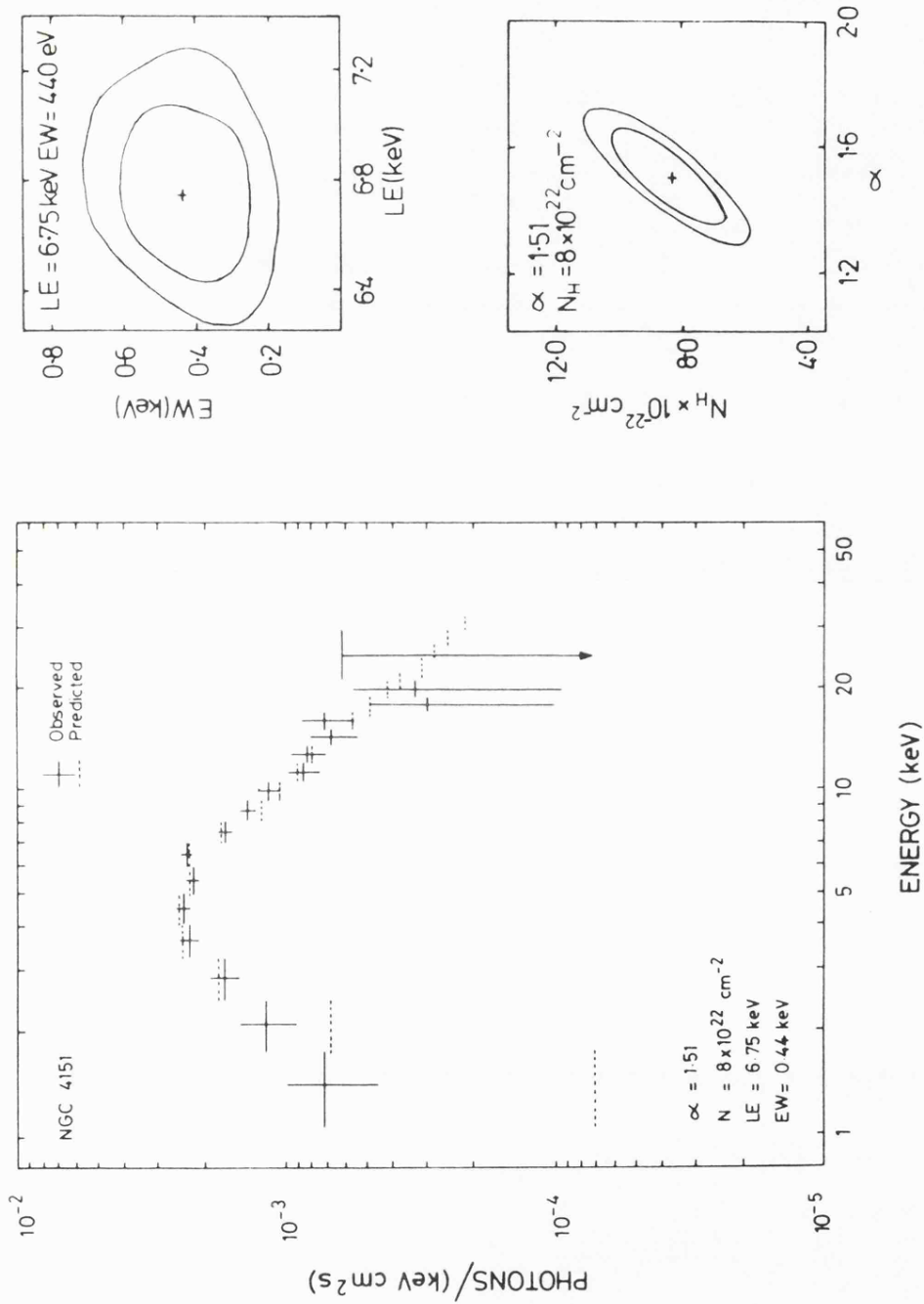


Fig 5.1 NGC 4151 : The Ariel-6 spectrum, also shown are the confidence limits on the model parameters.

have been reported previously, including an absorption edge at ~ 6.9 keV, Barr et al. (1977) and a possible fluorescence line at ~ 6.4 keV (Mushotzky et al.). More recently observations made with the HEAO-1 A2 instrument have detected an iron absorption edge at ~ 7.1 keV and the associated fluorescence line at 6.4 keV (Holt et al. 1980).

With only two PHA channels covering the 6-7 keV energy range in the Ariel-6 data, there was no requirement for the inclusion of an absorption edge. However, as the detected feature was midway between the expected positions of a cold iron edge and emission feature the possibility exists that our 'line' is in fact a hybrid created through our undersampling of the source spectrum.

It is readily apparent from Fig 5.1 that the best fitting continuum indicates a significant ($\sim 4.5\sigma$) excess below ~ 2.5 keV. By excluding the two lowest PHA channels from the fitting procedure we found that the required column density increased to $\sim 9.3 \times 10^{22} \text{ cm}^{-2}$, which is slightly higher than, but still consistent with, the value obtained by OSO-8 (Mushotzky et al. 1978). Our detection of a significant excess at low energies is consistent with that previously observed by the Einstein Solid State Spectrometer (SSS) on 1979 May 27th (Holt et al. 1980). By using the effective area of the SSS, Giacconi et al. (1979) and the data of Holt et al. we have attempted to deconvolve source spectrum from the SSS data, this is shown in Fig 5.2. Also plotted is the OSO-8 spectrum from Mushotzky et al. It can be seen that the combination of OSO-8 and SSS results accurately represents the spectrum of the source as seen during the Ariel-6 observations, but with a slightly different

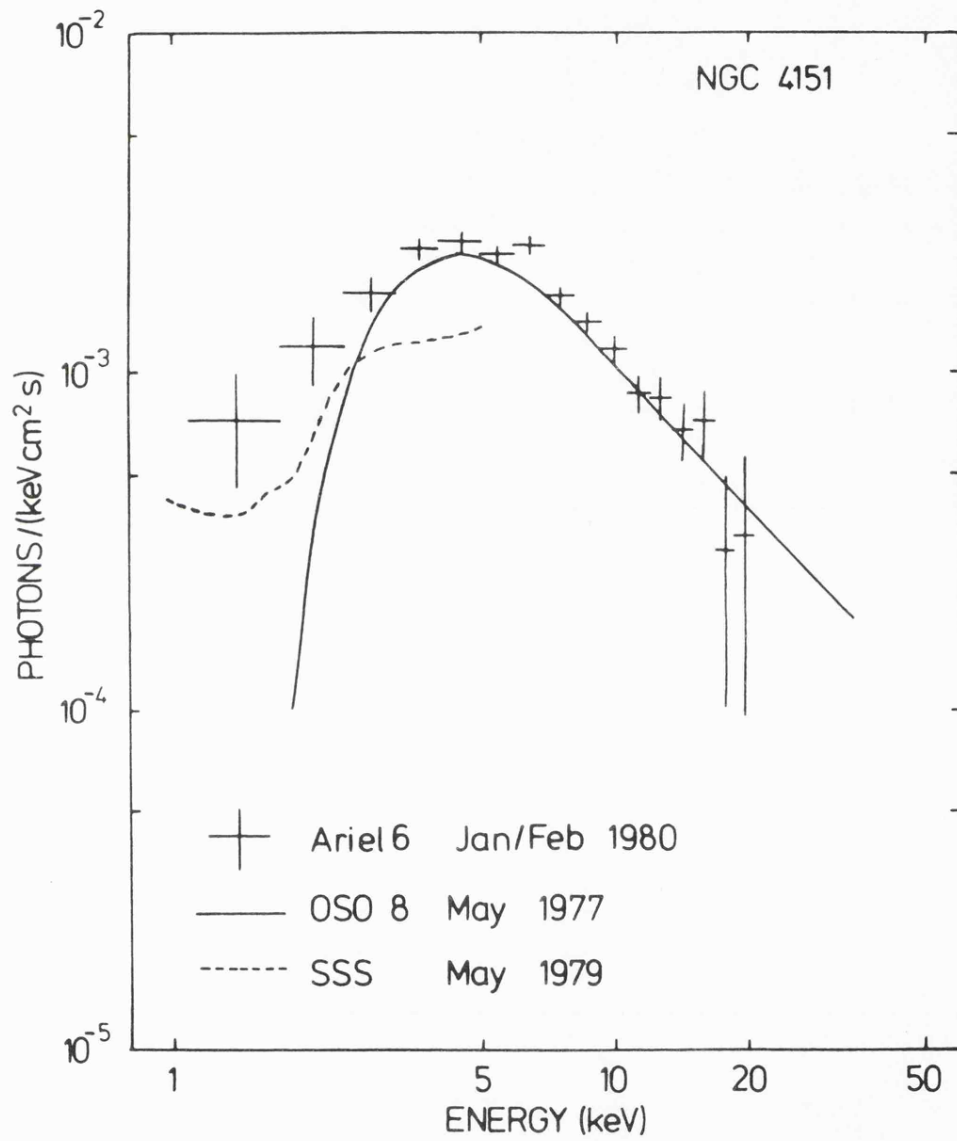


Fig 5.2

NGC 4151 : A comparison of Ariel-6, OSO-8 and SSS data.

normalisation. The detected flux was $(13 \pm 5) \times 10^{-11}$ erg $\text{cm}^{-2} \text{s}^{-1}$ and is within the range found during Ariel-5 observations over an ~ 4 year period (Lawrence 1980).

Discussion

The excess flux at low energies has been interpreted as the incomplete screening of the central emitting region by the clouds of cool gas in the BLR (Holt et al.). A covering factor of $\sim 90\%$ was calculated. At the time of writing the only significant detection of spectral variability in NGC 4151 at medium X-ray energies has been the observation of a large change in the low energy absorbing column, Barr et al. (1977), which is essentially a change in the covering factor of the central source. There have now been many subsequent observations by different instruments and no further reports of an excessive low energy column, which implies that the covering factor is approximately constant and is not as highly inhomogeneous as expected (Weedman 1977).

Hard X-ray measurements have shown that the spectrum extends to a few MeV with no evidence for a cut off and that out to 100 keV the shape has remained constant for ~ 5 years, (Coe et al. 1981, Paciesas et al. 1979, Baity et al. 1979). Order of magnitude variations have been observed in the flux at γ -ray energies and it is thought that this emission arises in a region separate from that of the X-rays (Coe et al. 1981).

The apparent stability of the X-ray continuum and its extension out to ~ 100 keV, over the period 1977 - 80 would appear to favour a comptonised thermal emission process rather than a pure comptonisation one, as the origin of the power-law

spectrum. Variability on time-scales of days, such as that reported by Lawrence (1980), may then be due to changes in the accretion rate onto the massive central body. Similarly the SSC model may be ruled out as this would entail reprocessing of the optical or infra-red flux, (see Beall et al. 1981), which has been shown to be stable, Lawrence et al. (1981) and is therefore incapable of generating the observed X-ray lightcurve (see Lawrence 1980 or Mushotzky et al. 1978).

In conclusion we have established that the spectral shape of NGC 4151 has most likely remained stable over the period 1977 - 80 and shown how this indicates a comptonised thermal origin for the observed X-ray spectrum. Secondly our observations have confirmed the presence of the low energy excess and shown it to be stable over a period of several months.

MCG 8-11-11

This source has the distinction of being the first Seyfert to be discovered as a result of its X-ray emission. Identified in the Morphological Catalogue of Galaxies as a barred spiral it was, subsequent to the X-ray detection, found to exhibit the broad Balmer lines characteristic of a Seyfert type 1 and to contain a compact radio source within its nucleus (Ward et al. 1977). Optical variability has been observed over time-scales of months and even over ~ 2 days (Miller 1979). MCG 8-11-11 has also been observed to vary at X-ray energies, Ward et al. 1977 reporting variability in $\lesssim 30$ days.

Ariel-6 Observations

Our observations were made during 1979 November, full

details of which are given in Table 5.1. It has been shown that the X-ray emission of the Seyfert galaxies is best modelled by power-law rather than thermal spectra (Mushotzky et al. 1980). Since we are unable to distinguish between either model in our data, we have therefore only considered power-law models. Using a power-law with low energy absorption we obtained a fit to the data that was almost acceptable; however by including an Iron line into the model we obtained a significant decrease in χ^2 , from ~ 1.3 to ~ 0.4 . The derived source spectrum is shown in Fig 5.3 and the parameters of Mushotzky et al. (1980) are also marked. Table 5.2 gives the values of our best fitting parameters. Using the modified F-Test of Bethelsdorf and Culhane (1979) we find the Iron line to be significant at the $\sim 98\%$ confidence level.

There is some evidence that the spectrum has softened since the HEAO-1 observation. Our 2 - 10 keV flux of $(3 \pm 1) \times 10^{-11} \text{ erg cm}^{-2} \text{ s}^{-1}$ is lower than that detected by the HEAO-1 A2 instrument during 1977 (Mushotzky et al.). Two further X-ray observations made in 1978 also found a lower X-ray flux than that of Mushotzky et al. (Mushotzky and Marshall 1980).

Discussion

The evidence of a decrease in flux and the presence of an emission feature is not overpowering, however there is a strong indication that MCG 8-11-11 was behaving in a manner identical to that observed in NGC 5548, where as the luminosity decreased an iron line 'emerged' from the continuum (Hayes et al. 1980). If we consider the type of variability to be the same in both

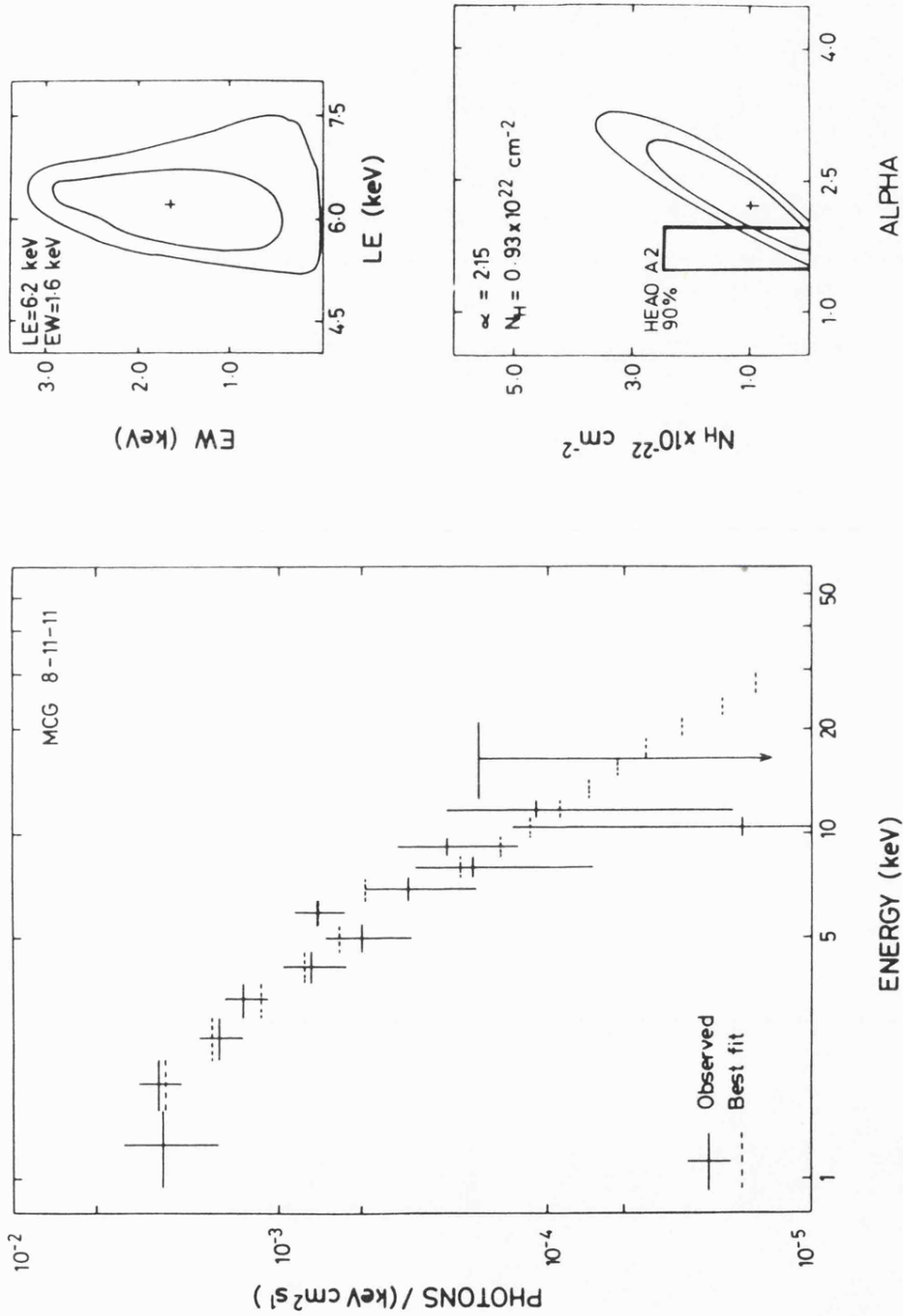


Fig 5.3 MCG 8-11-11 : The spectrum and confidence contours on the continuum and feature.

cases then we may assume that the models proposed for NGC 5548 are applicable to MCG 8-11-11.

It has been suggested that the line was generated by the fluorescence of the cool material in the BLR by the incident X-rays (Hayes et al.). However, the absence of a severe low energy cut-off in the X-ray spectra of both MCG 8-11-11 and NGC 5548 would appear to contradict this, unless by chance the covering factor was high in all directions but the line of sight, in both cases. A further requirement of the fluorescence hypothesis is that the ionising flux ($E > 7.1$ keV) must have been a factor ~ 3 greater than that detected, several weeks prior to the observation in which the line was evident. This increased flux was necessary in order to make the required covering factor less than 4π steradians, the equivalent width of the feature being directly proportional to the flux above 7.1 keV and the solid angle of the 'target' (the cool clouds), as seen from the X-ray source (see Section 4.3.4); the delay of several weeks is the light travel time from the source to the BLR.

Perrotti et al. (1981) report an observation of MCG 8-11-11 with the MIS0 balloon borne telescope during 1979 September 30th. Data were obtained in the 30 keV to 10 MeV range and were modelled by a power-law of index, $\alpha = 1.0 \pm 0.7$ with a high energy cut-off at ~ 3 MeV, where the spectrum steepens to $\alpha \sim 3.8$. The index of their low energy data is just consistent with our measurement and whilst their quoted normalisation is a factor ~ 2 below ours, it is not well determined. We cannot, therefore, reject the possibility that the high energy X-ray spectrum softened (with a consequent decrease in flux), between the MIS0 and Ariel-6 observations. If this is the case however, then

either a second break occurred in the hard X-ray spectrum at 50 - 100 keV or the flux at ~ 1 MeV varied by more than two orders of magnitude over the ~ 7 weeks separating the two measurements.

A second possible explanation for the Iron feature is that it was produced by the recombination of photoionised material local, $\lesssim 10^{16}$ cm, to the central X-ray source when the luminosity decreased (Fabian and Ross 1980). One of the conclusions of Fabian and Ross was that some of the lowest X-ray luminous sources may be observed solely by their iron line emission. Hayes et al. (1981) have searched for Iron emission in a sample of 13 Seyfert galaxies, they found no evidence for such features with an upper limit $\sim 10^{-11}$ erg cm $^{-2}$ s $^{-1}$ (3σ in 5.5 - 8.5 keV range). It must be noted however that this is not necessarily in disagreement with the proposal of Fabian and Ross, since the region of photoionisation could be in a radiative balance with the central body and simply decreasing the intrinsic luminosity purely changes the radius of the region, with only marginal effects on the ionisation state of the constituent elements (see for comparison the galactic source 3A1822-371 Section 4.4.2).

Due to the large uncertainties in the Ariel-6 spectral parameters we are unable to distinguish between emission at 6.4 or 6.7 keV and hence between the two possible Iron emission mechanisms. The many fortuitous circumstances that are required to produce the line by fluorescence however, force us to conclude that the feature is in fact a recombination line.

Tenerife (Sims et al. 1981).

Spectral fits were made to the X-ray data using simple power-law models with low energy absorption. A satisfactory fit was obtained with a power-law of index, $\alpha \sim 1.7$ and with no appreciable hydrogen column. The source spectrum is shown in Fig 5.4 and the best fitting model parameters are given in Table 5.2.

The optical fluxes measured by Sims et al. remained constant throughout the duration of their observation. Upon comparison with the observations of Lebofsky and Reike (1980), which were made close to those of Sims et al., see Table 5.3, we find that whilst the K band fluxes were consistent a significant increase ($\sim 7\sigma$) occurred in the V flux over ~ 2 weeks. The emission region is, by implication $\lesssim 4 \times 10^{16}$ cm.

Discussion

Our determined spectral parameters and estimated 2 - 10 keV flux of $(3 \pm 1) \times 10^{-11}$ erg cm⁻² s⁻¹ are all in good agreement with the earlier SAS-3 measurements. We also find the spectrum to be consistent with the average power-law index, $\alpha \sim 1.6$, observed in other Seyfert type 1 galaxies (Mushotzky et al. 1980).

It has been proposed that the fraction of the central X-ray source covered by the cool absorbing clouds in the BLR will decrease with increasing X-ray luminosity (Holt et al. 1980). Our spectrum of III Zw 2 supports this view; however Hayes et al. (1981) find no such correlation in a sample of 13 Seyfert galaxies and further work is obviously required to clarify the relationship between the cool material providing the absorption

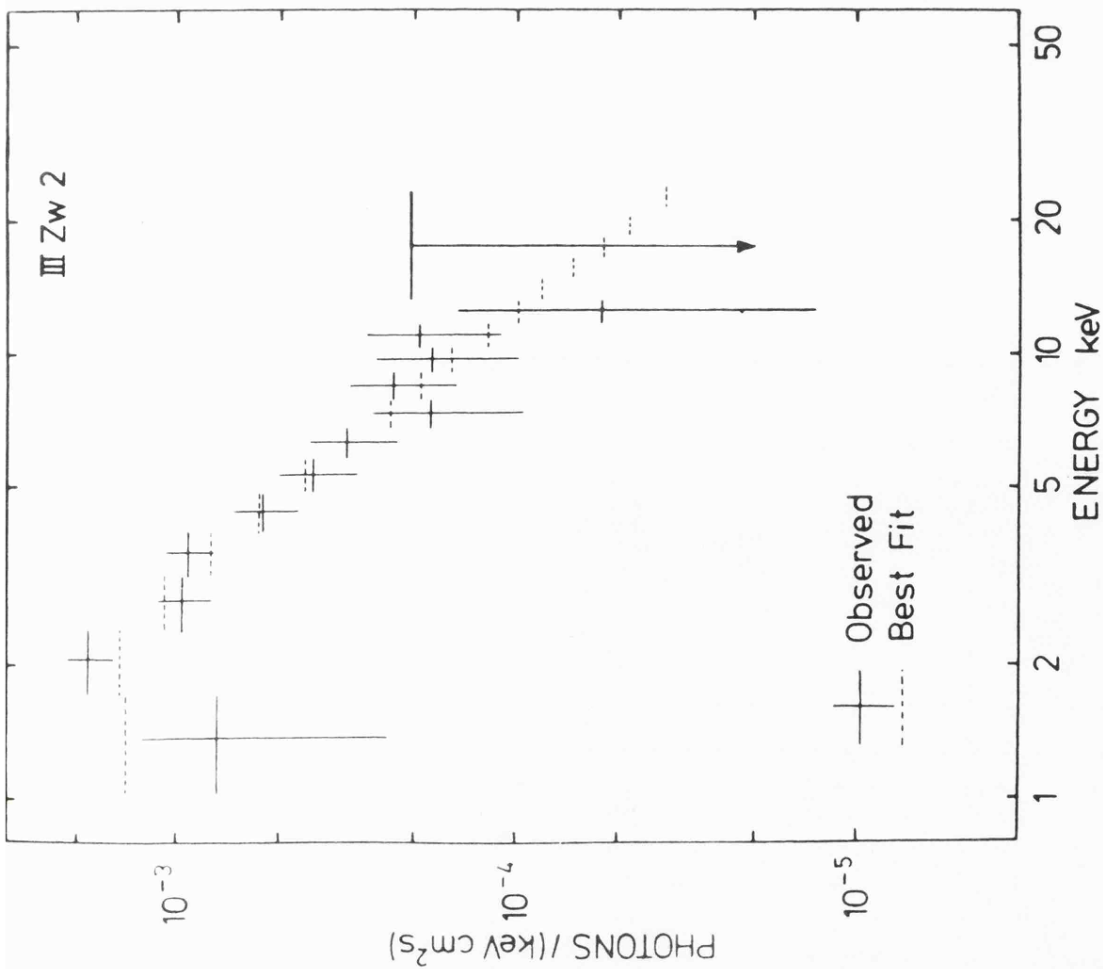


Fig 5.4 III Zw 2 spectrum obtained with Ariel-6.

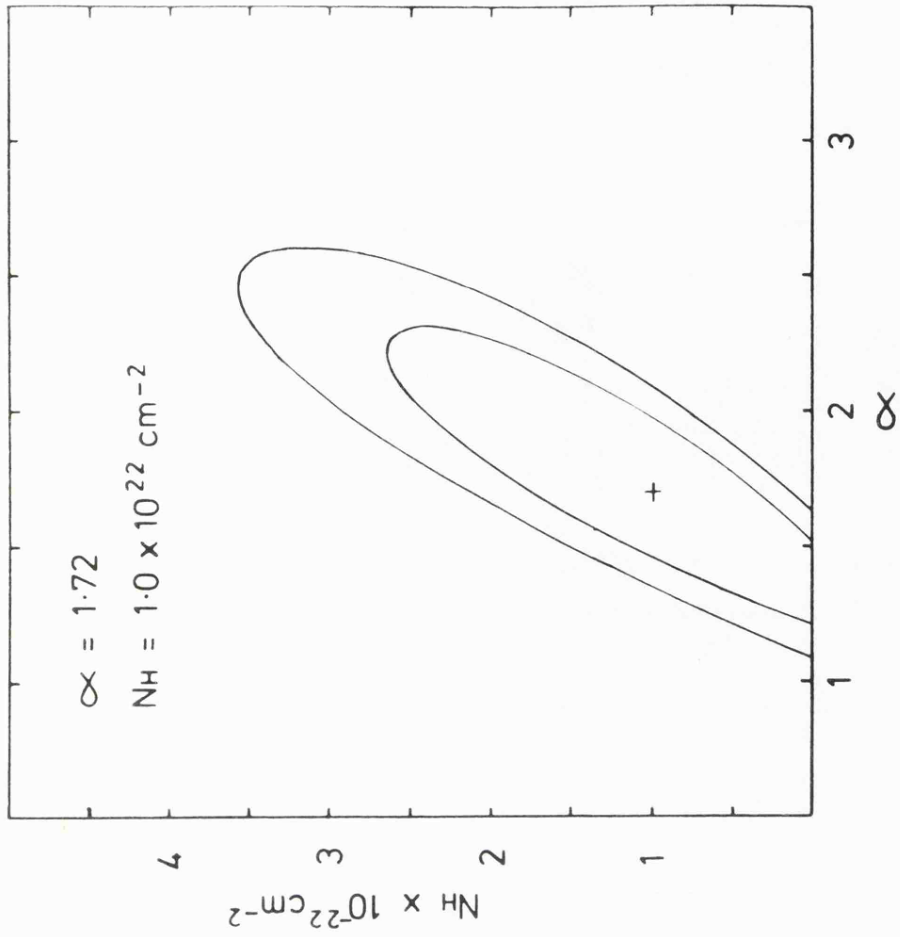


Table 5.3 V and K band fluxes for late 1979

	20 SEP*	2 - 6 OCT	12 NOV*	3 DEC*
K mJ	27.1 ± 0.5	26.6 ± 1.0	28.3 ± 0.6	26.3 ± 0.5
V mJ	4.17 ± 0.09	5.51 ± 0.17	-	4.48 ± 0.18

From Sims et al. (1981)

* Lebofsky and Reike (1980)

seen in several sources (i.e. NGC 4151, NGC 3783 and Mkn 464), and the X-ray luminosity.

Inability to obtain an accurate flux measurement combined with the absence of a measure of the radio flux at the time of the observations precludes modelling of the X-ray emission processes in a meaningful way. A determination of the magnetic field strength would also be necessary to allow the SSC mechanism to be usefully investigated.

5.3.2 BL Lac Objects

Sources of the BL Lac type were initially identified by their blue, non-thermal optical spectra with the absence of any emission or absorption lines. Their main attributes were thought to be rapid radio and large amplitude photometric variability combined with the presence of exceedingly high and often variable polarisation. As more members of the class have been discovered however, it has become apparent that there are in fact weak absorption features present (Weiler and Johnston 1980). These have enabled the determination of the red-shift, and hence luminosity, for a limited sample. It has been found that their general optical and radio properties as functions of luminosity, span the gap between the radio galaxies and the QSO's.

Mkn 421

Evidence that Mkn 421 was in fact a member of the BL Lac class of objects was provided by Miller (1975) who observed large amplitude photometric variability ~ 4.7 mag in a series of archival plates over the period 1930 - 75. Optically the

source appears to be a giant elliptical of approximately the same size as M87 with a mini BL Lac at the nucleus (Ulrich 1978, Mufson et al. 1980). The presence of weak absorption features have enabled Ulrich (1978) to determine a red-shift of ~ 0.03 and hence a distance of ~ 160 Mpc. Mkn 421 has an extended radio halo of ~ 3.5 diameter and consistent with the centre of this is a compact core of radius ~ 0.05 (Kapachi 1979, Weiler and Johnston 1980). The source was first detected at X-ray energies during 1975 when it was observed to flare by an order of magnitude (Ricketts, Cooke and Pounds 1976).

Ariel-6 Observations

Two observations of Mkn 421 were made during 1980 January, a total of $\sim 4\,000$ s data were collected (see Table 5.1). The results of spectral fitting to the data are shown in Fig 5.6, and the estimated parameters given in Table 5.2. A statistically satisfactory fit was obtained by a single power-law of photon number index, $\alpha \sim 2.9$. Visual inspection of the data suggests, however, that a two component power-law model may be more representative of the data. If we use the results of Hearn et al. (1979), who detected the presence of a significant soft X-ray flux and established an upper limit of $< 3 \times 10^{20} \text{ cm}^{-2}$ for any hydrogen column, then we may essentially neglect this parameter in our model, as the medium energy instrument is insensitive to columns below $\sim 10^{21} \text{ cm}^{-2}$. The resulting two component fits to the data show the 'soft' flux to be represented by a power-law, $\alpha = 3.4 \pm 0.4$ (or a temperature of $\sim 10^7$ K), and the 'hard' component by $\alpha = 1.0 \pm 0.8$; the difference being significant at the $\sim 2.6 \sigma$

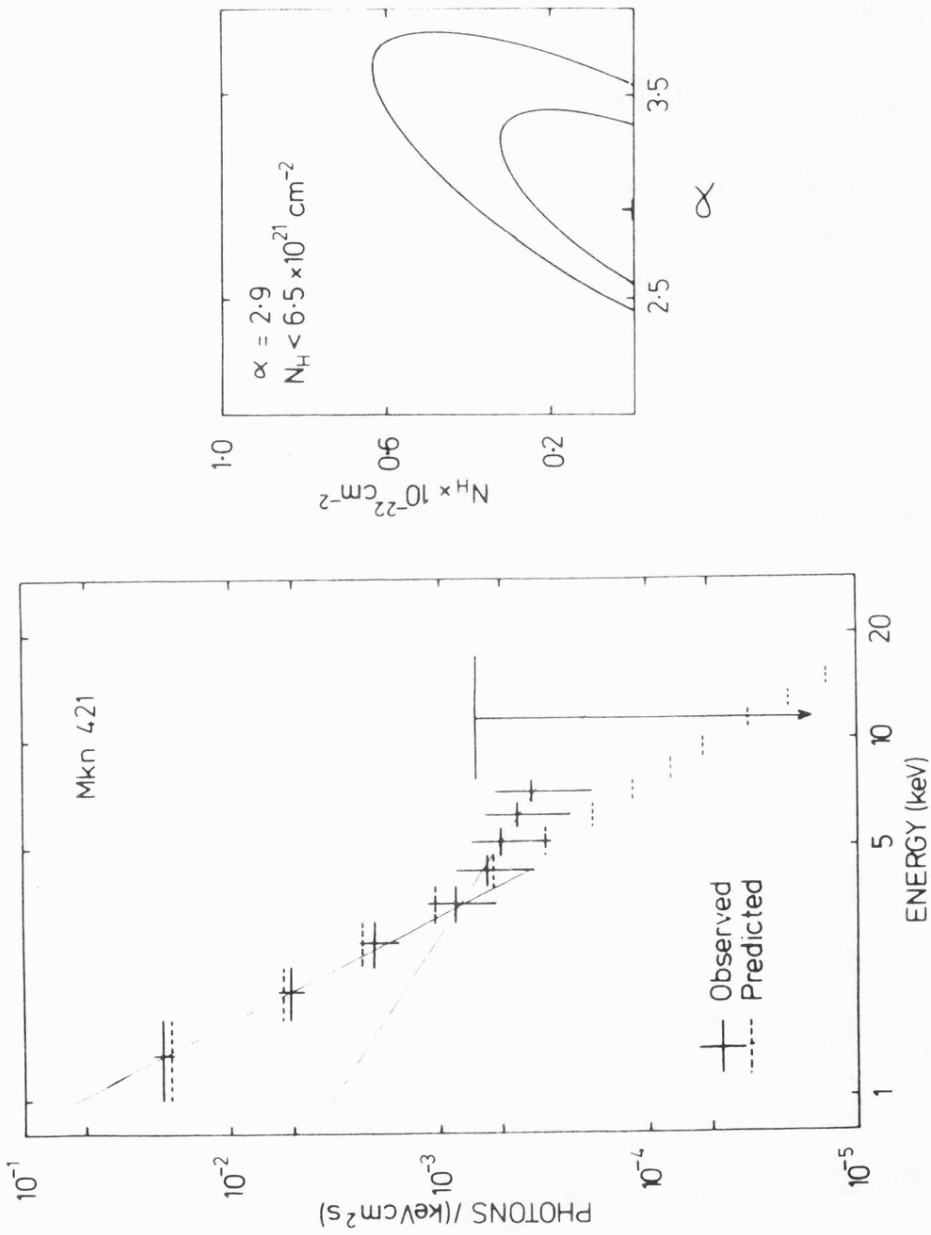


Fig 5.5 Mkn 421 spectrum obtained with Ariel-6.
 ---- shows the best fitting one component model,
 whilst — shows the two component model.

level.

Discussion

The indices for the soft and hard components are in very good agreement with the 1978 HEAO-1 A2 and 1977 OSO-8 results of $\alpha \sim 3.9$ and ~ 1 respectively (Mushotzky et al. 1978c, Mushotzky et al. 1979). However, neither the Ariel-6 soft spectrum, nor that of Mushotzky et al. (1978c) are compatible with that of Hearn et al. (1979), who found $\alpha \sim 2.1$ for energies < 4 keV.

From our data it appears that the spectrum of Mkn 421 has reverted to its 1977 state (as detected by OSO-8). It is worth while noting that the Ariel-6 2 - 10 keV flux of $(6 \pm 2) \times 10^{-11}$ erg cm⁻² s⁻¹ is also in good agreement with that seen by OSO-8 (Mushotzky et al.).

Even though our data do not facilitate a deep discussion of the energy generating mechanisms in Mkn 421, it is apparent that the hard spectral component is highly variable, but of approximately constant index; whilst the soft flux is approximately constant and appears to have a variable index or temperature. The simple inference is that the X-ray spectrum is luminosity dependent, it having two components and a break at 3 - 4 keV when in an luminous state and only a soft thermal(?) component when in a low state, $\sim 2.8 \times 10^{-11}$ erg cm⁻² s⁻¹ (Mushotzky et al. 1979). It is most plausible that the hard component is generated by the reprocessing of optical or infra-red photons (the SSC mechanism) and that the soft component is thermal emission from a hot corona surrounding the central massive body (see Margon, Jones and Wardle 1978, Mufson et al. 1980).

In conclusion we find the spectrum of Mkn 421 during early 1980 to be accurately represented by a two component model. The nature of the spectral variability since 1977 indicates that the hard and soft components originate independently of each other and that the former is most likely to be generated by the SSC mechanism, whereas the latter is probably thermal emission from the accreting plasma.

Chapter 6

Conclusions and

Forward - look

It has been the aim of this thesis to show how observations of spectral variability, made with instruments of only moderate resolution, can, by the nature of the variations, deduce some of the physical properties of X-ray sources. It is clearly seen in the proceeding chapters that the absence of a satisfactory attitude solution for the Ariel-6 observations meant that a search for, and study of, spectral variability was one of the few tasks which the satellite could perform successfully. As a conclusion to this work it is of value to re-state the main results that have arisen from the Ariel-6 observations, these are:

- 1) a detailed knowledge of the phase-dependency of the X-ray spectrum in the 4U0115+63 source enabled a distinction to be made between fan- and pencil-beam models. It was also obvious from our data that current theoretical models are insufficiently detailed to yield useful information when compared to the observational data. We find that the neutron star in the 4U0115+63 system spins down between X-ray outbursts, showing there to be little, if any, accretion of material from the Be companion.
- 2) The detection of a line in the spectrum of GX 1+4 and the variability of this feature have enabled the anisotropic distribution of material, around the neutron star pole in a pulsating X-ray source, to be seen. We have also found evidence that the polar cone is curved in the direction of rotation.
- 3) In systems which are thought to contain an accretion disc corona (ADC) our observations have shown that

such an ADC, if it in fact exists, is capable of attaining a stable equilibrium over a large range of accretion rates, strongly implying the presence of such phenomena in different guises in most disc fed systems (see Section 4.3 on 3A1822 - 371).

Observations of spectral variability, or the absence of it, on short timescales may clarify the nature of the ADC.

- 4) Detection of spectral non-variability in NGC 4151 suggests that the dominant means of X-ray generation is by the thermal compton mechanism. The stability of the low energy (<2.5 keV) spectrum over ~ 7 months also indicates that the fraction of the central source not covered by the clouds in the BLR, remains approximately constant.
- 5) The detection of an Iron emission feature in the spectrum of MCG 8-11-11, similar to that seen in NGC 5548, indicates that in both cases the line is the Iron recombination line and that it is not due to the fluorescence of cool material surrounding the central source.

The generation of an iron line may therefore be a common property of Seyferts when they undergo spectral softening.

- 6) Mkn 421 was found to have a two component spectrum and by comparison with previous observations it is apparent that the components vary independently of each other. We find that the low energy component is probably of thermal origin, whilst the hard X-rays

can be generated by the upscattering of infrared or optical photons.

In the light of the successful Ariel-6 observations it is of interest to briefly take note of the improvements in medium energy 'spectroscopy' that might become available during the next few years.

6.1 Future Missions

Missions such as AXAF during the 1990's will provide the high signal to noise of an imaging instrument, combined with an effective area at ~ 6 keV similar to that of Ariel-6 and an anticipated detector resolution of order ~ 100 eV (Lumb 1983). However for the remainder of the decade the forthcoming missions have instruments whose resolution is similar to that of Ariel-6, or at best a factor ~ 2 improvement.

Two satellites are currently in the first few months of active service, these are EXOSAT and TENMA. A third spacecraft, ASTRO-C is being prepared by the Japanese for launch during February 1987.

EXOSAT

EXOSAT was successfully placed in orbit on 1983 May 27th. The orbit of the spacecraft is unique among X-ray astronomy satellites in that it is highly elliptical with a period of ~ 100 hours duration. This enables continuous observations of X-ray sources for up to ~ 80 hours; the ~ 20 hours that are lost being due to the transit of the satellite through the radiation belts at perigee. The spacecraft is 3 axis stabilised and provides pointing to within $\sim 10^{\wedge}$.

The payload consists of two identical X-ray imaging telescopes operating in the 0.04 - 2 keV energy band, a Gas Scintillation Proportional Counter (GSPC) and a large Medium Energy Detector Array (MEDA), both of which operate over the 2 - 55 keV energy range. Mounted behind each telescope is a Channel Multiplier Array (CMA) which provides imaging to $\sim 10^{\wedge}$ but no energy information other than by the use of filters, and

a Position Sensitive proportional counter (PSD) which has moderate energy resolution ($\sim 45\%$ at 1 keV) combined with low resolution imaging ($\sim 1^\circ$). The MEDA consists of eight separate detectors, each with an $\sim 45^\circ$ FWHM field of view and a total effective area of $\sim 1800 \text{ cm}^2$. Their resolution at 6 keV is $\sim 20\%$. A second unique feature of EXOSAT is that half of the MEDA may be offset from the source to enable simultaneous monitoring of the neighbouring background. The GSPC has an effective area of only $\sim 170 \text{ cm}^2$ but has an energy resolution of $\sim 10\%$ at 6 keV; on bright sources therefore, the GSPC has the capability to distinguish between 6.4 keV fluorescence and 6.7 keV thermal features. All of the instruments are co-aligned, thereby pointing simultaneously at the source and providing monitoring from ~ 0.04 to ~ 55 keV.

It is now less than six months into the mission and whilst the MEDA and GSPC are functioning well, one CMA and one PSD are not operational. There are hopes however that the remaining CMA and PSD will continue to operate. Whilst this failure is unfortunate, it must be noted that one of the most important aspects of the mission is the capability to perform very long uninterrupted source exposures, this ability remains unimpaired.

TENMA (ASTRO -B)

This is a Japanese spacecraft which was placed in a low-Earth orbit during February 1983. The satellite is similar in size to Ariel-6 and it also makes use of only one ground station situated in Japan, necessitating a similar highly inclined orbit. A Gas Scintillation Proportional Counter (SPC) is the primary instrument, this has 10 modules with a total

effective area of $\sim 720 \text{ cm}^2$ and an energy resolution similar to the EXOSAT GSPC. One disadvantage of TENMA is that the pointing uncertainties made it necessary for the instrument to have a large $\sim 3^\circ$ FWHM field of view; it is possible therefore that the instrument may suffer from source confusion in crowded regions of sky such as the galactic centre. The improved spectral resolution and the stability of the background in a low-Earth orbit should make TENMA a very powerful medium energy spectroscopy mission over the next few years.

ASTRO-C

The primary scientific aim of this $\sim 400 \text{ kg}$, 3-axis stabilized, Japanese spacecraft will be to carry out a systematic study of variability in both galactic and extragalactic sources. For this reason the spacecraft will have a high onboard storage capability combined with a large telemetry bandwidth, thereby enhancing its performance during extended observations. ASTRO-C is similar to TENMA in that the spacecraft will be in a highly inclined low-Earth orbit and will use only one ground station, situated in Japan.

The main scientific instrument will be the large area counter (LAC) which is to be built in the United Kingdom in return for a share in the data over the ~ 5 years of the mission. The LAC consists of eight Ar/Xe filled proportional counters with a total effective area of $\sim 5000 \text{ cm}^2$. It will operate over the energy range 2 - 30 keV with a resolution similar to the EXOSAT MEDA. To allow for possible pointing uncertainties the instrument has a field of view of $\sim 1^\circ \times 2^\circ$ FWHM.

ASTRO-C is expected to be launched during February 1987,

making the LAC the only operational medium energy instrumentation available in the early 1990's.

Undeniably Ariel-6 had many faults and to some extent may be classified as only a limited success, in particular when compared to such successful satellites as Ariel-5. However, it has shown the capability of even a small instrument, with moderate resolution to contribute to our knowledge of the physical processes acting in a limited number of X-ray sources. This it has achieved, primarily, through the observation of spectral variability. With such missions as EXOSAT, TENMA and ASTRO-C to come, the next 10 - 15 years should provide the opportunity to remove some of the uncertainties from current theoretical discussions regarding the nature of the emission mechanisms acting in celestial X-ray sources.

References

- Anzer, U. and Borner, G. (1982) Submitted to Astron. Astrophys.
- Baity, W.A., Gruber, D.E., Matteson, J.L., Knight, F.K.,
Nolan, P.C., Scheepmaker, A., Wheaton, W.A., Hoffman, J.A.,
Primini, F.A., Lewin, W.H.G. and Peterson, L.E. (1979),
Proceedings of 21st COSPAR Conf. p 373.
- Barr, P., White, N.E., Sanford, P. and Ives, J.C., (1977),
MNRAS, 181, 43p.
- Basko, M.M. and Sunyaev, R.A., (1976) MNRAS, 175, 395.
- Beall, J.H., Rose, W.K., Dennis, B.R., Crannell, C.J.,
Dolan, J.F., Frost, K.J. and Orwig, L.E., (1981), ApJ. 247,
458.
- Becker, R.H., Boldt, E A., Holt, S.S., Pravdo, S.H.,
Rothschild, R.E., Serlemitsos, P.J. and Swank, J.H. (1976),
ApJ. 207, 167.
- Bethelsdorf, R.F. and Culhane, J.L., (1979) MNRAS, 187, 17p.
- Blandford, R.D., (1977) MNRAS, 180, 343.
- Bradt, H.V., (1980) Ann. N.Y. Acad. Sci., 336, 59.
- Brown, R.K., and Gould, R.J., (1970) Phys.Rev.D, 1, 2252.
- Chanan, G.A., Nelson, J.E. and Margon, B., (1978) ApJ., 226,
963.
- Charles, P., Thorstensen, J.R. and Barr, P. (1980) ApJ., 241,
1148.
- Clark, G.W., Bradt, H.V., Lewin, W.H.G., Markert, T.H.,
Schnopper, H.W. and Sprott, G.F., (1973) ApJ. 179, 263.
- Clark, G. and Cominsky, L. (1978) IAUC 3161.
- Coe, M.J., Bassini, L., Engel, A.R. and Quenby, J.J. (1981)
MNRAS, 195, 241.
- Cominsky, L., Clark, G.W., Li, F., Meyer, W. and Rappaport, S.,
(1978) Nature, 273, 367.

- Cowley, A.P., Crampton, D. and Hutchings, J.B., (1982)
ApJ., 255, 596.
- Davidson, A., Malina, R. and Bowyer, S. (1977) ApJ., 211, 866.
- Doty, J.P., Hoffman, J.A. and Lewin, W.H.G., (1981), ApJ. 243,
257.
- Elvis, M. (1976), MNRAS 177, 7p.
- Elvis, M., Tommaso, M., Wilson, A.S., Ward, M.J., Penston, M.V.,
Fosbury, R.A.E., and Perda, G.C. (1978), MNRAS 183, 129.
- Fabian, A.C. (1979). Proc.R.Soc.Lond.A. 366, 449.
- Fabian, A.C. and Rees, M.J., (1978), Proc.IAU/COSPAR Symp.
Ed. Baity, W.A. and Peterson, L.E. p381.
- Fabian, A.C., Guilberet, P.W. and Ross, R. (1982), MNRAS 199,
1045.
- Fireman, E.L. (1974), ApJ. 187, 57.
- Forman, W., Jones, C. and Tananbaum, H. (1976), ApJ. 206, L29.
- Ghosh, P. and Lamb, F.K. (1979), ApJ. 234, 296.
- Giacconi, R., Murray, S., Gursky, H., Kellogg, E., Schrier, E.,
Matilsky, T., Koch, D. and Tananbaum (1974), ApJ. 188, 667.
- Giacconi, R. et al. (1979), ApJ. 230, 540.
- Giacconi, R., Gursky, H., Kellogg, E., Schrier, E. and Tanan-
baum, H. (1971), ApJ. 167, L67.
- Glass, I.S. and Feast, M.W. (1973), Nature 245, 39.
- Griffiths, R.E., Gursky, H., Schwartz, J., Bradt, H., Doxsey, R.E.,
Charles, P.A. and Thorstensen, J.R. (1978) Nature 276, 247.
- Griffiths, R.E., Briel, U., Schwartz, D.A., Schwartz, J.,
Doxsey, R.E. and Johnston, M.D. (1979), MNRAS 188, 813.
- Hatchett, S. and Weaver, R. (1977), ApJ. 215, 285.
- Hatchett, S., Buff, J. and McCray, R. (1976), ApJ. 206, 847.
- Hayes, M.J.C., Culhane, J.L., Blisset, R.J., Barr, P. and Bell-
Burnell, S.J. (1980), MNRAS 193, 15p.

- Hayes, M.J.C., Bell-Burnell, S.J., Culhane, J.C., Ward, M.J., Barr, P., Ives, J.C. and Sanford, P.W. (1981) Proceed. of XV ESLAB Symposium. Ed. Andressen, R.D. p39.
- Hearn, D.R., Marshall, F.J., and Jernigan, J.G. (1979), ApJ. 227, L63.
- Holt, S.S., Boldt, E.A., Rothschild, R.E., Saba, J.L.R. and Serlemitsos, S.J. (1974), ApJ. 190, L109.
- Holt, S.S. and Kaluzienski, L.J. (1978), IAUC 3161.
- Holt, S.S., Mushotzky, R.F., Becker, R.H., Boldt, E.A., Serlemitsos, P.J., Szymkowiak, A.E. and White, N.E. (1980), ApJ. 241, L13.
- Holt, S.S. (1980), Vistas in Astronomy 24, 301.
- Holt, S.S. and McCray, R. (1982), Ann.Rev. of Astron. and Astroph. preprint.
- Huchtmeyer, W.K. and Wright, A.E. (1973), Astrophys.Lett. 15, 209.
- Hutchings, J.B. and Crampton, D. (1981), ApJ. 247, 222.
- Illarionov, A.F. and Sunyaev, R.A. (1972), Soviet Astron. 16, 45.
- Johns, M., Koski, A., Canizares, C. and McClintock, J. (1978), IAUC 3171.
- Johnston, M., Bradt, H., Doxsey, R., Gursky, H., Schwartz, D. and Schwarz, J. (1978), ApJ. 223, L71.
- Jones, C. (1977), ApJ. 214, 856.
- Joss, P.C. and Rappaport, S. (1984), Ann.Rev.Astron.Astro. preprint.
- Kapachi, V.K. (1979), Astron. and Astroph. 74, L11.
- Kelley, R.L., Rappaport, S., Bradheim, M.J., Cominsky, L. and Strothers, R. (1981), ApJ. 251, 630.

- Koo, J-W.C. and Haymes, R.C. (1980), ApJ. 239, L57.
- Kriss, G.A., Cominsky, L. and Remillard, R. (1980) IAUC 3543.
- Kriss, G.A., Canizares, C.R. and Ricker, G.R. (1980), ApJ. 242, 492.
- Kriss, G.A., Cominsky, L., Remillard, R., Williams, G. and Thorstensen, J.R. (1983) ApJ. preprint.
- Lamb, F.K. (1975), Ann.N.Y.Acad.Sci. 262, 331.
- Lamb, F.K., Pethick, C.J. and Pines, D. (1973), ApJ. 184, 271.
- Lampton, D, Margon, B., and Bowyer, S. (1976), ApJ. 208, 177.
- Langer, S.H., Ross, R.R. and McCray, R. (1978), ApJ. 222, 959.
- Langer, S.H. and Rappaport, S. (1982), ApJ. 257, 733.
- Lawrence, A. (1980), MNRAS 192, 83.
- Lawrence, A., Giles, B., McHardy, I. and Cooke, B.A. (1981), MNRAS 195, 149.
- Lebofsky, M.J. and Rieke, G.H. (1980), Nature 284, 410.
- Lewin, W.H.G., Vacca, W.D. and Basinska, E.M. (1983), ApJ. preprint.
- Lightman, A.P., Giacconi, R. and Tananbaum, H. (1978), ApJ. 224, 375.
- Lubow, S.H. and Shu, F.H. (1976), ApJ 207, L53.
- Lumb, D. (1983), PhD Thesis, University of Leicester.
- Lynden-Bell, D. (1969), Nature 223, 690.
- Margon, B., Jones, T.W. and Wardle, J.F.C. (1978), ApJ. 83, 1021.
- Marshall, N., Warwick, R.S. and Pounds, K.A. (1981), MNRAS 194, 987.
- Marshall, F.E., Boldt, E.A., Holt, S.S., Miller, R., Mushotzky, R.F., Rose, L.A., Rothschild, R. and Serlemitsos, P.J. (1980), ApJ. 235, 4.

- Mason, K.D., Middleditch, J., Nelson, J.E., White, N.E.,
Seitzer, P., Tuohy, I.R. and Hunt, L.K. (1980) ApJ. 242,
L109.
- Mason, K.O., Murdin, P.G., Tuohy, I.R., Seitzer, P. and
Branduardi-Raymont, G. (1982), MNRAS 200, 793.
- Mason, K.O. and Cordova, F.A. (1982a), ApJ. 255, 603.
- Mason, K.O. and Cordova, F.A. (1982b), ApJ. 262, 253.
- McCray, R., Shull, J.M., Boynton, P.E., Deeter, J.E., Holt, S.S.
and White, N.E. (1982), ApJ. 262, 301.
- McCray, R. and Lamb, F.K. (1976), ApJ. 204, L115.
- McHardy, I., Lawrence, A., Pye, J.P. and Pounds, K.A. (1981),
MNRAS 197, 893.
- Meszaros, P., Harding, A.K., Kirk, J.G. and Galloway, D.J.
(1982) preprint.
- Meszaros, P. (1982) Proc. of Workshop on 'Accreting Neutron
Stars', Garching, July 1982.
- Middleditch, J., Koski, A. and Burbidge, M. (1980), IAUC 3510.
- Miller, H.R. (1975), ApJ. 201, L109.
- Miller, H.R. (1979), ApJ. 227, 52.
- Mufson, S.L., Wisniewski, W.Z., Wood, K., McNutt, D.P.,
Ventis, D.J., Meekins, J.F., Byram, E.T., Chubb, T.A. and
Friedman, H. (1980), ApJ. 241, 74.
- Mushotzky, R.F., Serlemitsos, P.J., Smith, B.W., Boldt, E.A.
and Holt, S.S. (1978a), ApJ. 225, 21.
- Mushotzky, R.F., Holt, S.S. and Serlemitsos, P.J. (1978b),
ApJ. 225, L115.
- Mushotzky, R.F., Boldt, E.A., Holt, S.S., Pravdo, S.H.,
Serlemitsos, P.J., Swank, J.H. and Rothschild, R.H. (1978c),
ApJ. 226, L65.

- Mushotzky, R.F., Boldt, E.A., Holt, S.S. and Serlemitsos, P.J.
(1979), ApJ. 232, 17.
- Mushotzky, R.F., Marshall, F.E., Boldt, E.A., Holt, S.S. and
Serlemitsos, P.J., (1980), ApJ. 235, 377.
- Mushotzky, R.F. and Marshall, F.E. (1980), ApJ. 239, L5.
- Nagel, W. (1981), ApJ. 251, 278.
- Osterbrock, D.E. (1977), ApJ. 215, 733.
- Paciesas, W.S., Mushotzky, R.F. and Pelling, R.M. (1977),
MNRAS 178, 23p.
- Patterson, J. (1981), Nature 292, 810.
- Perotti, F., Della Ventura, A., Villa, G., DiCocco, G.,
Butler, R.C., Carter, J.N. and Dean, A.J. (1981), Nature
292, 133.
- Pounds, K.A. (1980) Proc. of NATO Summer School on X-ray
astronomy, Erice, Sicily, 1979, Published by D Reidel (1980)
- Pravdo, S.H. (1979), COSPAR Symp. on X-ray Astron., Innsbruck
1978, Pergamon Press p169.
- Pravdo, S.H., Boldt, E.A., Holt, S.S. and Serlemitsos, P.J.
(1977), ApJ. 216, L23.
- Pravdo, S.H., White, N.E., Boldt, E.A., Holt, S.S., Serlemitsos,
P.J., Swank, J., Szymkowiak, A.E., Tuohy, I. and Garmine, G.
(1979), ApJ. 231, 912.
- Pravdo, S.H. and Bussard, R.W. (1981), ApJ. 246, L115.
- Pravdo, S.H., Bussard, R.W., Becker, R.H., Boldt, E.A., Holt,
S.S. and Serlemitsos, P.J. (1978), ApJ. 225, 988.
- Pravdo, S.H. and Serlemitsos, P.J. (1981), ApJ. 246, 484.
- Rappaport, S. and Jass, P.C. (1977), Nature 266, 683.
- Rappaport, S., Clark, G.W., Cominsky, L., Joss, P.C. and
Li, F. (1978), ApJ. 224, L1.

- Rappaport, S. and van den Heuvel, E.P. (1981) IAU Symp.
No.98 on Bc Stars. Munich 1981.
- Rees, M.J. (1980) 'X-ray Astronomy', Ed. Giacconi, R. and
Setti, G.
- Ricketts, M.J., Cooke, B.A. and Pounds, K.A. (1976), Nature
259, 546.
- Rose, L.A., Pravdo, S.H., Kaluzienski, L.J., Marshall, F.E.,
Holt, S.S., Boldt, E.A., Rothschild, R.E. and Serlemitsos,
P.J. (1979), ApJ. 231, 919.
- Ross, R.R., Weaver, R. and McCray, R. (1978), ApJ. 219, 292.
- Savonije, G.T. (1980), Astron. and Astroph. 83, 375.
- Schnopper, H.W., Delvaille, J.P., Epstein, A., Webster, C.,
Charles, P., Bowyer, S., Hjellming, R.M., Owen, F.N. and
Cotton, W.D. (1978), ApJ. 222, 91.
- Seitzer, P., Tuohy, I., Mason, K.O., Middleditch, J., Nelson,
J.E. and White, N.E. (1979), IAUC 3406.
- Sims, M., Giles, A.B., Hall, R., Page, C.G. and McHardy, I.
(1981), unfinished paper.
- Strickman, M.S., Johnson, W.N. and Kurfess, J.D. (1980), ApJ.
240, L21.
- Tananbaum, H., Peters, G., Forman, W., Giacconi, R. and
Jones, C. (1978), ApJ. 223, 74.
- Tananbaum, H. (1980) 'X-ray Astronomy', Ed. Giacconi, R. and
Setti, G.
- Tennant, A.F., Mushotzky, R.F., Boldt, E.A. and Swank, J.
(1982), ApJ. 251, 15.
- Toor, A. and Seward, F. (1974), A.J. 74, 995.
- Trumper, J. (1979) Proc. of COSPAR Symp. on X-ray Astron.
1978. Ed. Baity, W.A. and Peterson, L.E., 3, 239.

- Tucker, W.H. (1978) 'Radiation Processes in Astrophysics'
MIT Press.
- Ulrich, M.H. (1978), ApJ. 222, L3.
- Wang, Y.-M. and Welter, G.L. (1981), Astron. and Astroph.
102, 97.
- Ward, J., Wilson, A.S., Disney, M.J., Elvis, M. and Tommaso, M.
(1977), Astron. and Astroph. 59, L19.
- Weedman, D.W. (1977), Ann.Rev.Astron.Astroph. 15, 69.
- Weiler, K.W. and Johnston, K.J. (1980), MNRAS 190, 269.
- Wheaton, W.A. et al. (1979), Nature 282, 240.
- White, G.T. and Ricketts, M.J. (1979), MNRAS 187, 757.
- White, N.E., Becker, R.H., Boldt, E.A., Holt, S.S., Serlemitsos,
P.J. and Swank, J. (1981), ApJ, 247, 994.
- White, N.E. and Holt, S.S. (1982), ApJ. 257, 318.
- White, N.E., Swank, J. and Holt, S.S. (1982) ApJ. preprint.
- Wilson, A.S. (1979), Proc.Royal Soc.Lond.A. 366, 461.

ABSTRACT

The Ariel-6 spacecraft was launched during 1979 and remained operational for ~ 3 years. The satellite payload is discussed, with an emphasis on the medium energy detectors, their calibration and performance. We present observations of spectral variability, in both galactic and extra-galactic sources, made with this instrument in the 1 - 50 keV energy range.

Three galactic sources were observed, these consisted of two X-ray pulsators, 4U0115+63 and GX 1+4; the former being fortuitously seen during outburst. Both sources were found to show a significant phase dependence in their X-ray spectra. In GX 1+4 an Iron emission feature was detected, the equivalent width of which was also phase dependent. Pulse timing was performed on the data from both sources and in the case of 4U0115+63 yields a revised set of orbital parameters. The third galactic source presented is 3A1822-371, we find that our data are not only consistent with the presence of an accretion disc corona in the system, but strongly suggests the presence of such a corona in many disc fed systems.

Three Seyfert galaxies, NGC 4151, MCG 8-11-11 and III Zw 2 were observed, this being the first reported X-ray spectrum of III Zw 2. NGC 4151 was found to have a spectrum consistent with that seen ~ 3 years earlier, whilst MCG 8-11-11 was softer than seen hitherto and now shows evidence for an Iron emission line. The BL Lac, Mkn 421 was found to have a two component spectrum; comparison with earlier reported spectra indicates that both components vary independently of each other and therefore arise in physically differing regions of the source.

Finally a forward-look is made which considers the improvements in medium energy spectroscopy that can be anticipated over the next decade or so.